Republic of Iraq
Ministry of Higher Education and Scientific Research
University of Babylon
College of Science for Women
Department of Laser Physics

Synthesis and Study The effect Chitosan Polymer-ZnO-Ag Nanocomposite Prepared by Pulse Laser Ablation Method and Pathogenisity and Virulence Gense of *Klebsilla Pneumaniae*

A Thesis

Submitted to Council of the College of Science for Women/ University of Babylon as Part of the Requirements for Obtaining a Master's degree in Laser Physics

By

Anwar Abdul-Razzaq Abbas Al-Jishami

B.Sc. (2012)

Supervised by

Assist. Prof. Dr. Amer Khudair Al-Nafiey

Prof. Dr. Ali Hussein Al Marzoqi

2022 **1444**

بسم اللّٰه الرحمن الرحيم

اللَّهُ نُورُ السَّمَاوَاتِ وَالْأَرْضِ مَثَلُ نُورِهِ كَمِشْكَاةٍ فِيهَا
مِصْبَاحٌ الْمِصْبَاحُ فِي زُجَاجَةٍ الزُّجَاجَةُ كَأَنَّهَا كَوْكَبٌ
دُرِّيٌّ يُوقَدُ مِن شَجَرَةٍ مُّبَارَكَةٍ زَيْتُونَةٍ لَّا شَرْقِيَّةٍ وَلَا
غَرْبِيَّةٍ يَكَادُ زَيْتُهَا يُضِيءُ وَلَوْ لَمْ تَمْسَسْهُ نَارٌ نُّورٌ
عَلَىٰ نُورٍ يَهْدِي اللَّهُ لِنُورِهِ مَن يَشَاءُ وَيَضْرِبُ
اللَّهُ الْأَمْثَالَ لِلنَّاسِ وَاللَّهُ بِكُلِّ شَيْءٍ عَلِيمٌ (٣٥)

صدق اللّٰه العلي العظيم

سورة النور ايت ٣٥

Dedications

To the one who gave me the honor to bear his name...

My dear father

To the light of my eyes, the light of my path, and the joy of my life

Her prayers and words were companions of brilliance and excellence…..

my mother

To the mountain where I take refuge and feel safe and strong

my husband

To my second mother and a tender heart...

My older sister

To my happiness, the soul of my life and the source of my strength

My children...

Mustafa and Youssef

To everyone who taught me and supported me, even with a smile

I give you all my love, gratitude and appreciation.

Anwar Al-Jishami

Thanks and appreciation

Praise be to God, Lord of the worlds, and praise be to God always abundant, never cease, above the praise of praise, and thanksgiving for thanksgiving for ever and ever, and prayers and peace be upon our master Muhammad, the seal of the prophets and his righteous family.

I extend my thanks and great appreciation and respect to the professors who supervised the research (Dr. Amer Khudhair Al-Nafiey) and (Dr. Ali Hussein Al-Marzoqi) for all the moral and scientific assistance they provided me in completing this research.

I extend my thanks and appreciation to the Department of Laser Physics Sciences with all its staff and affiliates, especially Dr. (Jinan Ali Al-Shamri) and to the Deanship of the College of Science for woman for their support during the study period.

Thanks, appreciation and gratitude to the Department of Biological Sciences at the College of Women's Sciences at the University of Babylon, especially the workers in the Advanced Molecular Genetics Research Laboratory, represented by Dr. Ali Hussein Al-Marzoqi, for their support and assistance during the research period.

And last but not least, thanks and appreciation to all my professors in all stages of my academic life and thanks to all my colleagues and may God grant them success in their scientific lives.

M.s.c Student

ANWAR

Summery

Synthesis of physical and biological materials and nanoscience are all topics of interest in medical, industrial and other applications. Incorporation of nanoparticles using fluid-based pulsed laser ablation (PLAL) technology leads to the production of high-quality nanocomposites that contribute to the production of antibacterial substances, including *Klebsiella pneumonia*.

After placing the nanoscale samples on glass slides and subjecting them to a series of tests, the composites (Cs-Ag-Zno)/(Cs- Ag)/(Cs- Zno) gave the following results: Examination of the optical properties UV-vis showed the presence of two peaks, one associated with Ag NPs and located at 400 nm and the other with zinc oxide and located at 244 nm. The absorption coefficient of the nanocomposite is at its maximum value in the range 200-550 nm and that the direct band gap of silver is (2.8) eV, the direct energy gap of zinc is (4.7) eV and the direct energy gap of Cs, Ag and Zn is at (2.7) eV While (2.5) eV is the indirect energy gap of silver and the indirect energy gap of (Cs-Ag-ZnO) composite is 2.6 eV and 4.2 eV for Zno .

There were also three peaks for each composite in the FTIR results of scanning the nanocomposites and we observe an O-H\NH_2 bond. So are C = O and N-H:OH bonds.

The search for the structural properties of the nanocomposite (Cs-Ag-Zno) revealed the presence of crystalline levels and the presence of peaks corresponding to the chitosan solution at (24.6118 °), in addition to the presence of corresponding peaks of silver and Zno nanoparticles. Nanoparticles were obtained at (30.3729 and 45.9902°) with Miller's

coefficients (100, 200), nanoparticles were FCC for silver nanoparticles and hexagonal for zinc oxide.

TEM testing revealed that spherical nanoparticles have a nanosize of 18.196nm. According to the results of FE-SEM, it was discovered that silver nanoparticles and zinc nanoparticles were tightly bound to the polymer (Cs) and appeared as bacilli of the ternary complex while they appeared as zinc and chitosan gel pieces while when silver nanoparticles were added to the polymer solution they formed concentric conical shapes.

When the bacteria *Klebsiella pneumonia*, which can cause a variety of diseases, was exposed to the generated nanocomposites, the results showed that the percentage of inhibition or killing was between (22-35) mm.

The percentage of killed bacteria increases with increasing concentration of nanocomposites. The results showed that bacterial DNA concentrations ranged between 0.03 and 0.291, and the highest concentration was at (Cs-Zno) composite.

Finally, five types of *Klebsiella pneumonia* genes were studied. (*Fimh 1*, *Ycfm entB, Kfu*, *rpmA*) and it turned out that they were affected by the nanocomposites in different ways), but in the second dilution, the effect of the nanocomposite (Cs- Ag -Zno) was clear, as it was observed that all studied genes were affected by this nanocompound when compared with the sample. Untreated with nanomaterials.

TABLES LIST

List of
Symbols & Shapes

Symbols	Meaning
α	Absorption Coefficient
A	Absorbance
ADT	Allowed Direct Transition
Ag	Silver
Cs	Chitosan
C.B	Conduction Band
C.S	Crystallite Size
DNA	Dioxy Nucleic Acid
Eg	Energy Gap
EDS	Energy Dispersive Spectroscopy
FE-SEM	Field Emission- Scanning Electron Microscopy
FWHM	Full Width at Half Maximum
hkl	Miller Indices
I	Transmitted Photon Intensity
I_0	Incident Photon Intensity
MBC	Minimum Bactericidal Concentration
MICs	Minimum Inhibitory Concentrations
MKC	Minimum Killing Concentration
NPs	Nanoparticles
O.D	Optical Density
Θ	Bragg's Angle
PCR	Polymerase Chain Reaction
ROS	Reactive Oxygen Species
SPR	Surface Plasmon Resonance
T	Transmittance
TEM	Transmission Electron Microscope
UV	Ultra Violet Region
V.B	Valence Band
UV -Vis	Ultraviolet-visible UV -Vis diffuse reflectance Measurements
XRD	X- ray Diffraction
β	Full Width at half maximum
λ	Wavelength
Zn	Zinc

1.1 Introduction

This thesis is concerned with studying three basic concepts: laser and nanotechnology, and the third is biological, which is bacteria, because of their important impact on daily life, as well as the result of advances in electronic, biological and physical fields. It has become necessary to connect these sciences together and try to find solutions and results to the problems of our lives.

The first term is laser The first concept is the laser, by which we mean the amplification of light by stimulated emission of radiation [1],Lasers have several basic properties, these properties are (monochromatic, directivity, coherence , brightness). monochromatic means that the laser beam has only one wavelength, directivity is the beam propagation in one direction and for very long distances without diffusing from its axis or very little diffraction , it does not exceed a few centimeters per kilometer, and the coherence is the difference between any two points on the wave of the laser beam that is constant when the beam is moving spatially and temporally. The laser is the only light source that has the coherence compared to traditional light sources. The brightness is that the power density of the laser beam per unit area is very high. .Solid state, liquid state, and gas-state lasers are the three basic laser classes. Lasers of all types mentioned above can also be used in many fields, including medical, biological, industrial, agricultural and various areas of life [2]. In this thesis, we will use the laser by pulsed laser ablation method in liquids to synthesize nanomaterials.

The other term is nano, which is a science that deals with the physical and biochemical properties of materials and their composition in nano dimensions, and the word nano means dwarf in Greek. (Richard Fayman) in a lecture titled (There's Lots of Room Below) at the American Physical Society in 1959, Norio Taneguk. Nature has used nanoparticles since the beginning of evolution [3].

When the particles (atoms or molecules) are spherical, the radius is less than one hundred nanometers, and the number of atoms ranges from a certain number to one million atoms, this agglomeration or assembly (nanoparticles) is called [4]. Each particle has a radius of 1 nm 25 atoms, most of them are located on the surface of the body, because the dimensions of the nanoparticles are less than the critical dimensions required for their occurrence, and this is different from the section that contains a number of atoms. Average free path, which controls electrical conductivity , is a physical phenomenon in which electrons move between two successive encounters with vibrating atoms, when the size of one-dimensional nanoparticles is called nanowires, they are nanostructures and structures with a radius of multiples of nanometers, but when they are scaled by nano in two dimensions, it is called a quantum well, or a body in a box, or an infinite potential well in quantum mechanics, and if they are in three dimensions, they are called quantum dots [5,6,7].

Metal nanoparticles are materials that are found at the junction of atoms and materials of large size. Due to their small size (less than 100 nanometers in at least one dimension), they have a large specific surface area and as many surface atoms as other materials, and particles can be obtained Metal nanoparticles by physical, chemical or biological methods, however, the use of the physiotherapeutic method (pulsed laser ablation) is of particular interest [8].

Nanomaterials have many applications in various fields of life, including agriculture, industry, environmental, and medicine, and there are a number of different materials and minerals that can be converted into nanoparticles with anti-bacterial and anti-fungal properties including silver, Zn and Ag and others [9-10-11]. In this thesis we will talk about the advantages of nanomaterials and their applications in the biological field and their ability to kill various pathogenic bacteria.

The third term is biological bacteria, and bacteria have recently been observed to develop resistance to drugs and antibiotics, including drug-resistant Staphylococcus aureus, *Salmonella typhimurium, Staphylococcus epidermidis, Escherichia coli, and Klebsiella pneumoniae*. The biological effects of nanoparticles, silver, zinc, chitosan polymer, etc., such as cellular uptake, cellular activation and intracellular distribution, are determined by size and shape, as well as surface and operational charge and basic structure, as well as the effect of these nanomaterials on bacterial genes responsible for perpetuating The life of bacteria that constitute the virulence factor and resistance to drugs and antibiotics [12-13]. From all that has been mentioned, in this thesis we will study the use of liquid laser pulse ablation in the synthesis of nanomaterials that aim to inhibit or kill *Klebsiella pneumoniae* bacteria and study the effect of these materials on bacterial genes and thus contribute to finding solutions to one of the important problems of life.

1.2 Nanomaterials Used in The synthesis of Nanocomposite

Nanoparticles have unique properties and advantages; Therefore, it has attracted the attention of researchers, and has achieved great development in nanotechnology. Among these properties is the surface area and the ability to act as an anti-bacterial, which causes many problems in health and environmental areas such as water pollution, enteritis, pneumonia and many other damages. Nanomaterials such as organic and inorganic metals and semiconductors such as (silver, zinc or zinc oxide, gold Au, polymer such as chitosan, etc.). We will focus on silver nanoparticles, zinc nanoparticles and chitosan nanopolymer. It inhibits or kills highly resistant Gram-negative and Gram-positive bacteria. It is also a good antibacterial because the decrease in size increases the surface area, and herein it increases the ability of nanoparticles as antibacterial particles [14].

1.2.1 Chitosan (Cs)

A After cellulose, chitin (β -(1-4)-poly-N-acetyl-D-glucosamine) is the second most abundant polysaccharide distributed in nature. Chitin is easily found in many organisms, especially in the exoskeletons of insects, lobsters, shrimp, and crabs. Chitin (poly-(β -1! 4)-2-amino-2-deoxy-D-glucopyranose) is the main source of chitosan as shown in Figure (1-1) [15],obtained by removing the acetyl group (CH_3-CO) from chitin. In addition to enzymatic processes, the preparation of chitosan depends mainly on chemical, physical or biological processes to remove minerals and proteins from crustaceans. Hydrochloric acid is often used as the preferred reagent during the purification process. As a second step, sodium hydroxide (NaOH) is used at 65-100°C for 0.5-72 hours. Purification and deproteinization processes primarily affect molecular weights (MWs) and deacetylated distribution[16]. Chitosan due to its many unique properties including biodegradation, biocompatibility and low toxicity, it has been used in a wide range of applications in many fields for example as a fluxing agent in water treatment and elicitor to activate plant defenses, food supplement during food preservation and in food additives, desiccant agent in cosmetics, cancer treatment, gastrointestinal diseases, respiratory tract and drug

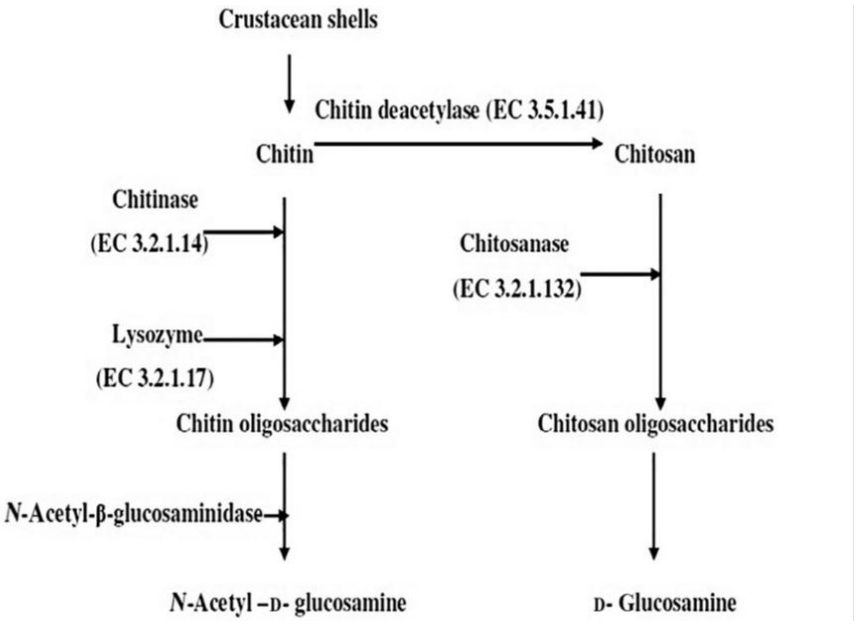

Figure (1-1)

Enzymatic Preparation of Chitosan [15]

delivery through various methods such as nanoparticles (NPs) where chitosan has been used as a carrier in polymeric nanoparticles to deliver drug prepared with chitosan derivatives because they contain functional groups Its chemical properties can be modified to achieve specific goals, making it a polymer with an enormous range of potential applications. Chitosan typically has a positive surface charge and mucosal adhesive properties, allowing it to adhere to mucous membranes and release drug load consistently Figure (1-2) shows the chemical structure of the polymer [18-19]. In addition, the broad antimicrobial activity of chitosan against bacteria and fungi has been reported.

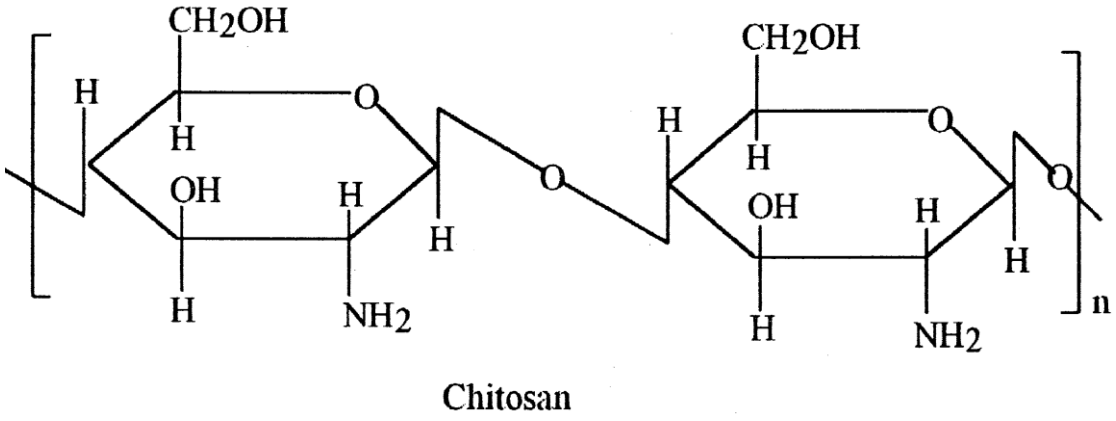

Figure (1-2): Structures of Chitosan [17].

Chitosan is highly dependent on the type of target microorganism furthermore, mechanisms of chitosan antimicrobial activity are related to its physical and chemical properties. Chitosan contains some functional groups that allow graft modification. Modified chitosan imparts special properties. These modifications can be used to chemically modify chitosan to improve its solubility and thus expand its applications. These chemical modifications produce many types of chitosan derivatives that have a continuous release which broadens their range of applications [20-21-22].

1.2.2 Silver (Ag)

A noble chemical element with a silver color, silver melts at 962 ° C, atomic number: 47.Atomic weight: 107,8682 atomic mass units. Density: 10.501 cm3. Nanoparticles of noble metals in liquids, among them silver nanoparticles, have become an important material for many applications [23]. Because of its optical, electronic, catalytic, and antibacterial qualities [24,25].

Silver nanoparticles have been used in several applications including optical sensors,cosmetics,pharmaceuticalindustry,foodindustry,diagnostics,orthopedics, drug delivery, and as anti-cancer agents, among others. Since the surface-to-volume ratio of nano-sized metal particles is unique and can significantly modify the physical, chemical and biological properties as well as its optical properties and high thermal and electrical conductivity [26].

It is necessary to know the method of preparing silver nanoparticles, because it is important from the point of view of the surrounding environment. Nanotechnology is attributed to the advances in nanomaterials fabrication techniques during the last two decades. The main challenge in the manufacture of nanomaterials is to control their properties such as shape, size distribution, morphology, chemical composition and crystalline environment. There are a wide number of methods for manufacturing silver nanoparticles which are readily available. The available methods for preparing silver nanoparticles as with all other nanomaterials are, from top to bottom or from bottom to top [27] as in Figure (1-3).

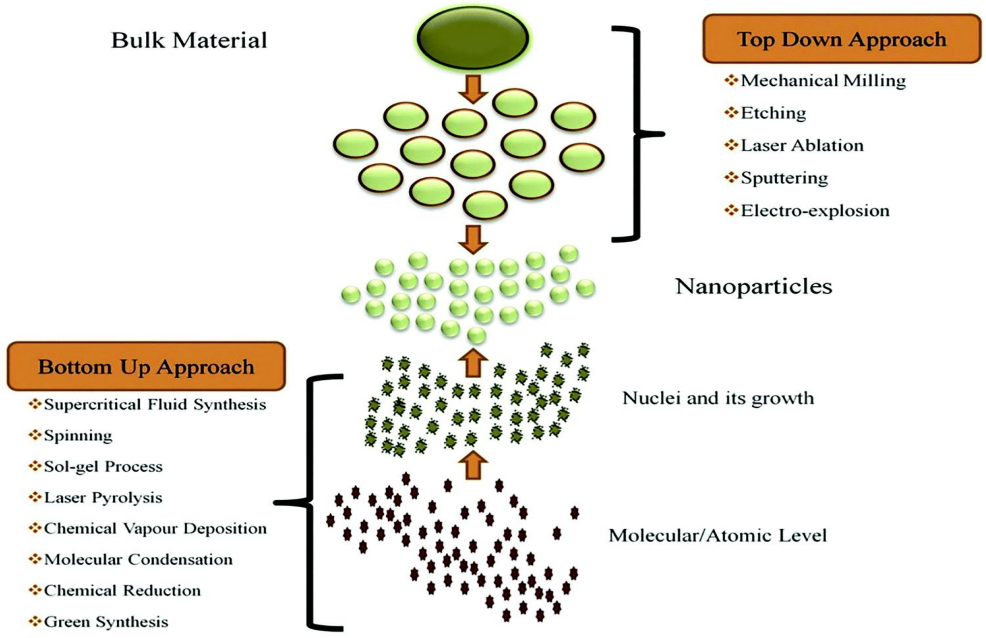

Figure (1-3): The Schematic Representation of The Top-Down and Bottom-up Approaches for Nanomaterials [28].

As a result of the remarkable properties of the mentioned nanomaterial structure as well as its unique interaction with living matter, it will generate Reactive Oxygen Species (ROS), which are the effective radicals that can kill bacteria. The nature of photodynamic therapy depends on the oxidation of living tissues and the abundance of oxygen in the environment in which the bacteria live. Also, the method of physical killing of bacteria is by absorbing nanoparticles by bacteria [29].

1.2.3 Zinc (Zn)

Zinc metal (Zn): It is one of the quantitative elements with atomic number (30).Its quantitative properties are that it is composed of hexagonal crystals and its melting point is low compared to in the rest of the metals, it is also considered as a strong reducing agent, having a white color and a solid, indestructible element. And clouds at normal temperatures, but it becomes

fragile after the temperature (100 C) until It can be pulled and hammered, in addition, it has a serious electrical conductivity .

Zinc oxide (ZnO): has a hexagonal structure with lattice parameters. It is a number of planes that have identical tetrahedral ions and ‹alternately stacked along the C-axis as shown in Figure(1-4) The tetrahedral symmetry of the zinc oxide, ZnO, resulted in a symmetrical structure as well as a phenomenon Piezoelectricity, the phenomenon of converting physical energy into energy Electricity by means of compression or vice versa, and this physical phenomenon appears in some materials that have the ability to generate electric potential when exposed to mechanical stress, as the pressure on the material's surface with a force as a result of the shifting of the positive and negative charge positions in the crystal, and consequently a difference in electric potential between the material's surface, and another characteristic that zinc oxide has is the polar surfaces, with the sixth electrode surface being the most typical electrode surface [30].

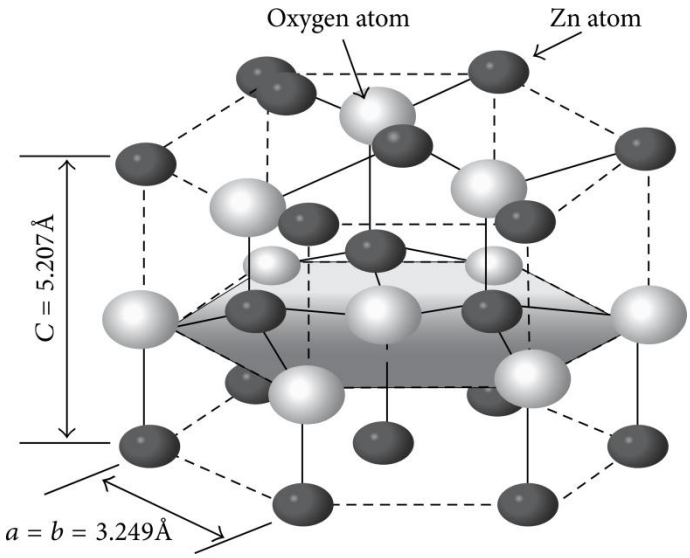

Figure (1-4): Diagram of (ZnO) [30].

ZnO nanoparticles (ZnO NPs) are increasingly used in industrial items such as rubber, paint, and cosmetics. ZnO NPs have become one of the most widely used metal oxide nanoparticles in biology over the past two decades. Due to its great ability to promote excess reactive oxygen (ROS) production, release zinc ions, and induce apoptosis, it is an inorganic element with remarkable potential in biomedicine, especially in the fields of cancer and antibacterial. Moreover, because zinc has a large energy gap (3.37 eV) and high exciton binding energy, it is known to maintain structural integrity in a frequently used material (60 meV) [31]. Although zinc is essential for human, animal and plant growth, adults need 8-15 mg of zinc per day, with about (5-6) mg per day lost via urine and sweat. However, zinc oxide nanoparticles are dangerous to microorganisms [32-33].

1.3 Synthesis of Nanocomposite (Cs-Ag-Zn)

To develop a practical method for producing antibacterial materials with improved functional qualities. Silver nanoparticles or zinc nanoparticles in Cs-based compounds have been shown to improve mechanical strength. Silver nanoparticles are among the first inorganic nanoparticles to be studied for antibacterial and wound-healing characteristics, and these products are frequently promoted as having the ability to kill or decrease germs. Many efforts have been made in recent years to build organic/inorganic hybrids, particularly those based on biopolymers and metal ions, in order to link the biopolymer's ability to the antibacterial properties of metal ions. The metal ion enhances the density of the positive charge of chitosan, which is believed to improve the adsorption of the negatively charged cell surface pelletion, resulting in cell growth inhibition, and it has also piqued interest in ZnO NPs due to features like as catalytic activity. Because of the anti-inflammatory zinc ion, its high stability, non-toxicity, cheap Cost, antibacterial qualities, as well as its solubility in aqueous solutions of organic or mineral acids, can be used in

cosmetics, decontamination, medical prevention, and clothing. It also has a key role in wound healing, especially from burns. Because of these advantages, the synthesis of Cs and ZnO as an alternative material for other nanoparticles [34]. Also, Ag NPs nanoparticles were used with chitosan and had great results, but it was noted that the concentration of Ag NPs nanoparticles Silver if it is high sometimes, this leads to change the properties of the nanocomposites (Cs-Ag), in addition to changing the color of the nanocomposite due to the high content of Ag, which is dangerous in some antibacterial applications, so the concentration of silver nanoparticles must be reduced. The activities of the compound were not ideal in a content where silver nanoparticles are low so it was necessary to strengthen the compound with another white metal oxide that could partially replace it, namely zinc and at the same time incorporated into the chitosan matrix, this would not only enhance the antibacterial property, but also maintain on the color of chitosan. Thus, nanocomposites (Cs-Ag-ZnO) are synthesized with high antibacterial activities that were successfully prepared by purification or any other scientific method [35].

1.4 Methods for Manufacturing Nanomaterials

The results of experiments used on organic and inorganic metals, various polymers and other materials led to the generation of nanomaterials with useful optical, electrical, magnetic and thermal properties, which made them applicable in many fields. However, these materials have drawbacks besides their advantages of high surface energy and easy agglomeration, which makes them unfavorable for long-term storage [36].

Nanomaterials are produced by several methods (physical, chemical, and others), such as spray method, electrodeposition method, spray pyrolysis method, sol-gel method, spin coating, and hydrothermal method [37]. In this paper, we will focus on the physical method for nanoparticle synthesis. Specifically, the pulsed laser ablation of liquid nanoparticles (PLAL) method.

The (PLAL) technique is effective, as it can avoid aggregation of nanoparticles by using ultrasonic dispersion and vibration in addition to changing the pH value of the solution. The liquid-phase pulsed laser ablation technique has several advantages, including: the chemical composition is simple and clean, and the final product is obtained in an easy way without the need for further purification, low cost and easy control of parameters. In addition, it is characterized by the preparation of nanomaterials at low temperatures, the production of more than one material at the same time, and homogeneous and pure compounds and thus the synthesis of nanomaterials that have a wide range of applications in fields including biosensors and nanoelectronic devices [38-39-40]. PLAL requires focusing high-energy lasers onto the surface of a solid target immersed in a liquid, which causes the laser to interact with the target and evaporate the surface in column halo plasma containing different types of particles such as atoms or ions and their combinations with high kinetic energy. Particles in the plasma corona collide and interact with the particles surrounding the liquid, producing new compounds containing solid and liquid target atoms [41].

"

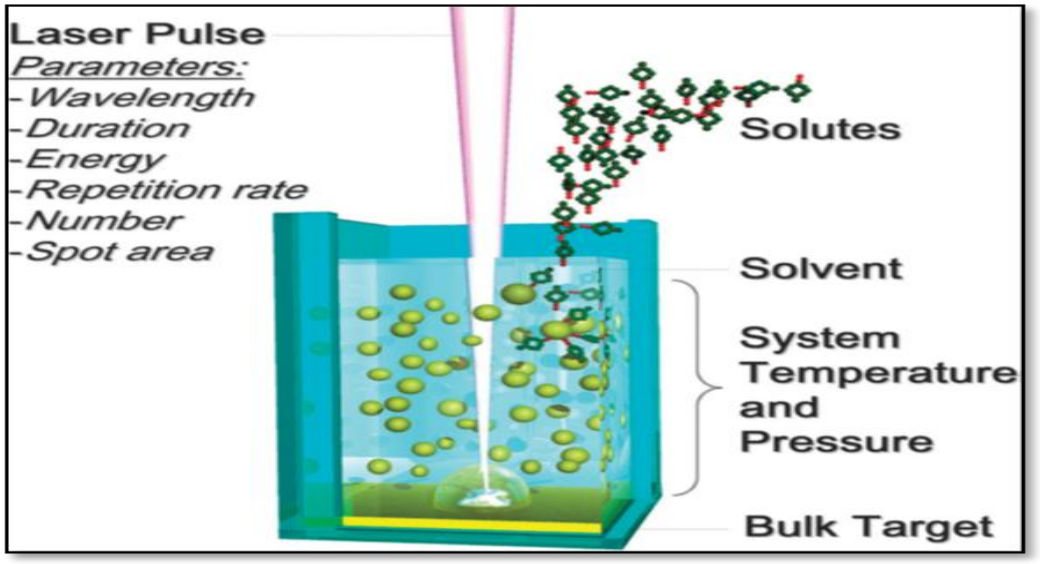

Figure (1-5): shows a schematic diagram of the laser ablation method in PLAL fluids [42].

Laser ablation was performed from a solid target immersed in a liquid medium inside an open vessel where laser pulses were fired at the target for a period of time to remove the metal surface portion. The first procedure for laser ablation is the interaction of the laser beam with the surface of the solid target, which causes the solid target to evaporate and dissolve into the liquid colloid solution. Chemical reactions can occur between solids and liquids, and the product of the reactions is usually nanoparticles (NPs) consisting of atoms of both the target and the formed liquid suspended in the colliding liquid. There are several factors that affect the laser ablation process, including: the laser wavelength, the laser energy, the type of liquid medium, the depth of the optical path of the laser beam inside the liquid, and the type of target material [43]. The success of the ablation process and the presence of nanoparticles in the liquid can be revealed by the optical absorption spectrum of metallic nanoparticles [45-46].

The most prominent type of laser used in the process of pulsed laser ablation in liquids is the Nd-YAG laser, which is one of the most important solid state lasers. The active medium is YAG crystal, which is Yttrium-Aluminum-Garnet doped with Nd+3 ions with a grafting percentage not exceeding (1.5%), the color of the crystal is purple. YAG crystal has high wear resistance, fracture hardness, and high optical quality. The Nd-YAG laser operates in a four-level system and in a continuous pulse mode. The active medium is pumped using a flash lamp, as an electric voltage is shed between the two ends of the lamp, which produces light rays that are absorbed by the crystal to irritate, or by using a semiconductor laser (Laser Diode). The Nd-YAG laser emits a beam with a wavelength of 1064 nm located in the infrared region. The high intensity of the laser pulse is efficient for frequency doubling and generates 532nm wavelength or 355nm thread harmonics generation because doubling the frequency leads to halving the wavelength [47-48]. Figure (1-6) shows the power levels diagram of the Nd-YAG laser.

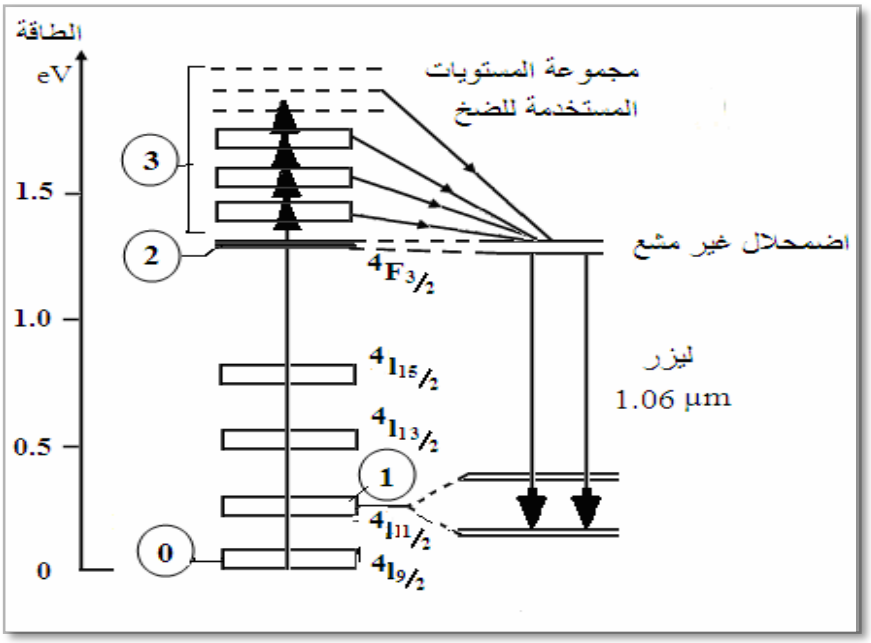

Figure (1-6) Scheme laser energy levels Nd:YAG[47].

1.5 *Klebsiella pneumoniae*

Klebsiella pneumoniae is a non-motile, aerobic, rod-shaped Gram-negative bacterium. These bacteria can spread through various tissues and cause life-threatening infections. It is found in the faeces of 5% to 38% of people and in the nasopharynx of 1% to 6% of the general population. Gram-negative bacteria such as *K. pneumoniae* are the second most common cause of bloodstream infections. Bloodstream infections usually occur as a result of infections in the urinary tract, digestive system, respiratory system, or after a catheter is inserted into a vein or urinary tract. The mortality rate associated with *K. pneumoniae* or pneumonia is higher than 20%. *K. pneumoniae* is resistant to many drugs. Antibiotics are one of the most troublesome problems for this type of bacteria [49], and this represents a very important challenge to the efficacy of antibiotics and a threat to conventional clinical treatment, so there is a need for new antibacterial strategies to overcome these challenges using different metals, including copper, zinc and silver. They have been investigated as potential antibacterial substances [50]

These minerals are synthesized as nanoparticles proportional to the size of the bacteria, as mentioned earlier. These nanomaterials are usually mixed with a biopolymer of natural bacterial strength, such as chitosan or other biopolymers such as PVA [51-52]. This addition (manufacture of nanocomposites) increases the effectiveness and efficiency of the polymer and thus increases the percentage of bacterial killing or inhibition [53], which is what we will address in this research. *K. pneumoniae* bacteria colonize the digestive tract as well as the urinary tract, respiratory tract, and blood. *K. pneumoniae* biofilms that form on medical devices (such as catheters and endotracheal tubes) provide an important source of infection in catheter patients. *K. pneumoniae* tends to be chronic due to *K. pneumoniae* in live biofilms that protect the pathogen from host immune responses and antibiotics. *K. pneumoniae* often presents with multiple drug-resistant phenotypes. It is usually caused by an extended spectrum of β-lactamases and carbapenemases, which makes it difficult to choose the right antibiotics. For treatment, at least 78 captive serotypes (K antigen) were identified for a few *K. pneumonia*. Serotypes (mostly including K1 and K2) have a unique (highly virulent) mucosal overgrowth. The phenotype is due to increased production of capsular polysaccharide (CPS), the most important virulence factor for *K. pneumonia*, and is determined by Abundant appearance of mucous colonies growing on agar plates. The chain test indicates hyper viscosity when the impregnation ring is capable of generating a viscous chain over 5 mm in length by stretching bacterial colonies onto an agar plate. A positive association of mucosa with successful establishment of infection was also shown. In addition to immunocompromised people, *Klebsiella* bacteria can affect healthy people, causing life-threatening infections that are often community transmitted, such as pus. Liver abscess, meningitis, necrotizing fasciitis, endophthalmitis, and acute pneumonia, especially serotype K1 and K2 [54,55]. The outer membrane proteins, excretory system type 6, contain genes encoding erupactin and its receptor, as well as *rmpA*, that confer a

mucosal phenotype. The general definition of hvKp refers to the hyper mutagenic phenotype, the genotype corresponding to virulence and clinical manifestations of metastatic infection. The capsule surrounding the surface of *K. pneumonia* acts as a major virulence factor associated with the viscous phenotype. Where the capsule may provide protection from immune responses, the capsule-mediated resistance to the actions of the bacteria tends to be defensive rather than offensive .*K.pneumonia* avoids phagocytosis, supplementation, antimicrobial peptides, and specific antibodies by using capsules that make it difficult for bacteria to attach. These capsules contain robust layers expressing an excessive mucosal phenotype that may enhance their viability. It was also found that all *Klebsiella pneumoniae* isolates produced enteropectin, while a much smaller proportion produced either aeropectin or ersenapectin. Aerobactin has been shown to play a role in enhancing the virulence of *K. pneumoniae*, in addition to the presence of bacterial bio-growth genes and iron transporter genes that supply the bacterial cell with life-important iron [56]. In addition to the many types of genes important in the life of bacteria, in this research we will address some types of these genes and show the effect of nanocomposites used on these genes.

1.6 Mechanism of Killing Bacteria Using Nanomaterials

When nanocomposites are used as an antibiotic against bacteria, the mechanism of killing Gram-negative bacteria and Gram-positive bacteria can be explained

as follows:

Gram-negative bacteria are mostly attacked by inactivating bacterial cells, while Gram-positive bacteria are degraded by inhibiting cell division. Nanomaterials damage the membranes of Gram-negative bacteria more than the membranes of Gram-positive bacteria, and the antibacterial ability of this nanocomposite is affected by the thickness of the cell walls of microorganisms. Bactericidal

activity is represented in four stages: release of metal ions, cell membrane penetration, and generation of ROS (reactive oxygen species). This is followed by DNA, protein, mitochondria, lipids, and membrane damage, which eventually leads to cell death. Silver nanoparticles have been used to inactivate or kill bacteria. When nanoparticles are irradiated, the energy absorbed by these particles quickly turns into heat and leads to irreparable damage, which means that it cannot be processed again as in Figure (1-7) [57-58].

In silver the size and shape of nanoparticles have an effect on the killing mechanism of living organisms, as small particles have a larger surface area, and therefore have a greater toxicity potential, and it is known that the shape of nanoparticles can greatly affect the physical properties, and the composition of silver nanoparticles, which is often used in the field biomedicine is (spherically, nanowire, nanorods, cubic) [59]. Also, increasing the concentration of nanoparticles also has an effect on the killing mechanism. The higher the number of particles, the higher the kill ratio [60]. The chemical and physical interactions between nanoparticles and cells (cellular uptake of silver nanoparticles) depend on time, dose and energy [61-62].

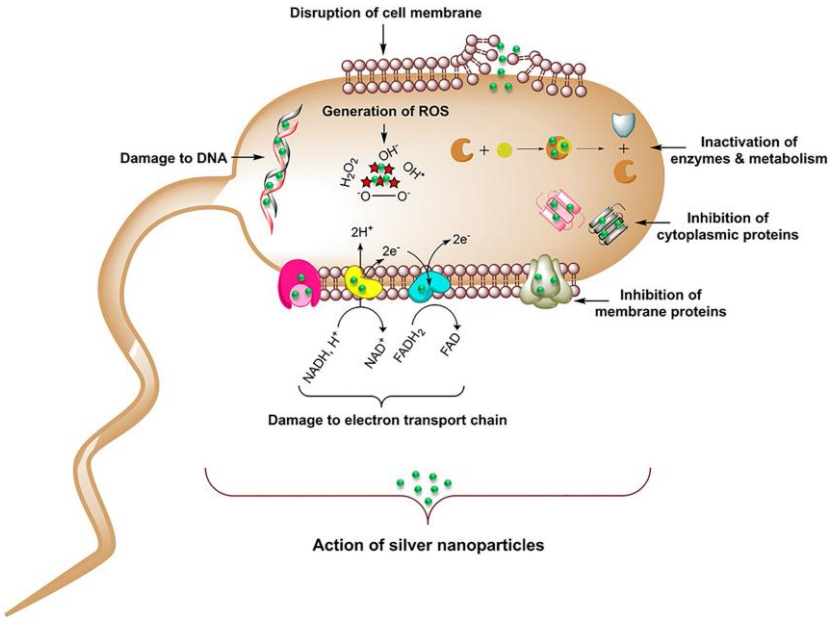

Figure (1-7) Schem of Produced Silver Nanoparticles on Apoptosis of Bacterial cells [63] .

As for chitosan, a variety of variables acting in a regulated and independent manner are known to influence the antibacterial activity. The most common antimicrobial activity of chitosan is based on its ability to bind to the negatively charged cell walls of bacteria. Cell rupture leads to altered membrane permeability, which is followed by binding to DNA, which prevents DNA replication and leads to cell death. Another way is that chitosan acts as a chelator, a substance that optionally binds to trace mineral elements that promote the formation of toxins while preventing the development of microbes. The antibacterial effect of chitosan depends on its polyclonal structure, since the pH of the environment KP is lower than that of chitosan and its derivatives, and the antibacterial activity also depends on lipopolysaccharides and cell surface proteins. The polycrystalline structure necessarily forms under acidic conditions, because grafted groups of certain derivatives may change the KP of chitosan (Cs) and protons by a value above the pH when the positive charge density of chitosan increases. As a result, the antibacterial property will

improve, or the nanoparticles will interact with the cell surface and change the cell permeability, forming an impenetrable barrier around the cell, preventing solutes from entering the cell. As shown in Figure (1-8), the cells on the surface of the chitosan microsphere showed different conditions: some were leaking intracellular material, some had already ruptured, leaving only the membrane. These results are consistent with the idea that Cs kills bacteria through bonding[64].

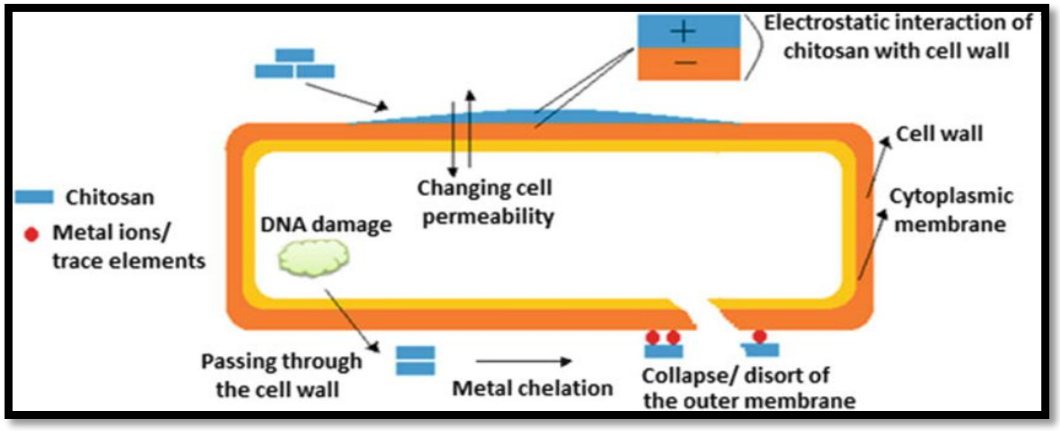

Figure(1-8) Antimicrobial Processes of Chitosan and Its Derivatives [64].

In terms of the zinc killing mechanism, ZnO-NPs have appealing antibacterial properties due to increased specific surface area with decreased particle size, which led to their effective use as an antibacterial through the production of ROS, which was a key factor for many mechanisms including cell wall damage due to local ZnO reaction, improved membrane permeability, NPs uptake due to loss of proton driving force, and adsorption of toxic dissolved zinc ions. As a result of oxidative stress, mitochondrial function was compromised, intracellular flow was disrupted, and gene expression was deregulated, resulting in cell growth suppression and death. Surface flaws on the ZnO abrasive surface texture have been linked to increased antibacterial activity in some circumstances. As illustrated in the illustration (1-9).

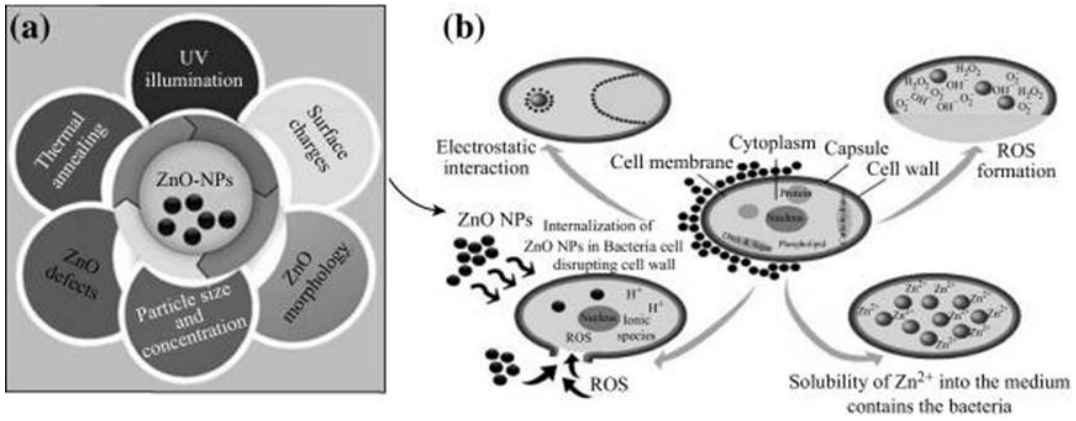

Figure(1-9) Correlation Between The an influence of Critical ZnO-NPs [65-66].

1.7 Previous Studies

1- To fabricate Ag nanoparticles, Yu-Hung Chen and Chen-Sheng used laser ablation method in 2002. Surfactants, SDS and CTAB were used to create highly distributed Ag particles. In SDS, particle diameters of 1.9–4.2 nm were generated using a laser intensity of 120 mJ/pulse, while in CTAB, particle diameters of 7.8–4.5 nm were produced using a laser intensity of 120 mJ/pulse. The anionic SDS and cationic CTAB are shown. The SDS-containing particles were stable for at least 1 month. Differences in laser power have been detected to influence particle size. Lower in SDS and CTAB, the 60 mJ/pulse laser intensity resulted in larger particle sizes of 6.8–2.7 nm and 9.4–5.9 nm, respectively [67].

2- Reza Zamiri el al. (2011) used a laser ablation method to generate silver nanoparticles (Ag NPs) with different amounts of aqueous chitosan solution. A nanosecond pulsed Nd:YAG laser was used to accomplish laminectomy, characterizing Ag NPs by transmission electron microscopy, UV-visible spectroscopy, and X-ray diffraction. The inclusion of chitosan enhanced the production efficiency as well as the stability of the

nanoparticles, according to the UV-visible absorption spectra. On the other hand, the decrease in nanoparticle size was more pronounced at higher chitosan concentration. Compared with distilled water, Ag NPs synthesized in chitosan aqueous solutions were more stable over a long period. He explained that chitosan is what protects the particles from agglomeration in the way that nitrogen atoms of amino groups in chitosan carry a free two-electron electron responsible for adsorption of NPs by a chelating mechanism [68].

3- M. Tajdidzadeh el al.(2014) studied the size, shape and stability of Ag-NPs. A Q-Switched Nd:YAG pulsed laser (wavelength = 532 nm, pulse energy = 360 mJ) was used to remove pure Ag plate for 30 min in order to create Ag-NPs in organic compounds such as ethylene glycol (EG) and biopolymers such as chitosan. . The media (EG, chitosan) allowed the production of well-dispersed NPs, with an average size of 22 nm in EG and 10 nm in chitosan in a spherical shape. NPs were compared to pure water in terms of particle size, shape, and stability. The stability of the samples was verified by analyzing the UV-visible absorption spectra after 1 month. The results showed that chitosan had higher NP formation efficiency than other media, and the NPs in chitosan solution were more stable than those in others after a month of storage, and because of its environmentally benign nature, this approach to synthesis of silver NPs can be considered a green method [69].

4- Yan Zhao et al. 2015 synthesized the core/shell Ag-ZnO nanostructure for the first time in liquid solution using a 248nm pulsed excimer laser. The thickness of the ZnO shell can be used to modulate the surface plasmon resonance absorption of core/shell Ag-ZnO nanostructures, which is in agreement with the limited difference in time-domain simulations. Moreover, compared to pure ZnO nanoparticles, the ultraviolet emission spectrum of the core/clamshell Ag-ZnO structures was stronger and turns blue [70].

5- The researcher Vu Khac Hoang Bui et al. 2017 made nanocomposites and combined them with chitosan to increase its antibacterial activity or reduce its effectiveness. It was shown that chitosan, due to its biological antimicrobial properties, is important in wound applications, but it loses its positive properties in alkaline media, so its properties must be modified by making it more complex by adding other metals and oxides to increase its effectiveness. It was considered that Ag NPs is one of these important elements or compounds, in addition to ZnO-TiO, and the effectiveness of chitosan increased in resisting bacteria [71].

6- S. Raj Kumar1 and P. Gopinath (2017) created Ag-ZnONPs as a biopolymer-encapsulated antimicrobial agent by coating chitosan (Cs) on silver zinc oxide nanocomposites using microwave-assisted site method. Field emission scanning electron microscopy (FE-SEM), X-ray diffraction (XRD), and Fourier transform infrared spectroscopy were used to examine the surface morphology, crystal structure, and functional groups of nanocomposites (FTIR). (MIC) and lowest killing concentration (MKC) of Cs-Ag-ZnO have superior efficacy against Gram-positive Staphylococcus aureus (S. aureus) and Gram-negative bacteria expressing recombinant green fluorescence protein (GFP) (E. coli). Further tests of the antibacterial activity of Cs-Ag-ZnO on live water demonstrated that the treatment inhibited bacterial growth with equal antibacterial efficiency. Cs-Ag-ZnO, had MKC values of 30 g/ml and 300 g/ml against S. aureus and GFP E. coli, respectively. Chitosan-coated Cs-Ag-ZnO had superior antibacterial activity than silver and zinc oxide-based nanocomposites, which are commonly employed as antibacterial agents [72].

7- The production, characterization, and antibacterial action of silver nanoparticles mediated by Allophylus serratus were described by Jemal, Kero, and others in 2017. Visual inspection confirmed the synthesis of silver nanoparticles: UV-Vis. spectrum, X-ray diffraction (XRD), Scanning

Electron Microscopy (SEM), Energy Dispersive Spectroscopy (EDS), and Fourier Transform Infrared Spectroscopy (FTIR) . The absorption spectra of produced silver nanoparticles from leaf and callus extracts revealed absorbance peak ranges of 440nm and 445nm, respectively, according to UV spectroscopy measurements. The X-RD pattern revealed crystalline, mostly spherical silver nanoparticles with sizes ranging from 42 to 50 nm in the sample . The XRD peaks 38.2°, 44.1°, 64.1, and 77°for leaf extract and 38.1°, 44.3°, 64.5°, 77.5°, and 81.33° for callus extract correspond to the planes of silver crystals (111), (200), (220), and (311) respectively and show that the silver nanoparticles are face-centered, cubic, and crystalline in nature. The existence of silver nanoparticles was also confirmed by SEM and EDS investigation. The FTIR data revealed the presence of biomolecules in extracts that act as reducing and capping agents in the production of silver nanoparticles. Silver nanoparticles were produced and tested for antibacterial efficacy against *Klebsiella pneumoniae* and *Pseudomonas aeruginosa* [73].

8- R. Kalaivani et al. (2018) UV–vis spectroscopy, fourier transform infrared spectroscopy, X-ray diffraction, and transmission electron microscopy were used to characterize chitosan-mediated silver nanoparticles (Ag NPs) . The inclusion of chitosan boosted the production efficiency of Ag NPs, according to the UV–visible absorption spectrum.Furthermore, at increasing chitosan concentrations, the size reduction of NPs was more noticeable. The XRD pattern revealed that Ag NPs are spherical and crystalline. The surface shape and size of the generated NPs were investigated using AFM and TEM images. The Ag NPs' size distribution and range were validated using a DLS picture. The antibacterial and antifungal properties of the produced Ag NPs were extremely strong. According to the study, crab waste could be a less expensive source of Ag NPs, which could be valuable in a variety of medical applications for biomedicine [74].

9- Mojgan Tajdidzadeh ,at el, (2019). describe the used of laser ablation in the natural polymer solution to manufacture zinc nanoparticles is described as a green method. The major goals are to use varying excision periods in a chitosan solution as a natural stabilizer for the polymer to lower the size of zinc nanoparticles and boost their stability. To excise the zinc plate immersed in the chitosan(Cs) solution from which the nanoparticles were formed, a pulsed Nd:YAG laser (532 nm) with a strength of 60 mJ/pulse and a pulse duration of 10 ns was utilized. At 5, 10, 15, and 30 minutes after ablation, the average particle sizes as well as the volumetric proportion of zinc nanoparticles in solution were determined, the particle size fell from 9.43 to 5.04 nm with spherical morphology, according to the findings. As the time of ablation progressed from 5 to 30 minutes, the fracture size grew from 0.24 to 8.5. Zinc nanoparticle stability and dispersion were also found to be substantially higher in chitosan(Cs) solution than in water. To compare the enthalpy of Zn-NPs in different media, the COSMO (conductor-like sorting model) solubility model was utilized. It was discovered that as the period of ablation increases, the size of Zn-NPs decreases .After six months of storage, it was shown that chitosan molecules are present, protecting Zn-NPs from aggregation and growth, proving that chitosan(Cs) solution is a superior environment for Zn-NPs than distilled water. Finally, the importance of the Zn and Zn spacing within similar particles when appearing in a solvent such as a natural material was proven by experimental results and theoretical modeling [75].

10- Ekaterina A. Gavrilenko et al(2019). They report on ZnO nanoparticles (NPs) created by a nanosecond pulsed laser (Nd:YAG, 1064 nm) through ablation of a metallic Zn target in water and air, as well as their comparison as prospective biological nanomaterials. The structure, content, shape, and flaws of the produced nanomaterials were all rigorously examined. It was discovered that the sample laser created in air contains some monoclinic

zinc hydroxynitrate in addition of the primary wuartzite ZnO phase, which is commonly prepared and reported by others. Both nanomaterials were then employed to modify biodegradable poly L-lactic acid wound dressings. The biomedical materials with bactericidal capabilities against *S. aureus and E. coli* bacteria were examined as-prepared model dressings. The advantages of air-prepared NPs over their water-generated counterparts are explored [76].

11- Sabah Alabbadi et al. 2020 developed chitosan nanocomposites with various weight ratios of silver and zinc oxide nanoparticles to improve antibacterial activity against Gram-positive and Gram-negative microorganisms. Because of the high antibacterial activity of the nanoparticles, all of the produced compounds displayed a spectrum of antibacterial behaviors, with the bi-metallic compounds showing a supporting antibacterial impact [77].

12- Ludmila Motelica 2020 and colleagues developed a biodegradable antimicrobial film that can be used for food packaging. By using a casting process, chitosan-based films were created as a biodegradable polymer with ZnO and Ag particles as filler/antimicrobial agents. To improve the antibacterial activity of the nanocomposites films, the nanoparticles were loaded with citronella essential oil Inhibition diameters of more than 30 mm for bacterial strains and more than 20 mm for fungal strains were found in tests on gram-positive, gram-negative, and fungal strains, indicating broad-spectrum antimicrobial action. By comparing antibacterial outcomes with plain Chitosan-ZnO,CEO or Chitosan-Ag,CEO films, the synergistic effect was demonstrated. according to the literature, are suitable for use as a fruit wrapper. When compared to the chitosan control membrane, the produced nanocomposites films had lower water vapor permeability values. SEM spectroscopy, fluorescence, visible

and ultraviolet spectroscopy, FTIR spectroscopy, microscopy, and thermal analysis were used to evaluate the samples [78].

13- Awwadc 2020, A.A. Menazeaa, b, Nasser S. A liquid pulsed laser (PLAL) was used to produce zinc oxide saturated with titanium dioxide (ZnO), which was then studied for its antibacterial properties. A different technique was used to verify the optical and morphological structure of the composite. The presence of TiO2doped ZnO was confirmed by FTIR analysis. The increased crystallinity of ZnO after doping with TiO_2 via PLAL technology was confirmed by XRD measurements. The optical conversion of TiO_2 doped ZnO was improved from 78.6 % to 92.3% . TEM images of ZnO revealed spherical, hexagonal or rectangular particles with clear rod-like shapes. The cell viability was also investigated for pure ZnO on paper and TiO2doped ZnO on paper. Pure ZnO had a cell viability of about 81.4 to 4.2%, but TiO_2 doped ZnO had a cell viability of about 91.6 to 5.1%. The antibacterial activity of the samples tested by MIC agreed that TiO2 fermented with ZnO raises the activity index. TiO_2 doped ZnO has been proposed for use in a variety of antibacterial applications [79].

14- R. B. Asamoah,et al . 2020 considered the antibacterial activity of two different nanocomposites, copper oxide with silver (CuO-Ag) and zinc. The following tests were carried out: XRD, XRF, TEM, UV-Vis spectroscopy, BET, and FTIR to examine the resulting particles. The compounds were found to have antimicrobial properties. Using the Kirby Power disc diffusion method and microdilution methods, the activity of the nanoparticles against Gram-negative and Gram-positive bacteria, Escherichia coli (ATCC25922) and Staphylococcus aureus (ATCC259233), was evaluated, respectively. CuO-Ag and ZnO-Ag had the same minimum inhibitory concentration (MIC) against E. coli and S. aureus in the Kirby-Bauer disc diffusion assay, which was 0.25 mg/mL. CuO-Ag has 98.8% and 98.7% efficiency over related Gram-positive and Gram-negative bacterial

species, respectively, while ZnO-Ag has 91.7% and 89.3 percent efficiency over related Gram-positive and Gram-negative bacterial species, according to the nanocomposites. Tested using precise dilution. presents a new method for analyzing each shape efficiency of transition metal-based nanocomposites in a relativistic manner [80]

15- Ke, Cai-Ling et al. 2021 by studying the properties of chitosan, its biocompatibility, biodegradability and non-toxic properties. Chitosan provides a broad spectrum antimicrobial. Patterns of antimicrobial action and factors associated with the antimicrobial effect of chitosan are discussed. the genetic response of microorganisms to chitosan, and applications of chitosan-based biomaterials, such as nanoparticles and membranes, have been described along with current clinical antibiotics or antifungal drugs [81].

16- Nasser S., et al.,(2021). Casting process was used to create a mixture of Chitosan-PVA embedded with varied ratios of gold/silver nanoparticles (Au NPs/AgNPs). Laser ablation was used to create gold and silver nanoparticles in a Chitosan-PVA blend solution. This environmentally friendly method for making metal nanoparticles provides a one-of-a-kind tool for nanofabrication. The large peaks at (407, 529) nm in the UV–Vis spectra of Chitosan-PVA doped with pure Ag NPs and Chitosan-PVA doped with pure Au NPs reveal the SPR peaks of Ag and Au NPs, respectively . The absence of distinctive peaks for the embedded NPs was confirmed by XRD, indicating that the produced NPs were dispersed uniformly and completely within the Chitosan-PVA matrix.The incorporation of Au NPs-Ag NPs in Chitosan-PVA matrix is confirmed by FT-IR data showing a decrease in the peaks of O–H stretching, N–H bending, and C–O stretching. The effective fabrication of AgAu NPs coreshell structure within Chitosan-PVA matrix is indicated by TEM pictures [82].

17- Avicenna, Syifa and others 2021 have used silver nanoparticles (Ag NPs) have been used in consumer products, cosmetics, and the food industry as an antibacterial agent. Using the pulse laser ablation synthesis approach, Ag NPs were generated in diverse mediums such as poly vinyl pyrrolidone (PVP), polyethylene glycol (PEG), and chitosan. A pulse Nd:YAG laser beam (1064 nm, 7 ns, 30 mJ) was directed and focussed on a silver metal plate set in a petri dish holding liquid media for 120 minutes using a silver mirror and a quartz lens with a focal length of 30 mm to make colloidal silver nanoparticles. All Ag NPs had a spherical form with poly disperse size in all mediums, including PVP, PEG, and chitosan, according to the findings . In PVP medium, the smallest Ag NPs, with an average size of 11.62 nm, were created. PVP is the suggested medium for creating Ag NPs with the best stability and the shortest size. Experiments with *Escherichia coli* and *Staphylococcus* aureus show that the produced silver nanoparticles have been successfully used as an antibacterial agent. The findings demonstrated that the synthesized silver nanoparticles were capable of completely eliminating bacteria in all media tested, including PVP, PEG, and chitosan, with a killing percentage ranging from 99.6 to 100 percent [83].

18- By using a laser ablation approach, Khaled A.Elsayed et al. 2022 ZnO-Ag colloidal bimetallic nanoparticles were created. UV-visible spectrophotometry, electron microscopy (SEM), energy-dispersive X-ray spectrometry(EDX),Raman spectroscopy, X-ray photoelectron spectroscopy (XPS), and photoluminescence were used to characterize the superimposed bimetallic nanoparticles (PL) . These tests validated the creation of the bimetallic nanocomposite and revealed that the synthesized bimetallic nanoparticles had a size distribution ranging from 30 to 130 nm. The anti-cancer activity was confirmed by assessing cancer cell cytotoxicity [84].

19- The biocompatibility and antibacterial activity of new zinc oxide (ZnO) nanoparticles (NPs) produced by Punica granatum peel and coffee ground extracts as the reducing and capping agents were studied by Hala M. Abdelmigid et al. 2022. Zinc acetate dihydrate and sodium hydroxide were used as reducing precursors to make chemically produced ZnO NPs. An ultraviolet-visible spectrophotometer (UV-VIS), X-ray diffraction (XRD), scanning electron microscope (SEM), transmission electron microscope (TEM), and Fourier transform infrared (FTIR) spectroscopy were all used to evaluate ZnO NPs. UV spectra for ZnO NPs PPE were 300 nm, 320 nm (ZnO NPs CE), 290 nm, and 440 nm (ZnO NPs), indicating ZnO NPs production. X-ray diffractograms confirmed their hexagonal shape. TEM images of biosynthesized ZnO NPs with particle diameters of 118.6 nm, 115.7 nm, and 111.2 nm, respectively, showed the hexagonal pattern and nanorod shape. FTIR analysis revealed the presence of proteins, carboxyl, and hydroxyl groups, which serve as reducing and stabilizing agents, on the surfaces of ZnO NPs. ZnO NPs is sensitive to *Staphylococcus aureus, Enterobacter aerogenes, Pseudomonas aeruginosa, and Klebsiella pneumoniae*. With IC50 values of 111, 103, and 93 g/mL, respectively, punica peel and coffee ground extracts are efficient reducing agents for the formation of green Zn ONPs and have less harmful effects on Vero cells than ZnO NPs [85].

20- This study was established by Sahar Naji Rashid et al. in 2022. Pulsed Liquid Laser Ablation (PLAL) can produce high purity nanoparticles. This method was used in this work to synthesize silver nanoparticles using an Nd:YAG laser with a wavelength (355 nm) and (532 nm) at energies (500) mJ and (600) mJ. Using UV-Vis, XRD, and SEM with EDX, AFM and FTIR analyses, the antibacterial activity of nanoparticles was evaluated against two Gram-positive bacteria (Staphylococcus aureus and Streptococcus mutans) and two Gram-negative bacteria (Escherichia coli"

Pseudomonas aeruginosa) isolated from the lumen of oral research revealed that PLAL-produced Ag NPs have antibacterial activity and can be used to combat both dangerous and harmful pathogens [86].

1.8 Aims of The study

1-Synthesis of (Cs-Ag-ZnO) nanocomposite by Pluse Laser Ablation method.

2-Studying the surface, structural and optical properties of this compound.

3-Application the nanocomposite as antibacterial on the *Klebsiella* bacteria and study the genetic effect.

2.1 Introduction

This chapter will cover knowledge of the structural properties of nanoparticles as determined by X-ray diffraction (XRD), UV_VIS spectroscopy, field emissionmhigh-resolution scanning electron microscopy (FE-SEM), transmission electron microscopy (TEM) and Fourier transform infrared spectroscopy (FTIR). As well as the optical properties of nanoparticles from the absorption coefficient and transmittance, as well as the direct and indirect energy gap. In addition to performing biological assays for bacteria such as spectrophotometer killing and inhibition tests, genome isolation and minimum inhibitory concentrations (MIC), examination of genes affected by nanomaterials.

2.2 Structural Properties

2.2.1 X-Ray Diffraction (XRD)

Under specific circumstances, X-ray diffraction examinations are utilized to ascertain the crystalline structure of the produced films. X-rays are electromagnetic waves with certain wavelengths that fall in the range between ultraviolet and gamma. In order to determine the crystal structure of the X-ray diffraction pattern that results from falling on the crystal, the English scientist W. Bragg devised a straightforward model. According to this theory, the crystal's various atomic levels allow for X-ray reflection [87]. Figure (2-1) depicts how X-rays are diffracted when they strike a crystal's surface. This diffraction is described by Bragg's Law by the following equation.

$$n\lambda = 2d_{hkl}\sin\theta.....(2-1)$$

Whereas:

n: an integer representing the order of interference θ: the angle of incidence of the X-rays.

λ: wavelength

d_{hkl}: distance between levels (hkl).

Only when the wavelength (λ) is less than or equal to twice the separation (d_{hkl}) between two subsequent levels in the crystal, as in the equation below, can the Barak diffraction condition become true:

$$\lambda \leq 2d_{hkl} \ldots\ldots\ldots\ldots\ldots \quad (2\text{-}2)$$

In order to achieve the bragg's condition and obtain the diffraction pattern of X-rays that complies with the law, a group of experimental methods were designed, such as Laue method, Rotating-Crystal method and Oscillating-Crystal method, and each of these methods is based on variables including The angle (θ) continuously or wavelength change (λ) by conducting a process of checking the composition of the material to know the nature of its crystal structure. When moving the sample at an angle (θ), the detector has moved at an angle (2θ), and therefore the angle written on the paper strip represents twice the angle in bragg's law on the condition that the X-rays are of single wavelength, so that the value of (d) can be calculated as in equation (2- 1) If (λ) and (θ) are known [88].

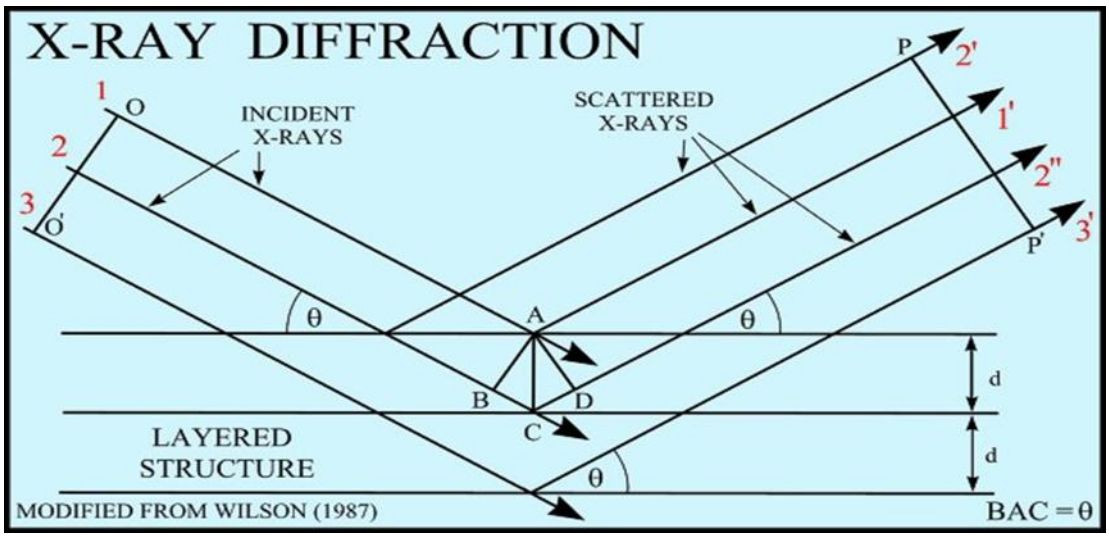

Figure (2-1) Bragg's diffraction

Using the Scherrers formula, the crystal size for each of the Bragg peaks is determined [89].

$$C.S = \frac{0.9\lambda}{B\cos\theta_B} \qquad (2\text{-}3)$$

Whereas

C.S : crystal size, β : maximum width at mid intensity (FWH M)

λ: The wavelength of the X-ray used (λ=0.15418nm) where (β =FWHM*π/180)

$\theta_{B:}$ diffraction angle.

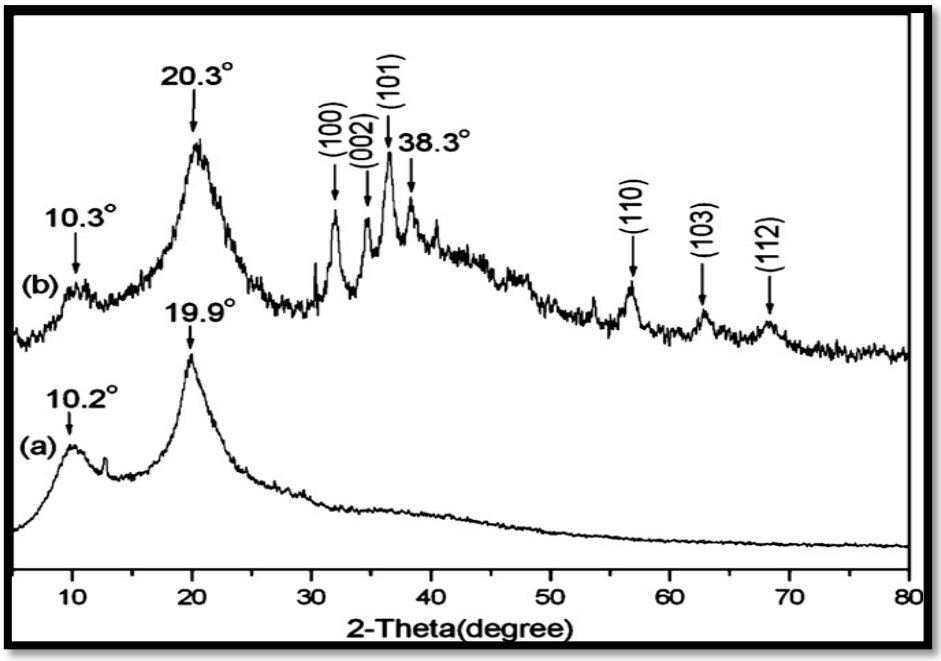

Figure 2-2 X-ray diffraction patterns of pure Cs film and Cs-Ag—ZnO blend films [35].

Using Figure. (2-2) X-ray diffraction patterns of the samples: (a) pure Cs film ,(b) Cs,Ag,ZnO blend The pure CS film (Figure. 2-2a) had two crystal forms, for *I* and form *II*, with respective significant crystalline peaks at 10.2° and 19.9° .However, doping Ag and ZnO had an impact on the two major Cs peaks at 10.3 and 20.3°. (Fig. 2-2b). This demonstrated that the normal structure of the polymer chains was disrupted by the presence of Ag and ZnO particles. In addition to the hexagonal zinc oxide (1 0 0), (0 0 2), (1 0 1), and (1 1 0), the diffraction pattern of the Cs-Ag-ZnO blend films revealed six additional peaks at 31.9°, 34.6°, 36.4°, 56.8°, 62.9° , and 68.2° that were attributed to the CS-Ag-ZnO blend films as can be seen in Figure1b, the peak at 38.3° showed the presence of additional of Ag. These findings showed that sol-cast transformation was used to make Ag and ZnO in mixed films [35].

2.2.2 FE-SEM Field Emission Scanning Electron Microscopy,

It is a method for viewing the molecular and nano world because the magnified images produced by using electrons rather than light waves have an extremely high resolution from the sample's surface and display details that are between one and five nanometers across. These electrons are produced by a field emission source that emits electrons in zigzag patterns while scanning the sample, causing the electrons to be freed and accelerate in the strong electric field gradient. Elemental electron columns in high vacuum are pinned by electron lenses to form a focused scanning beam that bombards the material. Secondary electrons are thus released from every area of the body. Because the energy of these secondary electrons is so low, only those produced at the sample's uppermost surfaces are released, while those produced in the deepest regions are quickly absorbed by the sample itself. Consequently, secondary electrons are highly surface-sensitive [90].

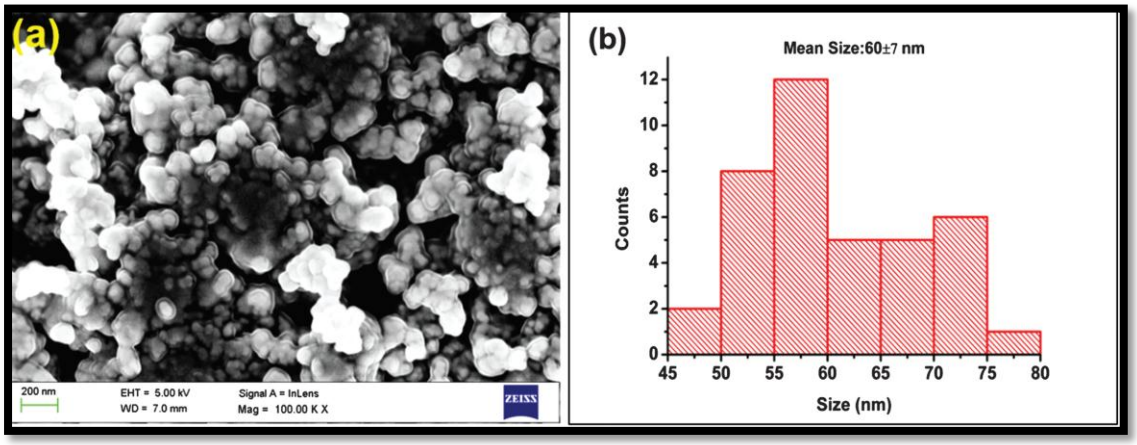

Figure (2-3) FESEM images of (a, b) Ag-ZnO NPs[72].

Using ImageJ software, the size of the nanocomposites was established by FESEM investigations to be 607 nm in diameter (in Fig. 2-3(b))[72].

2.2.3Transmission Electron Microscopes (TEM)

This type of microscopy sends a stream of electrons through an extremely thin specimen, interacting with the material along the way. The created powder was examined by Al-Sharif University in Iran using a TEM device of type JEOL 100 CX II (TEM) 100 kV, imaging with TEM.

As depicted in Figure (2-4). The interaction of the electrons moving through the substance results in an image. After being enlarged, the picture is subsequently focussed onto a fluorescent screen, a layer of photographic film, or a sensor like a CCD camera. Due to electrons' incredibly tiny de Broglie wavelength, extremely high resolution is possible.

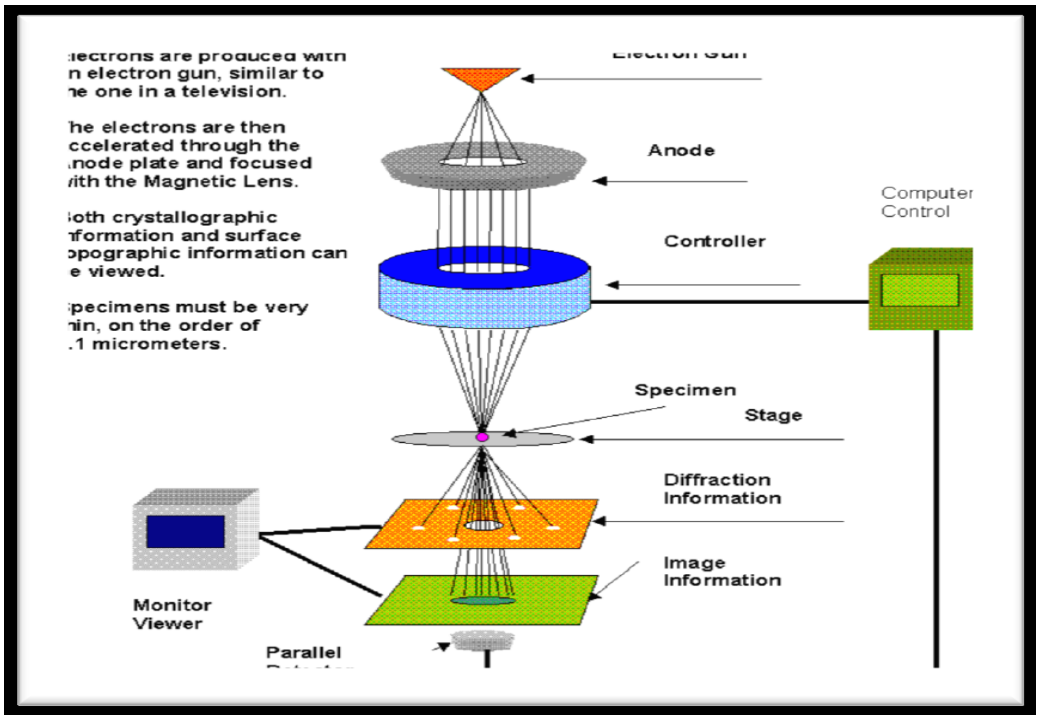

Figure (2-4) Transmission electron microscope schematic diagram (TEM) device in Al-Sharif University-IRAN

TEM picture shows films made in low light using a Cs-Ag-ZnO combination. Samples were coated on a copper TEM grid after being treated in 1 %acetic acid as part of the preparation process for TEM inspection . After being exposed to acetic acid, Cs and ZnO were dissolved. Ag NPs, which are tiny, granular, and have a uniform distribution, were the type of nanoparticles used as in Figure (2-5) Additionally, the usual particle size ranged from 10 to 20 nm [35].

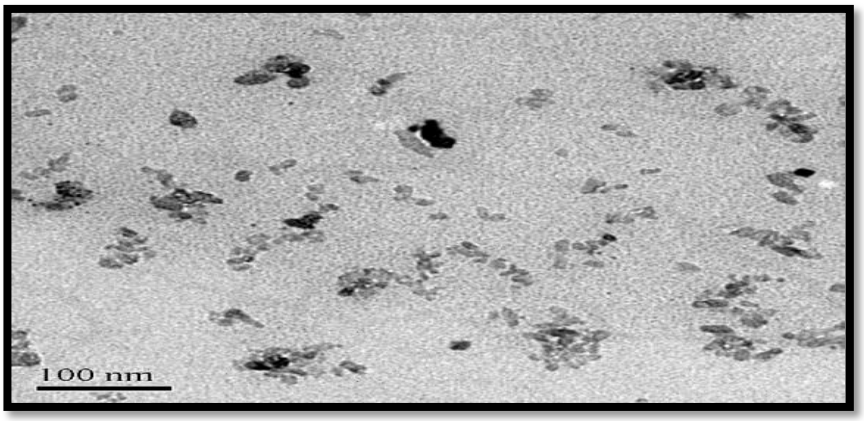

Figure (2-5) TEM picture of films containing 0.1 wt. Ag and 10 wt. Zno after being treated with an acid solution[35].

2.3 Optical Properties

The optical properties of solids are a critical tool for studying the energy bandgap, absorption coefficient as well as direct and indirect energy gap and other properties.

2.3.1Fundamental Absorption Edge

When the radiation energy absorbed is nearly equal to the energy gap, the absorption rate quickly increases. The energy difference between the highest point in the valance band and the lowest point in the conductive

band is the smallest at the absorption edge in crystalline materials. [91].

2.3.2Absorption Coefficient

The absorption coefficient is defined as the decrease in the flux of radiation energy or intensity with respect to a unit area in the direction of wave propagation within the medium, and it depends on the nature of the medium, the thickness of the film, and the absorbance of the film material for the incident rays. Through the absorption coefficient, it is possible to identify the nature of the electronic transitions. If the value of (α) is greater than (10^4 cm^{-1}), this means that direct electronic transitions occur between the valence and conduction bands, but if (α) is less than ($10^4 cm^{-1}$), this means the occurrence of Indirect electronic transmissions. In his law of radiation absorption, Lambert described the relationship between the intensity of incident radiation (I_o) and the intensity of transmitted radiation (I). in the following form [92].

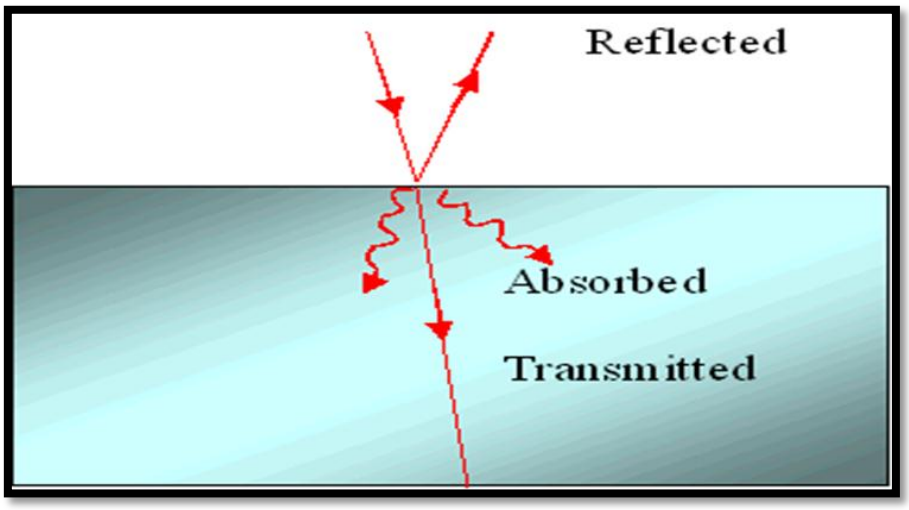

Figure (2-6) Absorption diagram .

$I=Io \exp(-\alpha ct)$ …. (2-4)

I Intensity of transmitted light

Io Intensity of incident light

c Concentration of solution(M)

t cortical path length

(α) Molar absorption coefficient is measured in units(Mcm^{-1})

And by solve the equation(2-4) We get

$\alpha t = 2.303 \text{ Log } (Io / I) /c$ …. (2-5)

Log (Io/It) stood for (A) If the light's frequency resonates with the transition frequencies of the atoms in the medium, thin film absorption will happen during the light's propagation. In this instance, the beam will weaken as it travels[93]. As only unabsorbed light will be transmitted, the medium's transmission and absorption are clearly connected . Numerous optical materials are colored as a result of selective absorption. The intensity of the falling radiation decreases exponentially ($e^{-t\alpha}$) during the material. The absorption coefficient is dependent on the incident photon's energy as well as the absorption coefficient, type of electronic transitions, and energy gap of the semiconductor [94-95]. The relationship shown below can be used to get the absorption coefficient.

$\alpha=2.303(A\backslash ct)$ ----------(2-6)

The practical results show the absorption of (α) can be described the nanocomposite Cs-Ag-Zn NPs as in Figure (2-7).

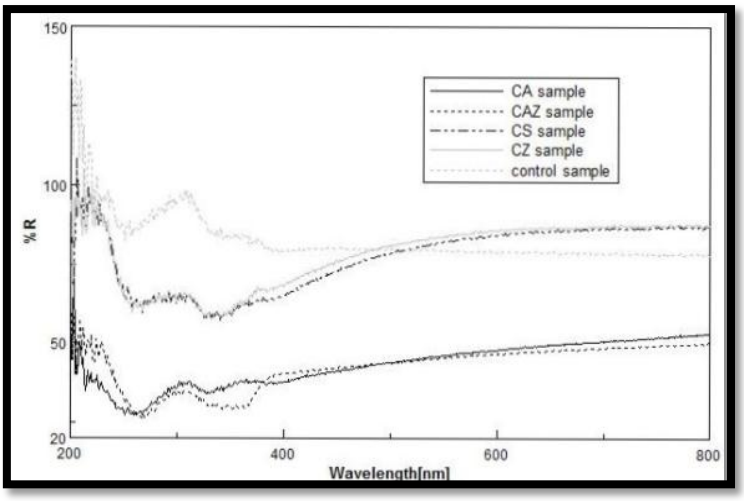

Figure (2-7) UV–vis spectra of the samples[10].

The following samples were subjected to treatment: the untreated sample, the treated samples with (Cs-Ag,- ZnO) \(Cs-Ag) \ (Cs-Zn) and chitosan [10]. Additionally, research is being done on using FTIR to pinpoint the functional groups in the nanocomposite C-Ag-Zno NPs.

2.3.3FTIR Fourier Transform Infrared Spectrometer

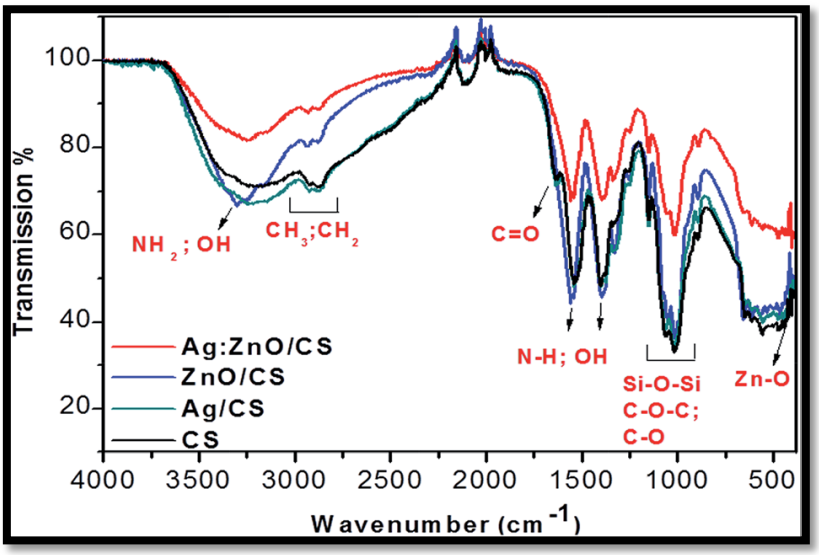

Figure (2-8) FTIR spectra of (Cs- ZnO), (Cs-Ag-ZnO), (Ag-Cs) films [34]

Chitosan's FTIR spectrum shows distinct bands at 3303 cm^{-1} which are attributed to the stretching vibrations peaks of the -NH2 and -OH groups, the absorption peaks at 1627 cm−1 are attributed to the bending vibration of the NH2 group and the stretching vibrations to the absorption band at 2926 cm^{-1} and 2856cm^{-1} , which is attributed to the asymmetric stretching of -CH3 and -CH2, and sources the bands at 13933 cm^{-1} and 10099 cm^{-1} , respectively. Si-O groups overlap. -Si and -C-O-C is mostly the reason for the high density of chitosan at 11000-1000 cm-1. The literature has already demonstrated that for these overlapping bands in the FTIR spectrum of Cs- Ag-ZnO, the bending vibration of the OH group and the bending vibration of the amino group were present at 1538 cm^{-1} .In general, the spectra of the studied samples can be observed superimposed for the Cs-Ag-ZnO and Cs-ZnO samples in the range 33000-3500 cm-1. The slight shift in these peaks indicates larger wave numbers and strong ZnO bonding to the hydroxyl, amino and amide groups of chitosan molecules [34].

2.3.4 Transmittance

The ratio (I/I°) is known as transmittance (T), which is the proportion of an incident light ray's intensity to a transmitted light ray's intensity , and it is given by the following relationship:

$$T=I/I_0 = e^{(-\alpha t)} \quad \text{.....(2-7)}$$

where (t) is the thickness of the material (cm) and (α)absorption coefficient cm^{-1}

Reflectivity (R) and absorbance (A) are related to the law of conservation of momentum and energy according to equation[96]:

$$T+A=1 \quad \text{.....(2-8)}$$

2.3.5 Optical Transitions

Depending on where the highest point is located at the top of the valence band and the lowest point is located at the bottom of the conduction band, semiconductors can undergo either direct or indirect electronic transitions [97].

2.3.5.1Direct Transitions

When the wave vector ($\vec{k}$) for the position of the bottom of the conduction beam and the position of the top of the valence band are equal, or when ($\Delta\vec{k} = 0$), a direct transition takes place. Momentum and energy are conserved throughout this transition, which is followed by an interaction between the incident photon and the valence band electron. During the ensuing partnership:

$$E_f - E_i = h\nu \quad \text{……(2-9)}$$

$$\Delta\vec{k} = 0 \quad \text{……..(2-10)}$$

whereas-:

The electron's initial and final energies in the valence and conduction bands, respectively, are denoted by the letters Ei,Ef .

This form of transition is known as an Allowed Direct Transition(ADT) and occurs in this type of semiconductor[98]. The absorption equation is given by the following relationship:

$$\alpha h\nu = A(h\nu - Eg)^r \quad \text{……(2-11)}$$

A: a constant that depends on the nature of the substance.

Eg: the energy gap.

According to the kind of electronic transitions that cause the optical absorption, the constant r has the values (3, 2) for an exponential coefficient.

r = 1/2 and r = 3/2 In the case of the allowed direct and forbidden direct transition respectively.

Where both transitions are not dependent on temperature.

2.3.5.2 Indirect Transitions

The indirect electronic transitions occur when there is a mismatch between the energies of the top of the valence band and the bottom of the conduction beam in the space of the wave vector (k), where the transition from the highest point of the valence beam to the lowest point of the conduction beam is in a non-vertical way. ($\Delta K \neq 0$) This transition is accompanied by a change in the crystal's momentum, and in order to achieve the law of conservation of energy and momentum, this change in momentum is compensated by the lattice either by phonon absorption or emission. The absorption equation for this type of semiconductor is given by the following relationship:

$$\alpha h\nu = A\,(h\nu - E_g \pm E_p)^r \quad \ldots\ldots\ldots\ldots \quad (2\text{-}12)$$

A: a constant that depends on the nature of the material

Ep: phonon energy .

The (+) sign means phonon emission

The sign (-) means phonon absorption

r: Exponential modulus.

These transfers also come in two varieties. When indirect transmission occurs, which is permitted, r = 2)). And in the case of banned indirect transmission, r = 3). In contrast to direct transitions, the emission or absorption process in these transitions is temperature dependent [99].

As a result, the energy difference between the lower part of the conduction band and the upper part of the valence band can be used to define the phrase band gap. Another definition of it is the energy required to excite (transfer) electrons from the top of the valence band to the bottom of the conduction band [100].

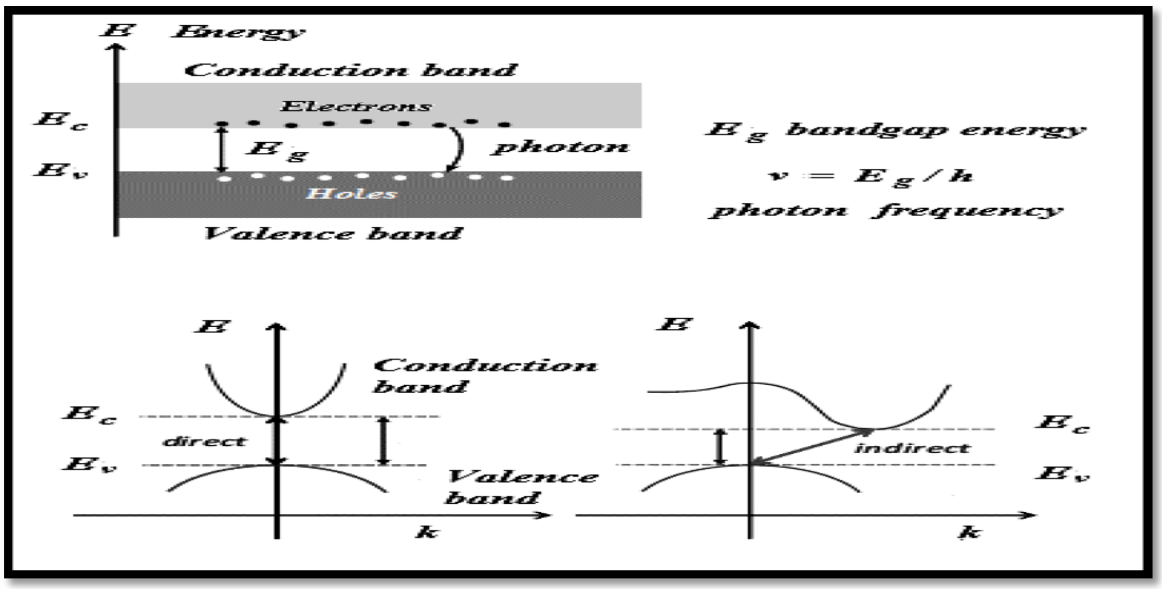

Figure (2-9) illustrates the energy gap and its types[101].

2.4 Biological part

As will be shown in the third chapter, bacteria acquired from patients are activated in the labs of the College of Sciences for Women in order to suppress the bacteria using nanocomposites

(Cs-Ag-Zn)\(Cs-Ag) and (Cs-Zn) and a chitosan polymer solution for comparison.

2.4.1 Minimum Inhibitory Concentrations (MICs)

After the kill rate is measured in millimeters, the Minimum Dilution Percentage (MDC) is determined. As the (gold standard) for detecting an organism's susceptibility to antibiotic resistance, minimum inhibitory concentrations (MICs) are used to evaluate the efficacy of all other susceptibility testing techniques. When disc diffusion techniques are ineffective or exceptional resistance cannot be ruled out by other testing methods, diagnostic laboratories use MICs to provide a critical response[127] .

2.4.2 Measuring The minimal Bactericidal Concentration (MBC)

The minimum bactericidal concentration was determined using all tubes that showed no growth to determine the lowest concentration of antibody used (MBC) and the lowest concentration that showed growth in the MIC assay for all samples. Bacteria were cultured from the MIC test plate on freshly produced solid feed agar plates by leaving lines on the agar surface. Plates were incubated at 37°C for 24 h. Using plates that showed no growth, the MBC of applied nanoparticles was calculated[127].

2.4.3 Extraction of Genomic DNA

Using Favrogen genomic kits, genomic DNA was isolated from the bacteria that had been collected in nutrient broth tubes and incubated for 24 hours before being frozen samples. DNA isolation required a 14-stage process using salting-out procedures [127].

2.4.4 Estimation of DNA Concentration and Purity

The affinity and straightness of the separated DNA were then verified using agarose gel electrophoresis after extraction of 1.5 percent of genomic DNA with agarose at 100 V for 10 min. from Sambrook & Maniatis, in 1989.

2.4.5 PCR Technique

In this study PCR, including conventional PCR, were used to identify mutant genes. The Bioneer (Korea) Organization provided the primers, which were then lyophilized as a result of various picomol fixations. After being lyophilized, the preparatory material was disintegrated in free DNase/RNase water to yield a final concentration of 100 pmol/l "and held as a stock at -20 C". This allowed for the preparation of a 10" M" concentration as the work primer.

2.4.6 Gene Detection Process

The pathogenic *Klebsiella* bacteria, which are Gram-negative, bacilli, and non-motile, are responsible for a number of illnesses, including pneumonia, urinary tract infection, bacteremia, and burns, as we described in the first chapter [102].

Klebsiella bacteria possess a number of genes, and the functional DNA units that make up the bacterial genes act through a diffusible byproduct. An RNA molecule may be the end result, or the effect can be achieved by translating intermediate RNA into a protein. Phenotype, which is an obvious aspect of an organism, is where the effect of a gene appears. Usually, the names of bacterial genes correspond to their phenotypes. Although mutations in the DNA sequence can be silent (they have no effect on the phenotype), they often result in altered traits. This set of

genes is responsible for bacterial virulence, pathogenicity, and antibiotic resistance [103]. Several virulence genes present in K. pneumoniae also contribute to its ability to spread disease. These genes were examined by PCR. In this study, we selected five types of genes important in the survival and resistance of bacteria to antibiotics. The first type is the gene responsible for the formation of adhesive *(fimH-1*). Type 2 is responsible for the outer membrane lipoprotein *(ycfM).* The third type, Enterobactin *(entB).* The fourth type is an iron transporter *(KFU*) with phosphotransferase function, and the last type is a mucosal phenotype regulator *(rmpA*) [104,105,106,107,108]. According to the following Table (2-1)

Table(2-1) Shows some genes of the *Klebsiella pneumoniae* bacteria selected in the study.

Gene	Forward	**Reverse**	**bp.**
Fimh1 type-1 (fimH-1) adhesin	GCTGAACGCCTATCCCCTGC	ATGAACGCCTGGTCCTTTGC	688
Ycfm outer membrane lipoprotein	CTTCTCCAGCATTCAGCG	ATCAGCAGTCGGGTCAGC	160
entB enterobactin	AGCATCGGTGGCGGTGGTCA	ATTTCCTCAACTTCTGGGGC	371
Kfu iron transporter with phosphotransferase function	TTT CGT GTG GCC AGT GAC TC	GAA GTG ACG CTG TTT CTG GC	797
rpmA regulator of mucoid phenotype A	CTTGCATGAGCCATCTTTCA	ACTGGGCTACCTCTGCTTCA	535

And figure(2-10) illustrating Safered-stained agarose gel electrophoresis of monoplex PCR. amplified products from extracted total DNA of *Klebsiella pneumoniae*. lane: (1 to 32 isolates) amplified with diagnostic *fimH-1* gene, show positive results at 688 bp. The electrophoresis was performed at 80 volt for 95 min [109].

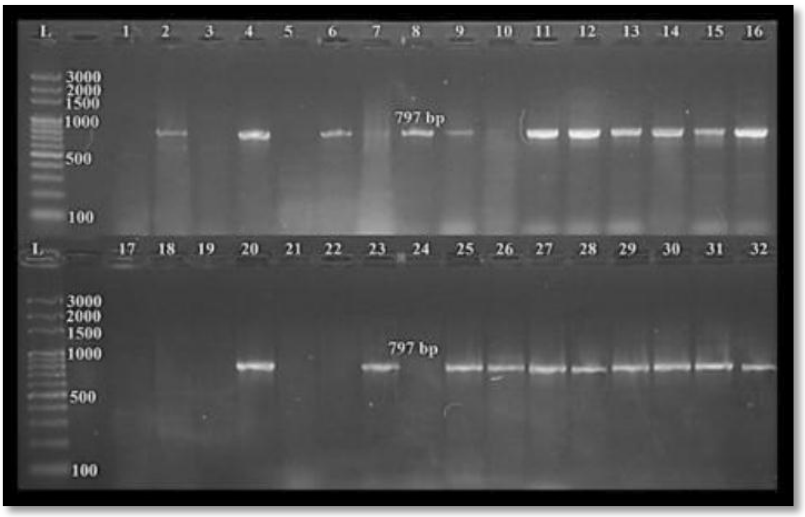

Figure(2-10) illustrating Safered-stained agarose gel electrophoresis of monoplex PCR[109].

3.1 Introduction:

The instruments, materials, and tools that were utilized to manufacture the triple nano composites of chitosan, silver, and zinc as well as the nanocomposites of each of silver, chitosan, and zinc are included in this chapter as the practical portion of the study. Along with conducting biological tests for bacteria such as killing and inhibition tests, DNA assays, and examination of genes affected by nano composites, laboratory tests also include the use of the UV-Vis spectroscopy, XRD system, FTIR, field emission scanning electron microscope (FE-SEM), and Transmission Electron Microscopes (TEM) to make structural and optical measurements In addition to measuring the percentage of killing and inhibition using a spectrophotometer, examining DNA using the Nano Drop device, and knowing the effect of the studied genes when using nanocomposites.

3.2 Instruments:

This section will explain the most important instruments that were used in the practical part of this study as in table (3-1).

Table (3-1) Used devices

No.	Instrument	Origins
1.	Sensitive scale	Germany
2.	Hood	Turkey
3.	Nd:YAQ Laser	Germany
4.	FTIR	Germany
5.	X-ray Diffraction	USA
6.	UV- Spectrophotometer	England
7.	Transmission Electron Microscopes (TEM)	Germany
8.	Incubator	Germany
9.	Nano drop device2000(measure the concentration of nucleic acid (DNA, RNA) and proteins from different spacemen's)	USA
10.	Refrigerator	Ishtar/Iraq
11.	Ultraviolet light transilluminator	UK
12.	Microwave oven	USA
13.	Spectrophotometer(mic)	Japan
14.	Horizontal electrophoresis unit	France

15.	Uv cabinet (PCR, Preparation and sterilization with uv) Cooling centrifuge 5424r (cooling centrifuge for Eppendorf tube using for spacemen which effected with temperature)	UK
16.	Centrifuge (Eppendorf tube using for spacemen which effected with temperature)	Germany
17.	Quantum Vilber Lambert (Gel documentation, for detect the fluorescent dye on spacemen like agarose, cellulose papers, animal tissues … etc.)	France

3.3 Material:

In This study will clarify the most important materials that were used in the practical part of this study.

Table 3-2 Used Materials

No.	Materials	Origins
1.	Chitosan polymer powder	commercial
2.	silver plate	commercial
3.	Zinc plate	commercial
4.	distilled water	Labs of the College of Sciences for women
5.	Acetic acid	Labs of the College of Sciences for women
6.	alcohol	commercial
7.	Mueller Hinton Agar	England
8.	Nutrient agar media	England
9.	Nutrient agar, MacConkey	Himedia
10.	Agarose	Canada
11.	DNA loading dye	USA
12.	DNA ladder marker (100&500bp)	UK
13.	Primers	USA
14.	Isopropanol	England
15.	Promega DNA purification kit	USA
16.	Nuclease-Free Water	USA
18.	Master mix	UK

3.4 Tools:

This study will explain the most important tools that were used in the practical part of this study

Table 3-3 Used Tools

No.	Tools
1.	agricultural dishes
2.	Small tubes
3.	Swab
4.	Big tube
5.	beaker
6.	Quartz cells
7.	Cotton
8.	Micro Pipette
9.	holder
10.	Heater
11.	Sensitive balance
12.	Micropipettes 5 -50 µl, 100-1000 µl , 0.5 – 10 µl
13.	PCR Tubes

3.5 Work Diagram

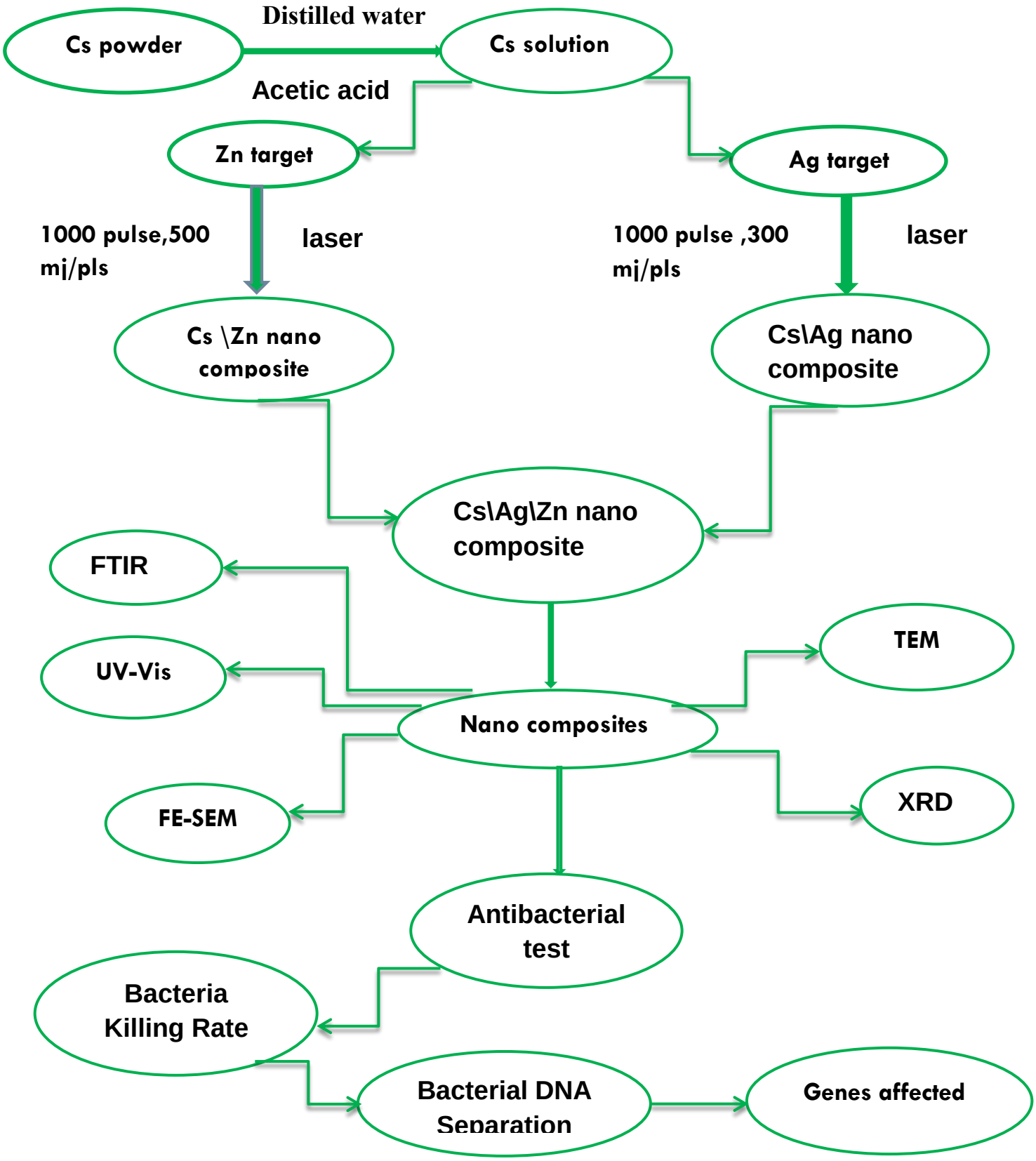

3.6 Laser Ablation System Used in The Experiment

Figure (3-1) shows a pulsed laser device for ablation of colloidal nanoparticles of a solid target immersed in different solutions. It consists of a Q-Switch Nd:YAG pulsed laser source of wavelength (1064nm), with second harmonic generation 532nm, and third harmonic generation 355nm.

Figure(3-1) Q-switch Nd-YAG laser.

Table (3-4) shows the main parameters of the Q-Switch Nd:YAG laser used in the research.

wave length	1064 nm
Energy Per Pulse	(300–500) mJ
Frequency	(6) HZ
number of pulses	(1000) Pulses
Pulse Duration	10 n sec
ambient temperature	(5 – 40) °C
diffraction	0.1 m rad
beam diameter	3 mm

3.6.1 Nano Composites Preparation

Chitosan polymer powder with a molecular weight of 1500 g/mol. To make the chitosan solution, use 2 grams of the powder, 287.5 milliliters of distilled water, and 32.5 milliliters of concentrated acetic acid. Nd: YAG laser is used by PLAL as the source for the ablation process. A convex lens with a focal length of 10 cm was employed to focus the laser beam such that it was perpendicular to the silver and zinc plate.

The Nd: YAG laser was used to bombard a high purity (99.99 percent) silver plate that was submerged in 2 ml of chitosan solution. The laser pulses had an energy of 300 mJ per pulse, 1000 pulses per second, and a wavelength of 1064 nm. In order to create the (chitosan-Ag-Zn) nanocomposite, we first raised the silver plate, dipped a high purity zinc plate (99.99 percent) in the chitosan/silver solution, then bombed it with the same laser parameters as the silver plate but at a higher energy of 500 mJ/pulse. For silver and zinc plates separately, the same procedure was used for chitosan/silver solutions and chitosan/zinc solutions as shown in Figure (3-1). In order to conduct the FE-SEM and XRD investigations, the final compounds, (chitosan-silver)\ (chitosan-zinc) and (chitosan-Ag-Zn) solutions, were deposited separately on three aluminum plates in a drop-by-drop fashion.

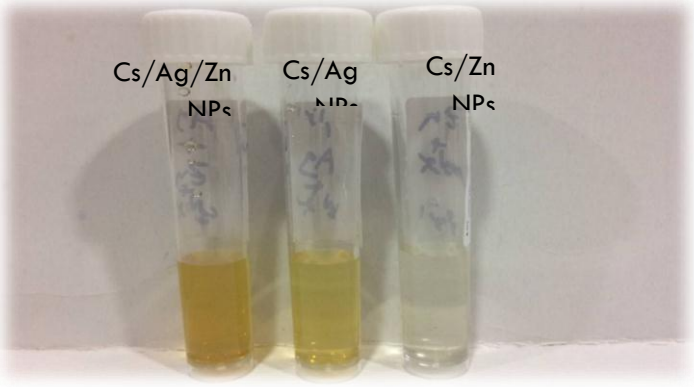

Figure (3-2) The obtained nanocomposites

3.7 Optical Instruments

3.7.1 Absorption Spectrum Measurement (UV-Visible)

Spectrophotometer From the near infrared to the ultraviolet, this spectrometer operates over a large portion of the electromagnetic spectrum. There are two major irritants in this device:

1- Deuterium lamp No. 1 (190 -360 nm).

2- Tungsten lamps (360-1100 nm).

The spectra of tungsten lamps were measured at room temperature in a CECIL CE 7200, and these cells are made of quartz in England. The test was carried out in the College of Sciences for Women .Advanced Laser Laboratory, and this college is one of the colleges affiliated with the University of Babylon, as shown in Figure (3.2).

Figure (3.3)UV- Spectrophotometer

3.7.2 FTIR Fourier Transform Infrared Spectrometer

As shown in the Figure(3-4), this apparatus was developed in Germany and is used to assess the mixture of chemical and functional linkages in the materials examined using analytical spectroscopy (FTIR). By adding a few drips to the (model: ALPHAB). The equipment was at room temperature. The work was done at the Advanced Physics Laboratory/College of Science for woman and the Laser Physics Department/University of Babylon.

Figure (3.4) Fourier Transform Infrared Spectrometer FTIR

3.8 Structural Morphology

3.8.1 Field Emission-Scanning Electron Microscopy (FE-SEM)

It is a kind of electron microscope that uses an electron beam to scan a sample rather than light waves to produce images of the material. These electrons are produced by a field emission source (an electronic canon), and as the sample is scanned in zigzag patterns, they are propelled by a strong electric field gradient. Electronic lenses fix the high vacuum columns of initial electrons to prepare the

narrow scanning beam that bombards the material. As a result, secondary electrons and back-scattered electrons are produced throughout the body, with the deep region producing the majority of them due to their low energy. Because the secondary electrons are quickly absorbed by the surfaces, they are very sensitive to those surfaces.

1640 HITACHI business Japan), in which the detectors of this apparatus take in the released electrons and transform them into an optical image that can be imaged. viewed on a screen or in a digital image, creating a three-dimensional appearance.

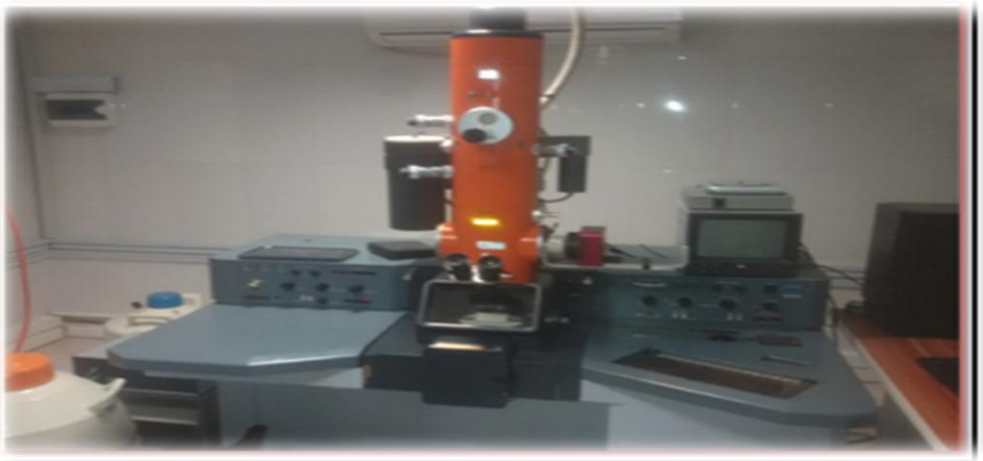

Figure. (3-5) image of a high-resolution scanning electron microscope.

3.8.2 X-ray Diffraction Measurement (XRD)

X-ray diffraction measurements to reveal crystal size, lattice modulus, and chemical composition for diffraction. The device's form is depicted in the Figure (3-5). A machine of the kind (ADX 2700 Powder Diffraction) Made in the USA was used for the test.

Figure (3.6) X-ray diffraction measurement

3.9 Preparation of Bacteria Samples

Here, we'll go through how to make a carrier and preservation media for bacteria as well as a nutrient medium for them.

3.9.1 Preparation of the nutrient Medium

19 gm of Nutrient Agar powder was dissolved in 250 ml of distilled water and 19 gm of Mueller Hinton Agar in 250 ml of distilled water the solutions were then placed in glass vials and mixed well until homogeneous before being heated on a hot plate (heater) until The melting is complete and the substance reaches the boiling point, at which time it is sterilized in an autoclave at 121 ° C for 21 minutes. After the sterilization process is completed, the solution is left until it cools down and then poured into plastic dishes, where the pouring process is carried out in the hood device so that no pollution occurs, then the dishes are placed in the refrigerator and become ready for use.

3.9.2 Bacteria Transport and Preservation

Patients with lung infections being treated at Hillah Surgical Hospital had bacteria that caused *Klebsiella pneumoniae* infections; samples were taken from these patients, containing a carrier medium (transport swab) to ensure sample safety, and the samples were then transferred to the college laboratories. The bacteria were cultivated in a nutrient medium for the purposes of isolation and identification. They were then kept sterile for 24 hours in the incubator at a temperature of 37°C before being cultivated in nutrient solution. To accomplish this, a smear is removed from the bacterial culture's surface using a loop, and the dishes are then placed in an incubator set to a low temperature. It was prepared for the experiments after being grown and inhibited at a temperature of 37 °C for 24 hours.

In order to know the ability and effectiveness of bacteria, the following was used:

1. Nutrient Agar Medium (Oxoid-UK)

for the isolation, cultivation, and preservation of bacterial strains.

2. Average MacConkey agar (Mast-UK)

to isolate gram-negative bacilli and distinguish fermented lactose from non-lactose-fermented bacteria.

3. Simmons' Citrate Broker (Oxoid -UK)

This method was used to discover the bacterial ability to deplete citrate as the sole carbon source.

4: Christensen Urea Intermediate (Biolev-Italy)

(MR-VP) Medium (Oxoid-UK)

Following the manufacturer's instructions, the basal medium was made, sterilized at 121 °C for 15 minutes, cooled to 50 °C, and then mixed with 50 mL of 20 percent urea to make one liter of media (50 mL of urea to 950 mL of medium). They had a pH of 6.8 to 6.9 to by virtue of this medium and a sterile solution from

Mast-UK. This technique was used to determine bacteria's ability to produce urea enzyme.

This method was used to detect the bacteria's ability to complete and perform a partial glucose analysis.

6-Peptone Water Media (Mast-UK)

This medium was used to detect the ability of bacteria to produce Indole

7. Normal movement

This medium was prepared with a supply (0.4 g) of nutrient agar to nutrient broth, then dispensed into tubes, sterilized at (121 °C/for 15 min), and used to detect bacterial motility.

8. Kligler Iron Agar Medium (Biolife - Italy)

This method was used to detect the ability of bacteria to produce (H_2O) and fermentable sugars with acids and gas production.

9. Medium agar gelatin.

The 4.4 g of gelatin (Oxiod-U.K. Company) was added to the nutritional agar medium to create this medium. It was used to check whether certain bacteria could produce hydrated gelatin.

10.Eosin methylene blue medium.

This medium was used for a specific cultivation (*Klebsiella*), which produced the special color "green metallic luster.

11. Mueller-Hinton-Agar

The Muller Hintonn agar medium was prepared according to the manufacturing company, sterilized at 121C° for 15 min, then cooled to 50 C°. This medium was used to detect the" antibacterial activity of" (Cs- Ag-Zn) nanomateria.

3.9.3 Reagents and Solutions:

1-Methyl red dye

0.1 g of methyl red dye reagent is dissolved in 300 ml of 95% ethyl alcohol, bringing the volume to 500 ml with water, and using this indicator of complete glycolysis, the reagent is prepared.

2- Voges- Proskauer reagent

It contained the following ingredients:

a) α-naphtho l; It was made by combining α -naphthol and 100ml of 100% ethyl alcohol .

b) (sodium hydroxide solution, sodium hydroxide solution); It was prepared by combining 40 g of NaOH and 100 ml of distilled water; It is used for partial glucose analysis.

3-Kovac

This reagent was made by mixing 5 g of (dimethylamine benzyl aldehyde) with 35 ml of concentrated hydrochloric acid and 75 ml of amyl alcohol. This reagent was used for the determination of indole.

4- Catalase

This reagent, which was made with H_2O_2 as a diluent and kept in a darkened bottle to analyze the bacterial ability to produce catalase, was at a concentration of 30 percent.

5-oxidase

Tetra- Methyl- Phenylene- Diamine- Dihydrochloride, 1 g, was dissolved in 100 mL of distilled water to create this reagent.

6-Frazier

The preparation of this reagent involved dissolving 5 gm of HgCl2 in 20 ml of strong HCL (98%) and 100 ml of distill water. It was utilized to find out whether bacteria could analyze gelatin.

7-Iodine solution

To make this reagent, 6 gm of iodine crystals and 5 gm of potassium iodine were dissolved in 20 ml of distillate water, and the solution was heated and stirred to dissolve the crystals. Before cultivation, 0.2 ml from this solution was added to every 10 ml of tetrathionate broth medium.

8- Dilution Solution

PSS was created by dissolving 99 gm of NaCl in 1000 ml of distill water, distributing it in tubes, and autoclaving it at 121°C for 15 minutes. It was then used for direct stool specimen analysis, isolation, and as a diluent.

9-Gramm stain alternativess

The solutions were created using the necessary microbiological techniques .

10-Methyl violet solution

This solution was prepared by dissolving 0.5 g of methyl violet in 100 mL of distilled water.

11-Iodine solution.

To make this solution, 20 ml of distilled water was used to dissolve 1 g of crushed iodine crystals and 2 g of potassium iodine (KI), which were then combined to make 100 ml and stored in a dark bottle. The working solution was created by mixing 1 ml of this solution with 5 ml of distilled water.

12-Color remover solution

Acetone was used as a decolorizer at a concentration of 95%.

13- Safranin elixir

Making this solution involves dissolving 0.5 grams of saffron tincture in 10 ml of alcohol, then adding 100 ml of distilled water and storing the concoction in a dark bottle.

3.9.4 Biochemical Tests

a. the oxidase test

Selected bacterial colonies were used to line the lines of nutrient agar medium, which were then incubated at 37 degrees Celsius for 24 hours. When colonies were stained violet, a few drops of monoamine oxidase reagent were added to the expanding colonies. The result was satisfactory .

b. Catalase Test

When lining the "nutrient agar medium with selectedd bacterial coloniess that have been incubatedd for 24 hours at 37 degrees Celsius, then transfer the ring "growth yield to a clean slide and add one "drop of sample solution (30 percent water). When gas bubbles materialize, the outcome is favorable .

c. Test for Indole Production

Bacterial colonies that were" incubatedd for 24 hours at 37 degrees Celsius were selected and then cultured in tubes containing peptone water. Then Kovac reagent was added in a few drops. The arrival of the pink ring color indicated a successful outcome.

d. Methyl red assay

The selected bacterial colonies were grown in tubes containing "MR-VP (MR-VP broth) and incubatedd at 37 degrees Celsius for 24 hourss. "Five drops of methyl red reagent were then addedd to read the result. A positive result and a comprehensive glucose analysis were indicated by the appearance and observation of a red hue.

e. the Voges-Proskauer test

The particular bacterial culture was seeded into the tubes containing the "(MR-VP broth), which were then incubatedd at 37 degrees Celsius for 48 hours. After 15 minutes, the result was read by adding (0.6m ml of -naphthol reagent) and (0.2 ml of 400 percent NaOH solution). Positive outcome brought about by glucose's incomplete analysis, which yields acetone or (acetyl "methyly-carbinol) .

f-Test for hydrogen sulfide production.

The tubes that contained a slant of (Kligler iron agar medium) were seeded with the specific bacterial culture by sticking to the bottom of the medium & striking on the slant, incubating it at (37 degrees Celsius) for (24 hours.) Then read "the result. The" result appears once in black, which means a positive result.

h. Urease manufacturing

The particular bacterial culture was seeded into the tubes that had a slant of urea agar, and the tubes were then incubated for 24 hours at 37 degrees Celsius. then review the outcome. A red appearance indicated a successful outcome.

j. Motility examination

Tubes containing motility-enhanced media for bacterial culture were incubated at 37 degrees Celsius for 24 hours. Asuccessful outcome was indicated by the dispersal of "growth outside the spinous zone.

k. Citrate analysis

The citrate agar mile, which was present in the citrate agar tubes, was hit when they were attached to the bottom. After that, let it sit at (37°C) between (24 - 48 hours). A shift from green to blue in the middle of the spectrum indicates a convincing result.

3.9.5 Preparation of McFarland Turbidity Standards

To create solutions with particular optical densities, McFarland turbidity standards are made by combining varying volumes of 1 percent sulfuric acid and 1 percent barium chloride. An "optical density of 1.5x 108 colony forming units (CFU /Ml), the density of a bacterial suspension, is provided by 0.5 McFarland turbidity standard. Commercially, the 0.5 McFarland standard is available .

3.9,6 Effectiveness of Inhibitory Nano Compounds Against Bacteria

The College of Sciences for women laboratory used the following procedures to destroy and suppress germs during the planned investigation. Figure (3.7) illustrates the actions that were taken at the University of Babylon to prevent pollution.

Figure (3.7) Culture of bacteria in nutrient dishes

First: distilled water was used to activate Gram-negative bacteria, and the bacteria were subsequently cultivated in dishes containing nutrient media for bacteria. .

Second: Pierce the prepared dish four times.

*A 50 ml solution of chitosan polymer is intended to be added to the first hole. It is employed to contrast the polymer's impact on bacteria when acting alone with that

of the polymer when reinforced with nanomaterials (control). To evaluate the percentage of inhibition.

* The second hole is used to introduce chitosan and nano-silver compound at a rate of 50ml. In order to calculate the percent

* The third hole is used to inject chitosan and nano-zinc compound at a rate of 50ml.

* In order to calculate the percentage of inhibition, the fourth hole is used to inject the triple compound chitosan, silver, and nano-zinc at a rate of 50ml.

Third: the dish were moved to the incubator and remained there for 24 hours at 37°C. After the incubation period, the diameters of each hole harboring bacteria were measured.

Figure (3-8) Addition of materials to the dish containing bacteria.

3.9.7 Spectrophotometer (UV-mic)

The dilution method was used to estimate minimum inhibitory doses (MIC). In this experiment 3 ml of nutrient medium, 2.5 ml of assorted nanoparticles and 0.5 ml of bacteria were put into each tube. Thus, the final result was obtained in each tube, which is 6 ml. The positive control (media and test

object) was kept in one control tube per test batch, and the tubes were incubated at 37 °C for 24 h. Then the kill ratio was calculated for each tube with a wavelength of 600 nm.

Figure (3-9) Spectrophotometer Device

3.10 Genotyping Assays

3.10.1Isolation of genomic DNA

Using favrogen genomic kits, genomic DNA was isolated from the bacteria that had been collected in nutrient broth tubes and incubated for 24 hours before being frozen samples. DNA isolation required a 14-stage process using salting-out procedures .According to Manufacture Company, the process was ineffective:

1- We fill a 1.5 ml micro centrifuge tube (not provided) with the necessary number of bacterial cells, and we centrifuge it at maximum speed for 1 minute (14,000 rpm or 10,000 x g). Afterward, discard the supernatant.

2- We add 200m l of FATG Buffer and, using a vortex or pipette, re-suspend the pellet. 5 minutes of room temperature incubation is required.

3- We mix the sample with 200 ml of FABG Buffer for 5 seconds.

4- We incubate the sample and lysate for 10 minutes at 70 °C or until they are clear. Every three minutes during incubation, flip the tube over.

5- We mix the sample for 10 seconds while adding 200 ml of 96–100% ethanol. (Checking the pipes for any precipitation.

6- A 2 ml collection tube is filled with an FABG Column. Transferring the sample mixture and any precipitated to the FABG Column should be done with caution. After 5 minutes of centrifuging at maximum power (14,000 rmp or 10,000 XG), discard the 2 ml collecting tube. A new 2ml Collection tube should be filled with the FABG Column. The FABG Column is washed with 400ml of W1 Buffer. Discard the flow-through after centrifuging for one minute at full power (14,000 rmp or 10,000 X G).

7- In step 7, the FABG Column is once more put into the 2 ml collection tube. The FABG column should be cleaned using a 600 ml wash buffer (ethanol added). After one minute of full-power centrifugation, discard the flow-through (14,000 RPM or 10,000 XG). When you first open, be careful to add ethanol to the Wash Buffer.

8- We refill the 2 ml collection tube with the FABG Column. To dry the column, centrifuge for an additional three minutes at high power (14,000 rpm or 10,000 x g.

9- We insert a fresh 1.5 ml in micro centrifuge tube with the dried FABG Column.

10- We add 100 ml of TE, or preheated elution buffer, to the membrane center of the FABG Column. (Important Step: For successful elution, make sure the elution solution is distributed across the membrane center and completely absorbed.)

Table (3-5)

Components	Amount
Buffer Fabg	40 ML
w1 buffer	45ML
buffe wasr(cop)	25 ML
Buffer for elution	30 ML
FATG Buffer	30 ML
FABG pillar	100pcs
collection tube, 2 ml	200 pcs

Isolation kit Components

3.10.2 Calculating DNA Concentration and Purity

By introducing 2.5 ml of the extracted DNA to the Nano drop, which measures concentration in ng/L and purity, the DNA concentration of samples was measured. By examining the optical density (O.D) 260/280 nm ratio, it was able to determine whether protein contamination was present in the samples. For the purpose of eliminating DNA contaminants, a 260/280 ratio of 1.7–1.9 was advised. (2002) Sambrook and Russell

3.10.3 Gel Electrophoresis

Electrophoresis of gel in this chapter, we will explain how the gel electrophoresis reagents process works, as we discussed in the second chapter on gel electrophoresis.

3.10.3.1 Gel Electrophoresis Reagents

1-Agarose Powder (Biotech).

2- Biotech TBE Buffer with a 1X concentration.

3- Bromide ethidium (Biotech).

4- Ladder Marker for DNA (pioneer).

3.10.3.2 Protocol of Gel Electrophoresis

3.10.3.2.1 Preparation of the Tris Borate EDTA Buffer (1X TBE)

According to Sambrook and Russell (2001), this solution was created by combining 900 milliliters of distill water with one liter of (1X) TBE buffer from Promega (Germany).

3.10.3.2.2Agarogel preparation

- 1-X TBE (100 ml) was poured into a beaker.
- To the buffer, we added (2 gm) of agarose powder.
- A microwave oven was used to heat the solution for two minutes, until it was boiling.
- We added 0.5 ml of (10 mg/ml) Ethidium Bromide to the agarose solution.
- To mix the agarose and prevent bubbles, it was swirled.
- The solution was allowed to cool to a temperature between 50 and 60 C.

3.10.3.2.3DNA Loading & Electrophoresis

Samples were carefully placed into each well of the gel, then electricity was turned on at 70 V for 1 h to allow DNA to transfer from the negative electrode (-) to the positive electrode (+).Using a UV transilluminator set at 350 nm, the safer colored bands of the gel were observed, and images were taken

3.13.4 PCR

A successful PCR technique depends on the reaction conditionsss, which include the chemicals, temperature, and prevention of contamination. The reaction parameters must be tuned to produce the best specificity and product yield because

prior research has shown that PCR is sensitive to these variables. Standardd PCR amplificationn conditionss were employed with primer sequences.The most important factor in PCR programming may be the temperature at which primers hybridize to complimentary sequences on the template DNA. Calculations based on melting temperature (TM) are used to establish the annealing temperature for PCR primers. At a temperature termed as tm, half of all DNA strands disintegrate. Calculating the TM of PCR primers involves using the guanine and cytosine (G+C) content. Typically, the annealing temperature is 2 to 12 °C below the melting point (TM) .

The concentration found in primers is the ideal concentration. A weaker PCR output occurs from a drop in primer concentration, while an increase may produce primer dimer artifacts that make it difficult to interpret the data .. PCR-dependent processes work well with samples of partially purified DNA and thus do not require preparations of highly pure DNA. PCR failure can result from the presence of inhibitory compounds in the DNA extraction process, such as those used for protein denaturation and cell lysis. The components listed in table (3.6) were used in a master premix of Bioneer..

Table (3.6) PCR procedure Master Mix component list.

Tap Polymerase DNA	1 u/ µl
ach: dNTP dATP , dCtP , dGtP , dtTP)	250 Mm
tris-HCl (ph 9.0)	10 mM
K Cl	30 m mM
mg Cl2	1.5 mM

4.1 Introduction

This chapter presents and discusses the results of physical analyses by UV-Vis, XRD, FTIR, FE-SEM and TEM for nanocomposites (Cs)\ (Cs-Ag)\ (Cs-Zno) and (Cs-Ag-Zno) prepared by the liquid pulsed laser ablation method (PLAL).

From the biological part, studying the effect of these compounds in killing and inhibiting *Klebsiella pneumonia* bacteria, then calculating the percentage of killing and extracting DNA from the dead bacteria, identifying the affected genes, and discussing the results obtained

4.2 Physical Part

4.2.1 Optical Properties of Nanocomposites

In this section, an explanation of all the optical properties of the nanocomposite will be dealt with, according to the laboratory tests performed

4.2.1.1 UV-Vis absorption

The UV absorption in Figure (4-1) shows the 400 and 244 nm peaks for each Ag and ZnO NP, respectively, which is due to the effect of the pulsed laser, which resulted in a blue shift for both (Ag and ZnO NPs) due to the occurrence of the quantum confinement phenomenon as silver and zinc oxide particles are linked to the polymer chain, and this is consistent with the reports [31, 69, 74].

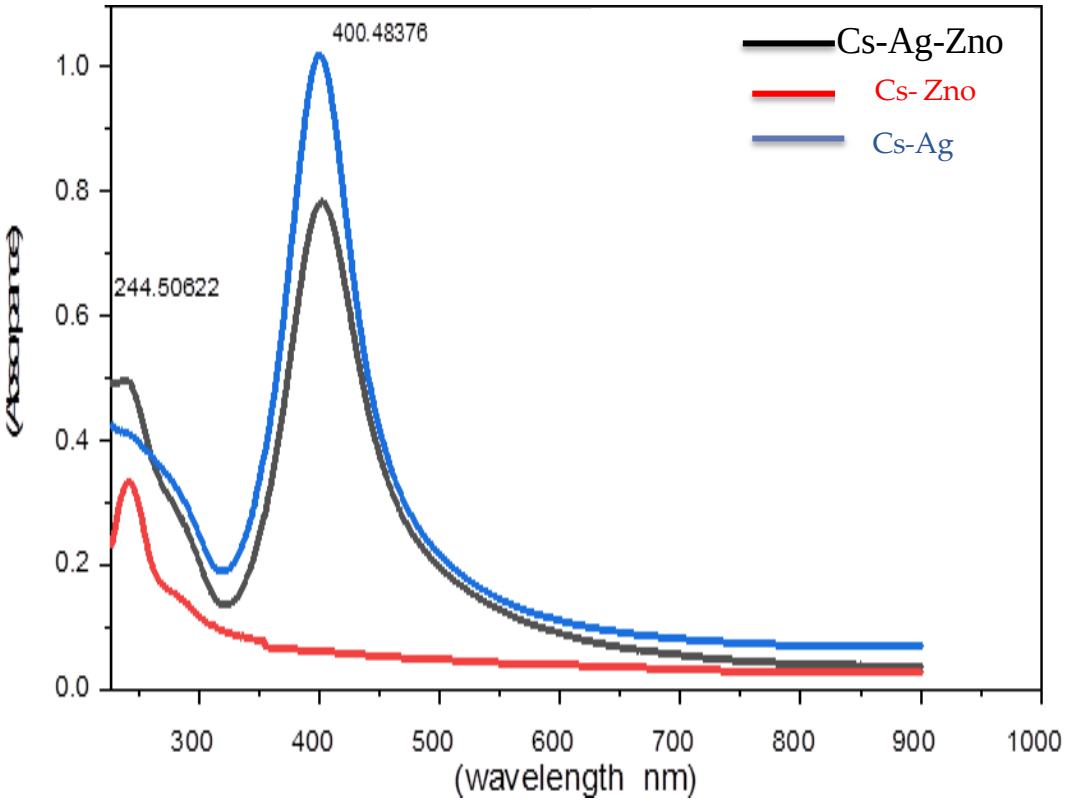

Figure (4-1). UV–vis spectra of the samples: (Cs-Ag-Zno) \(Cs –Zno) and (Cs-Ag).

4.2.1.2 Absorption Coefficient

The absorption coefficient of the prepared samples was also calculated according to equation (2-4) in the second chapter (Beer-Lambert's law). The results showed that the absorption coefficient shown in Figure (4-2) is the highest value of the absorption coefficient when it is imposed. (Cs-Ag-Zno) is tripartite in the (200-550) nm region with a peak at 400 nm and a low absorption coefficient of 600-900 nm and this matches the research [110].

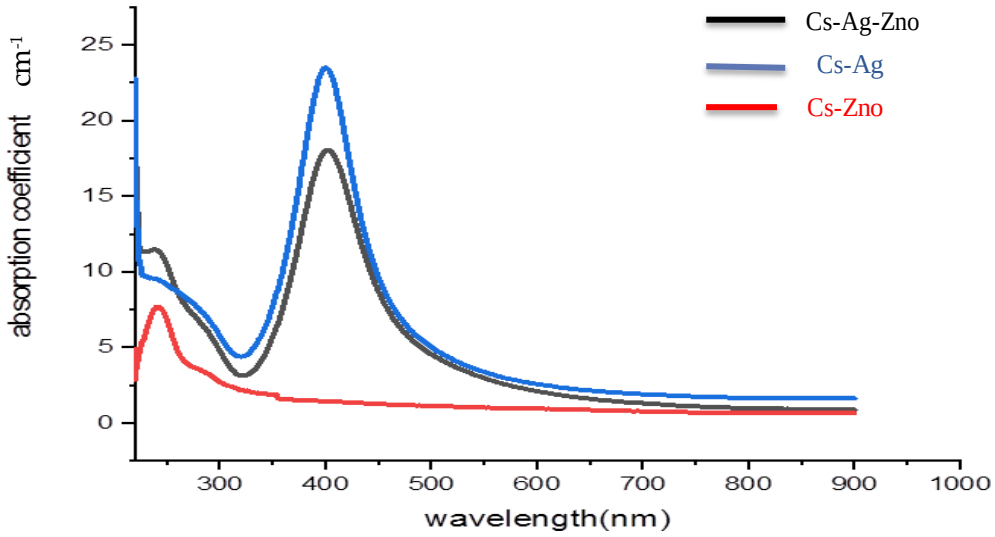

Figure(4-2):The absorption coefficient for each (Cs-Ag-Zno) \(Cs-Ag) and (CS-Zno).

4.2.1.3 The Energy Band Gap

The energy gap is calculated by the following equation

$$\alpha = A/h\nu(h\nu - E_g)^r \qquad (4\text{-}1)$$

Where A is a constant depends on the nature of the material , hν is the energy of a photon , r is a quantity that describes the electronic transition between the valence and conduction bands in nature, where h is Planck's constant.

The estimated value of the direct band gap of the compound (Cs-Ag) is (2.8) eV, for the compound (Cs-Zno) the direct energy gap is (4.7) eV, and for the nanocomposite (Cs-Ag-Zno) the direct energy gap is at (2.7) eV as in (Fig. 4-3). We see that the creation of secondary levels between VB and CB caused the narrowing of the direct energy gap. The gap may be large in the chitosan-zinc compound due to the oxidation of zinc nanoparticles. This means that there are structural defects in the zinc

nanoparticles generated in the solution containing a percentage of water and acetic acid this matches research [111,112,123,124].

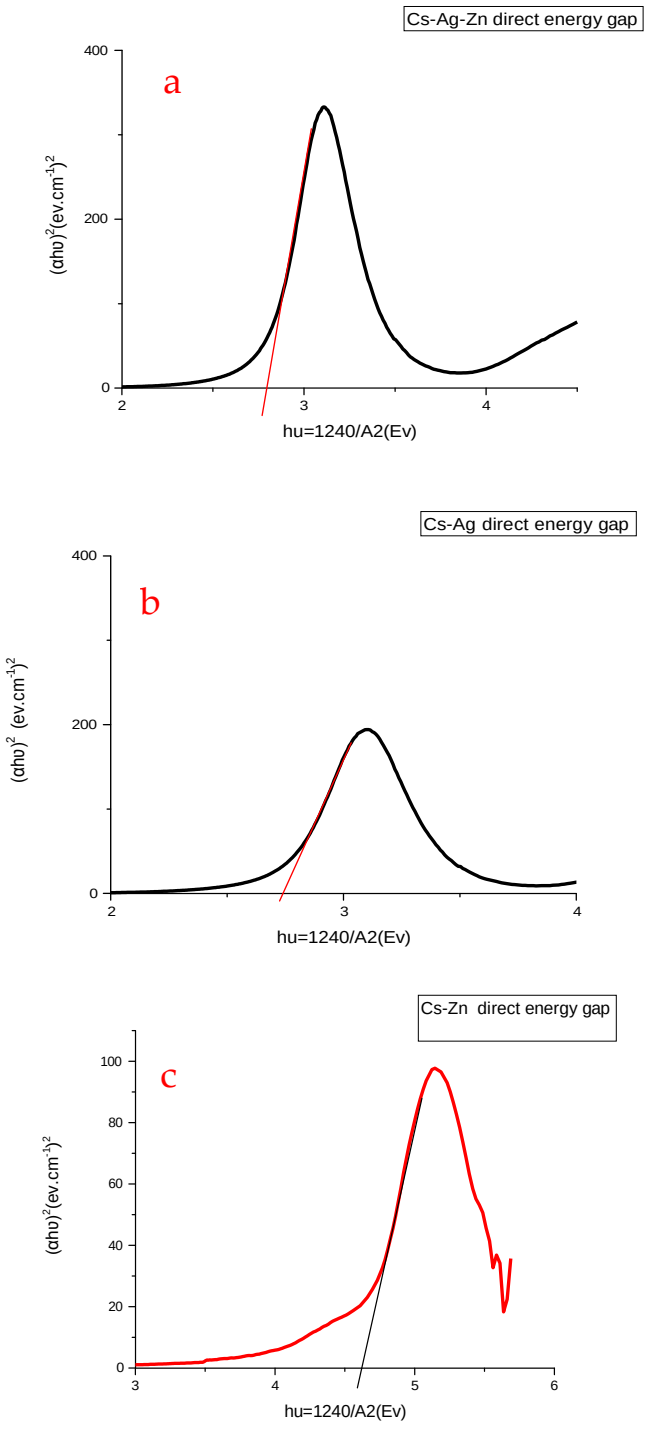

Figure(4-3) shows the direct energy gap for (a)Cs-Ag-Zn (b) Cs-Ag (c) Cs- Zno.

The indirect energy gap for silver (2.5) eV while the indirect energy gap of zinc (4.2)eV, and for composites (2.6) eV as in Figure (4-4) [113]. Table (1-4) shows the values of the energy gaps

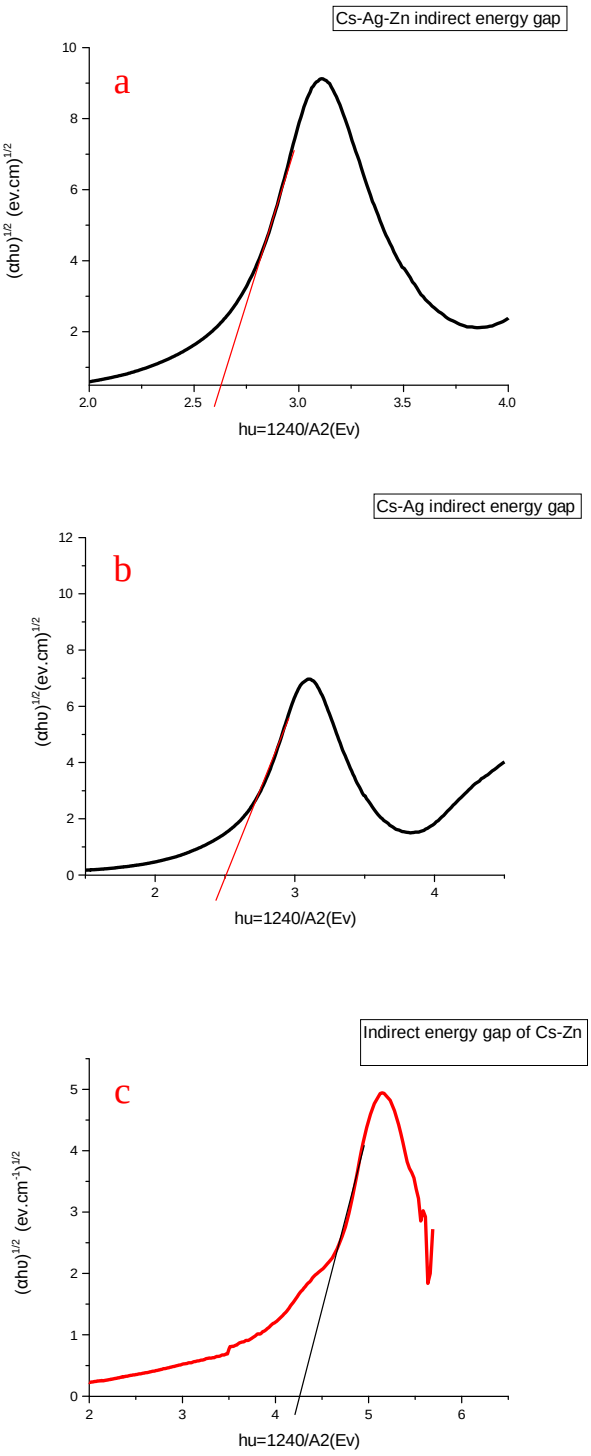

figure (4-4)shows the indirect energy gap for (a)Cs-Ag-Zno (b) Cs-Ag(c) Cs-Zno

Table (4-1) values of energy gaps for nanocomposites

compound	direct energy gap eV	Indirect energy gap eV
Cs-Ag	**2.8**	**2.5**
Cs-Zno	**4.7**	**4.2**
Cs-Ag-Zno	**2.7**	**2.6**

4.2.2 Fourier Transform Infrared Spectrometer (FTIR)

The FTIR spectrum of the samples is shown in Figure (4-5). The peaks are present as shown in Table (4-2). These results indicate that laser bombardment of the chitosan solution had no effect on the polymer chain. Both Ag and Zno nanoparticles required high energy for their formation and thus did not appear in sufficient quantities, as three peaks appeared for each nanocomposite, 3343.93 cm^{-1}, 348.65 cm^{-1}, 3347.67 cm^{-1}. The hydroxyl acid followed by the NH2:OH bond was clarified, the other peak was at 1983.80 cm^{-1},1984.10 cm^{-1},1983.38 cm^{-1} which are C = O bonds, as well as another peak for the compounds at 1638.65 cm^{-1}, 1639.52 cm^{-1},1640.60 cm^{-1} From the N-H:OH spectra of the studied samples can be observed superimposed for the Cs-Ag-ZnO and Cs-ZnO, Cs-Ag samples in the range 3300-3500 cm-1. These peaks indicates larger wave numbers and strong ZnO,Ag binding to the hydroxyl, amino and amide groups of chitosan molecules [34,35].

The table (4-2)Shows the apparent peaks of the functional totals of the prepared samples .

Grape.	O-H\NH$_2$	C=O	N-H:OH
CS- Ag-Zn	3343.93 cm^{-1}	1983.80 cm^{-1}	1638.65 cm^{-1}
Cs-Ag	3348.65 cm-1	1984.10 cm^{-1}	1639.52 cm^{-1}
Cs-Zn	3347.67 cm^{-1}	1983.38 cm^{-1}	1640.60 cm^{-1}

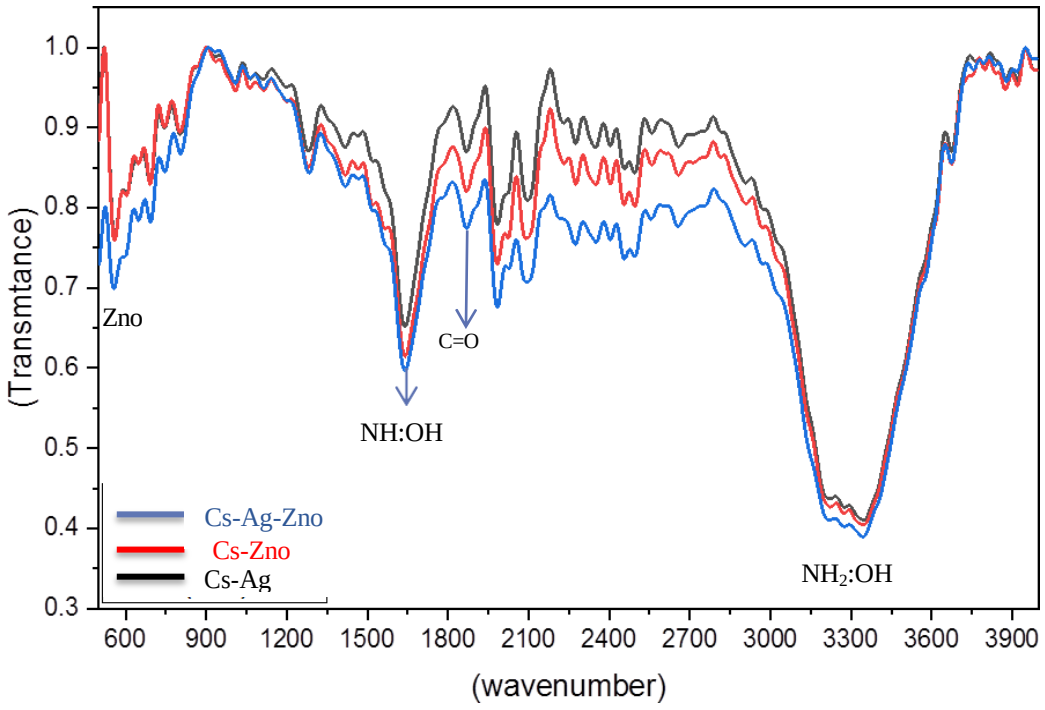

Figure (4-5) FTIR Spectral analysis.

4.2.3 X-Ray Diffraction (XRD)

The structural properties of the nanocomposites (Cs-Ag-Zno)\(Cs-Ag)\(Cs-Zno) were measured by X-ray diffraction, and as in the figures (4-6,7 ,8), which shows the pattern of the XRD.

We note from the figure for the (XRD) titration of the nanocomposite (Cs- Ag- Zno) the presence of peaks belonging to the chitosan solution at (24.6118 °) in addition to the presence of peaks belonging to silver nanoparticles 45.9902 ° and zinc oxide nanoparticles at 30.3729 ° with Miller's coefficients (100, 200)as in table(4-3), FCC and hexagonal folded nanoparticles were obtained and this matches the research [35,72].

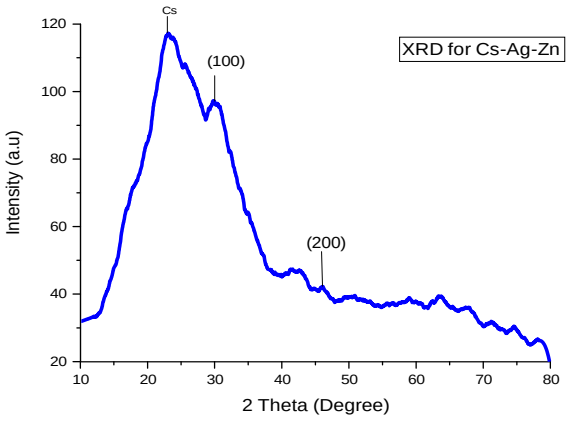

Figure(4-6) XRD for Cs-Ag-Zn.

Table(4-3) XRD paramters for nano composite Cs-Ag-Zno.

2 Θ Deg.	d(nm)	FWHM(rad)	C.s	hkl
30.3729	0.294051	0.018	7.77	100
45.9902	0.197183	0.0118	12.6	200

From Figure (4-7), we notice that there are five clear peaks at 14.1576°,16.9901°,23.4601° belongs to chitosan and (45.9880°)it returns to silver with miller coefficients (200) respectively, and this corresponds to the results of the research[114].

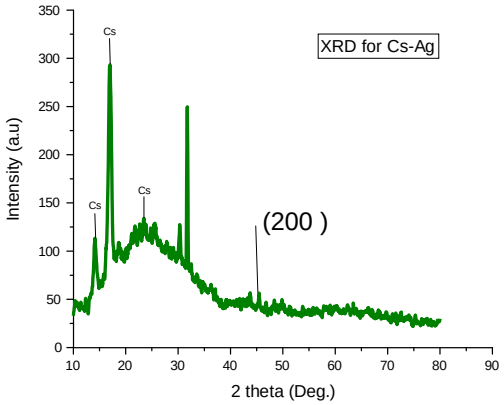

Figure(4-7) XRD for Cs-Ag.

Table (4-4) XRD paramters for nano composite (Cs-Ag).

2 Θ	d(nm)	FWHM(rad)	C.S	hkl
45.9880	0.19923	0.00139	30.4	(200)

We note from the figure for the titration (XRD) of the raw nanocomposite (Cs- Zno) the presence of peaks belonging to the chitosan solution at (14.2085°,17.0302°,25.6266°) in addition to the presence of apeak belonging to zinc nanoparticles at 31.8012° with a Miller factor (100), and this corresponds to the research[115].

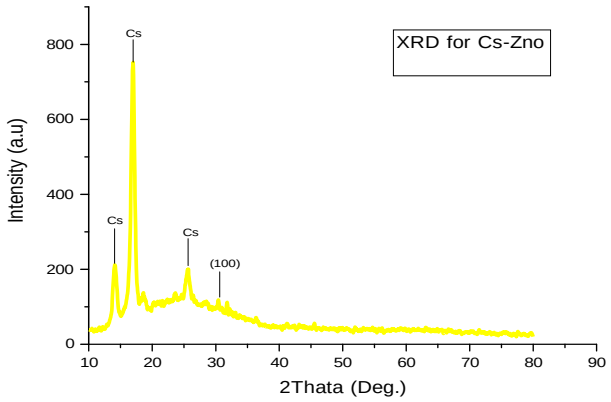

Figure (4-8) Granular size and XRD for Cs-Zno.

Table (4-5) XRD parameters for nano composite (Cs- Zno)

2 Θ	d(nm)	FWHM(rad)	C.S(nm)	hkl
31.8012	0.281163	0.oo558	25.108	(100)

We note through the analysis that chitosan has prominent peaks where chitosan is semi-crystalline, it gives deacetylation, which is usually done in the solid state and thus obtaining an irregular structure, while the peaks of silver nanoparticles appear at the angles mentioned in Table (4-4) and therefore the silver nanoparticles are FCC, followed by zinc nano particles at an angle of 31.8012 degrees. The nanoparticles have a hexagonal shape. Average crystal size of the nanoparticles is (21.89) nm, and this is consistent with the results of the research [34-35].

4.2.4 Field Emission-Scanning Electro Microscop (FE-SEM)

The (FE-SEM) assay showed that when zinc nanoparticles merged with the chitosan solution, these particles clearly overlapped with the polymer bonds and appeared in the form of gel pieces for Zno, chitosan with sizes (83-180) nm, while when silver nanoparticles were added to the polymer solution they formed concentric conical shapes with sizes (48-208) nm, and this was clearly evident when the triple compound (Cs-Ag-Zno) was formed, where nanoparticles appeared in the form of rods with sizes (185-286) nm as shown in Figure (4-9) these results are consistent with the research [72].

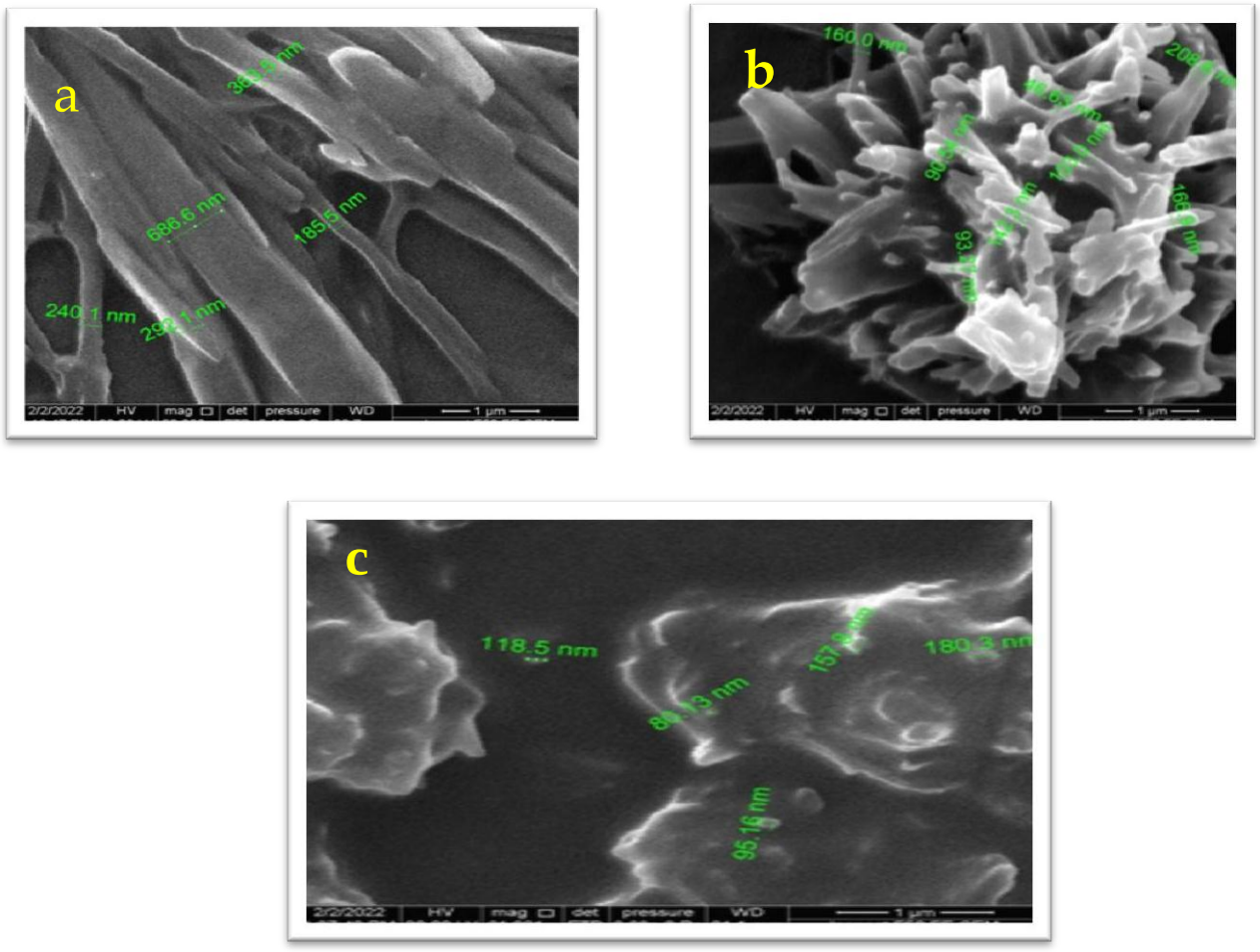

Figure (4-9) : FE-SEM (a)Cs-Ag-Zno(b) Cs-Ag (C) Cs- Zno.

4.2.5 Transmission Electron Microscopes (TEM) for the nanocomposite.

The assay (TEM) showed that spherical nanoparticles were obtained at a rate of 18.196 nm, and this is shown in Figure (4-10) and this is important and necessary in our study to fit the purpose of the study, that is, the size of nanoparticles is important in the process of killing and inhibiting bacteria, as we explained it in the first chapter. This is consistent with the research results [63,64,65,66].

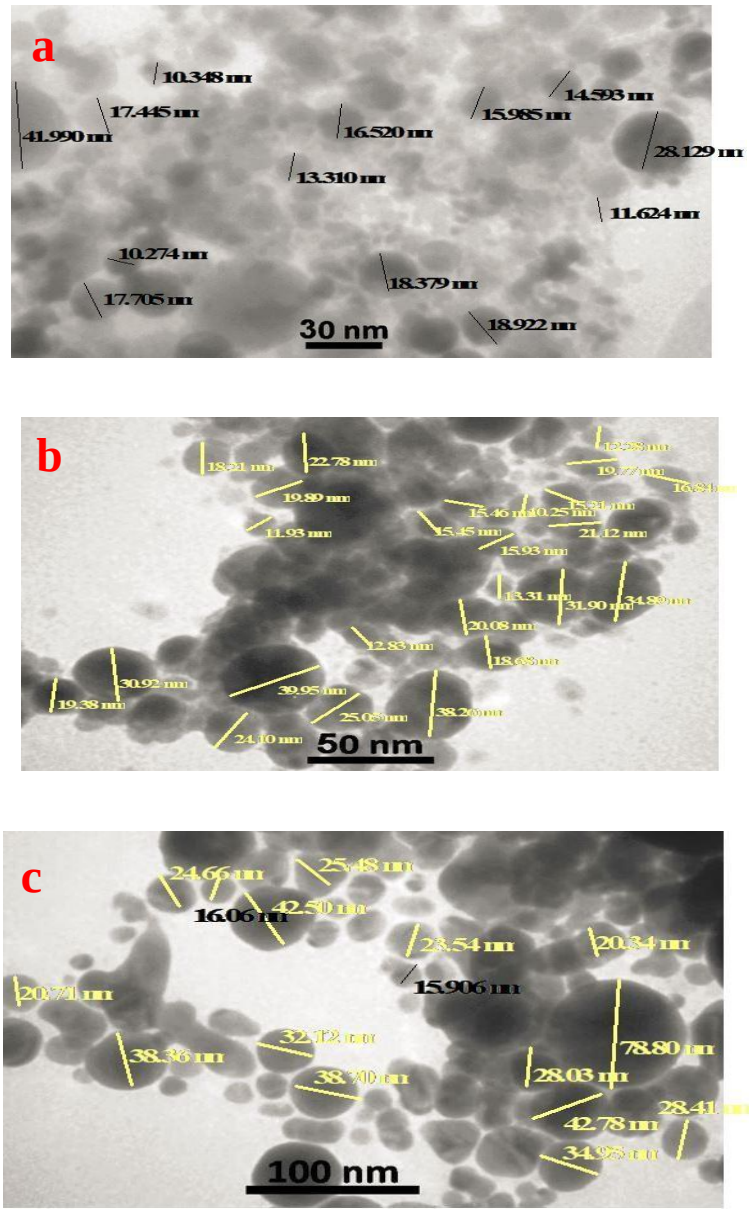

Figure (4-10): Shows the results of the TEM assay for the (Cs- Ag-Zno) nanocomposite (a)30 nm(b)50nm (c)100nm

4.3The Biological Application of Nanocomposites

4.3.1 The Effect of Nanocomposites as Bactericidal

Killing ratio of *Klebsiella peneumonia* bacteria when Cs ,(Cs-Ag-Zno), (Cs-Ag) and (Cs-Zno) were added to bacteria at 500 µL per compound. The result was that after a 24-h.Incubation period at 37°C, the nanocomposite (Cs-Ag) had the highest killing rate by 35 mm followed by the nanocomposite (Cs-Ag-Zno) by 29 mm, a compound of (Cs- Zno) by 26 mm and finally a Cs polymer by 22 mm, as shown in Figure (4-11). The antibacterial activity of NPs mainly depends on the electrostatic attraction between the NPs and the surfaces of positive and negatively charged bacterial cells. This attraction is critical for the activity of NPs as bactericidal agents. That the cause of bacterial cell death is mitochondrial damage and dysregulated expression of several programmed proteins, the present results showed, like previous studies, that NPs damage mitochondria and DNA leading to cell death. This is due to the cytotoxicity of NPs such as [99-108].

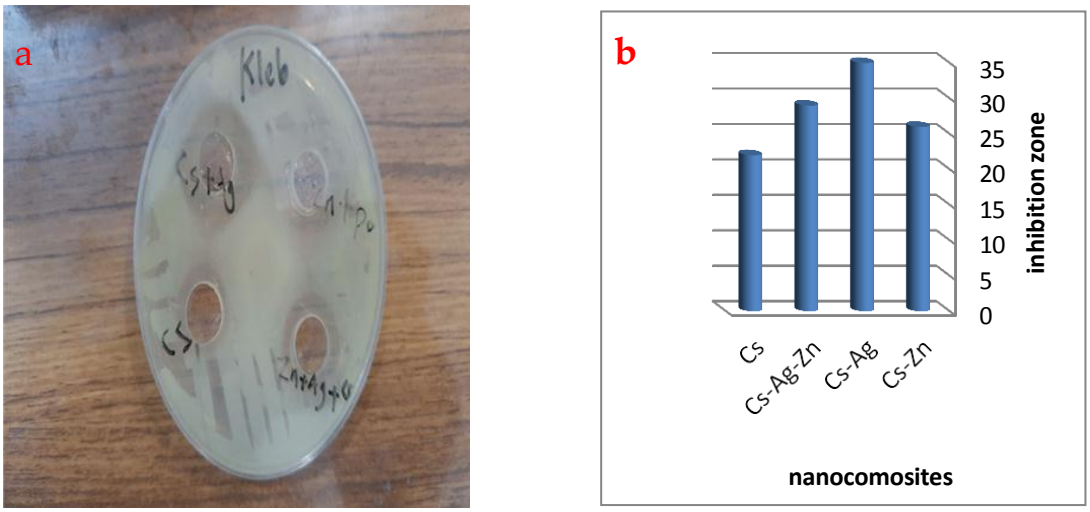

Figure (4-11): (a,b)The percentage of killing when nanocomposites are added.

4.3.2 Size of Inhibition Zone (Millimeters)

After determining the bactericidal killing rate on *Klebsiella peneumonia*, the next step is to determine the minimum inhibitory concentration (MIC) and make a dilution of each compound starting from (0.1) to (0.0001) for the nanocomposites (Cs-Ag), (Cs- Zn) and (Cs-Ag –Zn) as well as the biopolymer (Cs) for comparison of results. Using a spectrophotometer with a wavelength of 600 nm, it was found that the highest percentage of bacterial inhibition up to the fourth dilution was at the nanocomposite (Cs-Zn) at the first and second dilutions as in Figure (4-12), followed by the compound (Cs-Ag) in the fourth dilution, for the triple compound(Cs-Ag-Zn) at the second and third dilution, and for chitosan in the second, third dilution and this is consistent with the research [81,80,79,52]. As shown in Table (4-6).

The small size of the nanomaterials, which were shown by TEM and XRD assay, had the effect of increasing the killing rate and thus obtaining the bacterial DNA required for the examination of infected genes [116,117].

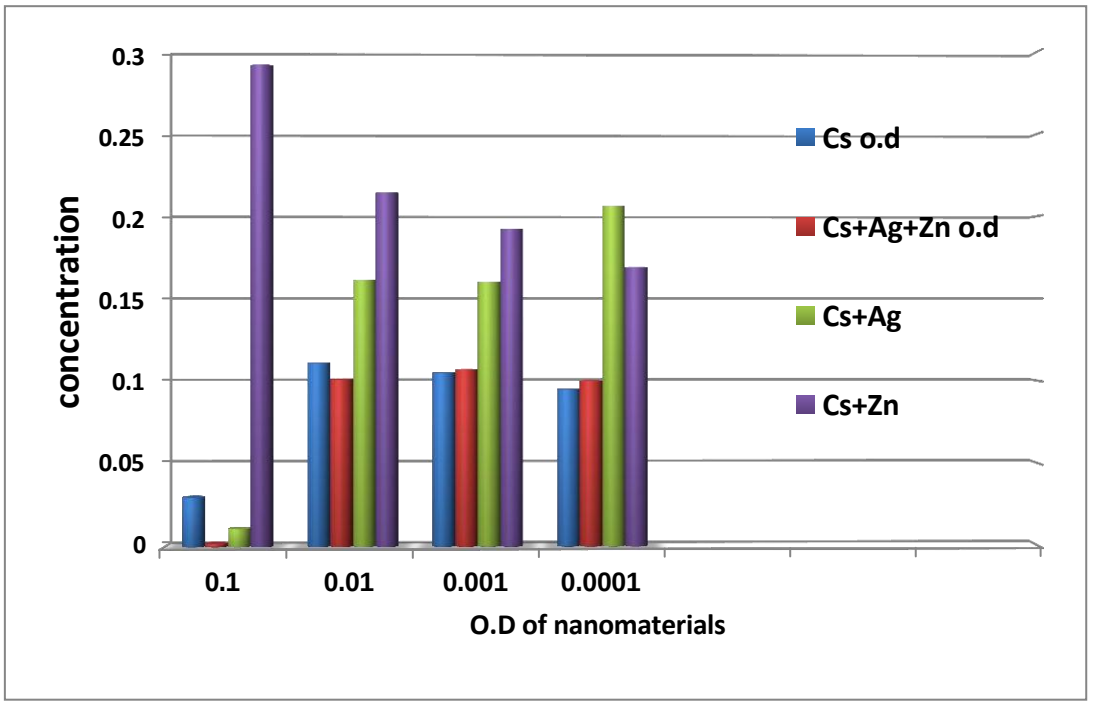

Figure (4-12) Shows the ratio between concentration and O.D for nanomaterials.

Table (4-6) Minimum inhibition concentrations and minimum bactericidal concentration.

Concentration	Cs O.D	Cs-Ag-Zn O.D	Cs-Ag O.D	Cs-Zn O.D
0.1	0.03	0.002	0.011	0.291
0.01	0.111	0.101	0.161	0.214
0.001	0.105	0.107	0.16	0.192
0.0001	0.095	0.1	0.206	0.169

After calculating the killing percentage and making the dilutions, the DNA of all samples is electrophoresis . Table (4–7) shows the amount of

DNA obtained from diluted samples of nanocomposites in addition to diluted chitosan, which amounted to (16) samples, and two samples (17–18) were added for comparison. They represent samples of bacteria used in the experiment without adding any nanocompound or polymers.

Table (4-7) shows the DNA extracted from each sample. Samples (1,2,3,4) are samples treated with chitosan polymer from the first to the fourth dilution, respectively, and samples (5,6,7,8) are samples treated with a nanocomposite (Cs-Ag-Zn) Dilute, samples (9,10,11,12) are the samples treated with the nanocomposite (Cs-Ag) diluted, and the samples (13,14,15,16) are the samples treated with the diluted nanocomposite (Cs-Zn), while the two samples (17,18) represent the control samples not treated with nanocomposites or biopolymer for the purpose of comparison.

Table (4-7) The concentration of DNA extracted from bacteria

#	User name	Nucleic Acid Conc.	Unit	A260	A280	260/280	260/230	Sample Type	Factor
1	NanoDrop	0.3	ng/µl	0.006	0.002	2.39	-0.33	DNA	50
2	NanoDrop	17.3	ng/µl	0.346	0.268	1.29	0.8	DNA	50
3	NanoDrop	-0.6	ng/µl	-0.013	-0.013	0.98	0.17	DNA	50
4	NanoDrop	14.7	ng/µl	0.295	0.269	1.1	0.85	DNA	50
5	NanoDrop	-2.4	ng/µl	-0.049	-0.049	0.99	0.46	DNA	50
6	NanoDrop	37.8	ng/µl	0.756	0.576	1.31	0.76	DNA	50
7	NanoDrop	13.2	ng/µl	0.264	0.215	1.23	0.76	DNA	50
8	NanoDrop	27.3	ng/µl	0.545	0.382	1.43	0.74	DNA	50
9	NanoDrop	7	ng/µl	0.14	0.116	1.2	0.72	DNA	50
10	NanoDrop	39.8	ng/µl	0.796	0.595	1.34	0.76	DNA	50
11	NanoDrop	1.6	ng/µl	0.032	0.019	1.66	1.68	DNA	50
12	NanoDrop	6	ng/µl	0.12	0.103	1.17	0.9	DNA	50
13	NanoDrop	25.7	ng/µl	0.513	0.415	1.24	0.7	DNA	50
14	NanoDrop	12.5	ng/µl	0.25	0.064	3.93	0.7	DNA	50
15	NanoDrop	6.7	ng/µl	0.133	0.129	1.03	0.91	DNA	50
16	NanoDrop	12.7	ng/µl	0.253	0.228	1.11	0.77	DNA	50
17	NanoDrop	43.7	ng/µl	0.875	0.474	1.84	1.59	DNA	50
18	NanoDrop	155.6	ng/µl	3.112	1.661	1.87	1.9	DNA	50

4.3.3 Influence of Isolated MDR Genomes by Nanoparticles

DNA isolated from untreated bacterial cells and bacterial cells treated with nanoparticles were analyzed. According to Figure (4-13) of agar gel electrophoresis, the nanocomposites had positively marked effects on the genome of pathogenic bacteria after 24 h of exposure to the nanocomposites.

In addition, in vitro studies have revealed that nanoparticles have genotoxic effects and interact directly with DNA, with these effects occurring inside bacterial cells causing genotoxicity. However, there are indications that genotoxicity may occur as a result of indirect DNA damage caused by cellular formation of reactive oxygen species (ROS), antioxidant depletion, or altered DNA repair protein synthesis. [118]. Experimentally introduced Zn NPs and Ag NPs into bacteria and damaged the bacterial DNA by interfering with chitosan [119]. Zinc usually ensures a strong contact with these materials. In a different study it was speculated that after Zn treatment the DNA lost its cellular proteins and no longer had the ability to replicate as Zn NP also hinders the division and growth of bacterial cells [120].

Proteins interact with nanometals, including nanosilver, making these nanometals toxic as a result of which they bind to protein molecules, inhibiting cellular metabolism and leading to the death of microorganisms [121].

It is believed that after entering the bacteria, the nanoparticles inactivated their enzymes and led to bacterial cell death due to the high activity of Zn NPs and AgNPs, which is attributed to the low and oxidized state electron transfer [122].

Agarose gel electrophoresis was used to assay DNA fragmentation.

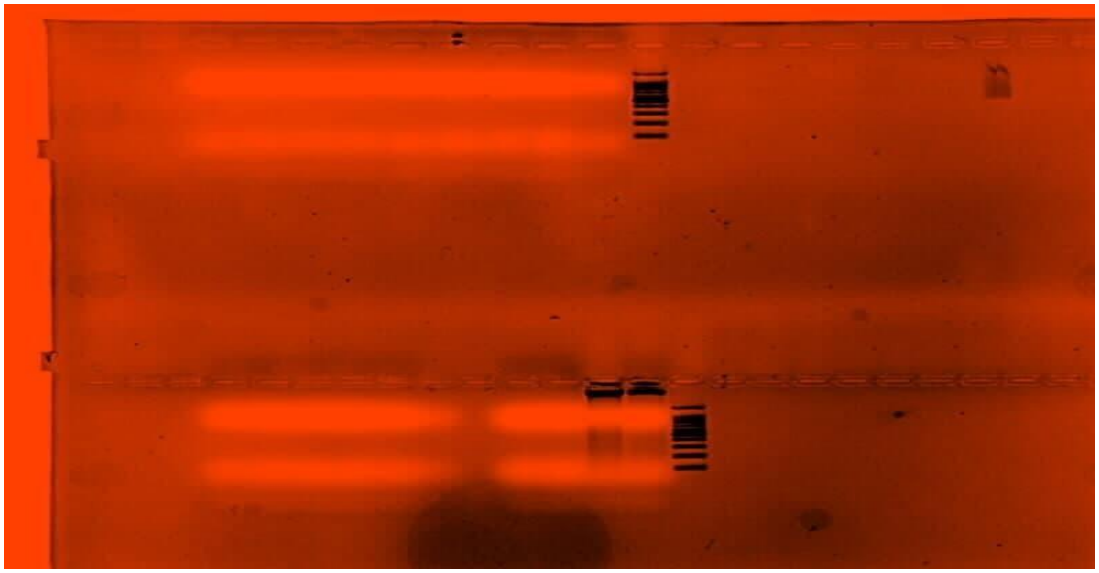

Figure (4-13): Agar gel electrophoresis was used to examine how the nanoparticles affected on DNA of *Klebsiella pneumoniae* .

4-3-4 Effect of Nanoparticles on Virulence Genes

Five different types of genes that constitute virulence factors in bacterial resistance were selected as shown in the second chapter of Table (2-1). After assessing the effect of nanocomposites on bacteria, bacterial DNA concentration and DNA extraction are measured by electrophoresis. The effect of these compounds on the proposed genes was studied and it was found that the nanocomposite (Cs-Ag-Zn) at the second dilution (0.01) had more effect than the rest of the compounds as shown in Table (4-8) sample no. 6.

This diluted compound caused the destruction of the five adhesion genes *(fimH-1*), the genes responsible for the production of adhesion proteins that lead to the formation of bacterial adhesion filaments on the bacterial wall. The host cell and thus the bacteria were prevented from gathering and forming bacterial colonies and preventing their adhesion to the surface of the host, as well as destroying the gene for transferring iron to the bacterial cell, which hinders its growth and ability to reproduce *(kfu*).

Also, the destruction of the gene responsible for the important line of defense for bacteria is the outer membrane surrounding the bacterial mucosa *(rmp)* that facilitates the entry of nanoparticles and antibiotics and thus kills bacteria by inhibiting them and thus affecting and distorting mitochondria and proteins as well as disrupting cell signals within bacteria. The gene *(entB*) that supplies the bacteria with iron from the surrounding bacteria, and finally the gene *(ycfM)* responsible for Exogenous lipoproteins that feed bacteria. Therefore, the compound lost the ability of bacteria to resist the antibiotic by weakening it and then killing it [105].

As for the nanocomposite (Cs-Ag) in the first and third dilution, it did not show any effect on these genes, as well as the fourth dilution of chitosan, as shown in Table (4-8), sample no. (9-11-4), respectively. The fact that the nanocomposites did not completely affect the mentioned genes does not mean that these compounds did not affect the various other genes (virulence factors) of the bacteria that were not studied in this research which is evident from the rate at which the bacteria were killed. Dealing with nanomaterials.

When comparing the nanoscale samples with the two control samples (18-17), we find that the bacteria treated with nanomaterials have clearly affected the bacterial genes, as shown in Figure (4-14).

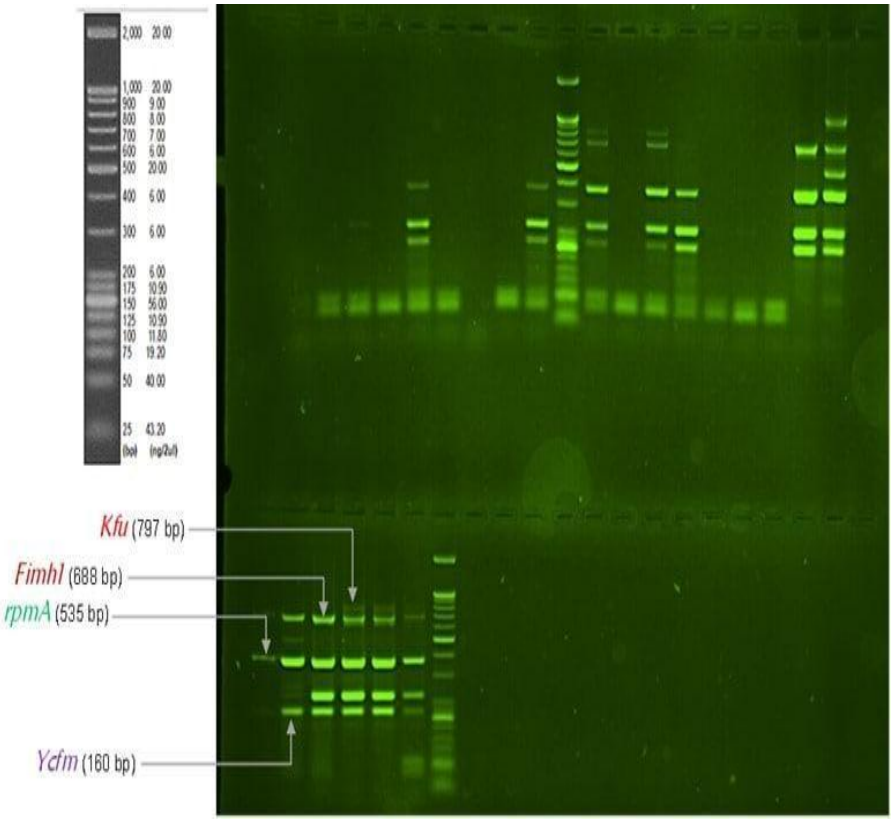

Figure (4-14) shows the genes affected by nanocomposites.

Table (4-8) show the effect of nanocomposites on the bacterial gene

Sample Number	Sample	Virulence
1	Cs 10^{-1}	*Ycfm*
2	Cs 10^{-2}	*Ycfm*
3	Cs 10^{-3}	*Ycfm*
4	Cs 10^{-4}	*Ycfm-entb-rpma-Fimh1*
5	(Cs-Ag-Zn) 10^{-1}	*Ycfm*
6	(Cs-Ag-Zn) 10^{-2}	*NON*

7	(Cs-Ag-Zn) 10^{-3}	*Ycfm*
8	(Cs-Ag-Zn)10^{-4}	*Ycfm "entb-rpma "Fimh1"*
9	CS-Ag 10^{-1}	*Ycfm-entb- rpma- Fimh1-Kfu*
10	Cs-Ag 10^{-2}	*Ycfm*
11	Cs-Ag 10^{-3}	*Ycfm_entb_rpma_ Fimh1_kfu*
12	Cs-Ag 10^{-4}	*Ycfm_entb_rpma_ Fimh1*
13	Cs-Zn 10^{-1}	*Ycfm*
14	Cs-Zn 10^{-2}	*Ycfm*
15	Cs-Zn 10^{-3}	*Ycfm*
16	Cs-Zn 10^{-4}	*Entb_rpma_Fim1_ kfu*
17	Con.	*Ycfm -Entb_rpma_Fim1_ kfu*
18	Con.	*Ycfm-rpma-Fimi-kfu*

Table (4-9) Compared with previous studies of the effect of nanocomposites in killing bacteria.

Nanocomposites	Preparation Method	Bacterial Application	kill Rate	Ref.
Cs-Ag	chemical method	*E. coli and S. aureus*	More than 90% if the incubation hour is increased	125
CS-ZnO	chemical method	*Different types of bacteria*	90%	126
Cs-Ag-Zn	chemical method	*S.aureus, E.coli, K-pneumoniae*	(61.33-65.33)mm	77
Cs-Ag-Zn	Laser ablation by Nd:YAG(500,300 J\ple,1000ple\sec,1064 nm)	*K-pneumoniae*	(22-35)mm	Our study

4.4 Conclusions

1- It turns out that the proposed technique is successful for obtaining (Cs- Ag-Zn)\(Cs-Ag)\(Cs-Zn) nanocomposites and it was a simple and affordable technology. This has been proven by examination UV-vis of nanocomposites, which showed the presence of two peaks at (244.400) nm belonging to zinc and silver particles, respectively.

2- From examining the energy gap, we notice that the energy gap of the compound (Cs-Ag-Zno) and the compound (Cs-Ag) was small, and the

energy gap of the compound (Cs-Zno) was large. This may be due to the fact that the oxidation process was not organized or due to the presence of defects and deformities due to impurity.

3- FTIR scan from nanocomposites showed The pulsed laser ablation process did not affect the synthesis of chitosan, and at the same time, the Zno NPs pulsed laser was obtained.

4- The study of the structural properties showed that the nanocomposites that were produced have a crystalline and non-random structure, with an average crystal size of (21.89) nm, as well as the presence of peaks belonging to each of Cs, Ag and ZnO, and that these particles take the hexagonal shape as well as the FCC.

5- The assay (FE-SEM) showed the fusion of nanoparticles with the chitosan solution, whereby nanoparticles were obtained in the form of bacilli for the triangular conical compound of silver and chitosan and an irregular gel-shaped shape for zinc and chitosan, while the assay (TEM) showed that nanoparticles with a size of 18.196 nm were obtained.

6- The nanocomposites were applied to the *Klebsiella pneumoniae* bacteria, showing the effect of these compounds on the bacteria, and the percentage of killing increased with the increase in the concentration of these compounds.

7- By comparing the results with other researchers, it was found that the proposed method for the synthesis of nanocomposites was a simple, inexpensive, and short-time method .

8- Five *Klebsiella pneumonia* genes have been studied. (*Fimh 1, Ycfm entB, Kfu, rpmA*) and it turned out that they were affected by the nanocomposites in different ways), but in the second dilution, the effect of the nanocomposite (Cs-Ag -Zno) was clear, as it was observed that all

studied genes were affected by this triple compound when compared with the sample untreated material

4-5 Recommendations

1- Manufacture of other nanomaterials in the same way and study their optical and structural properties.

2-Changing the concentration of a substance by changing its physical parameters and studying its various properties.

3-Synthesized nanocomposites can be applied to other bacteria or fungi

4-Focus on other types of genes that are related to drug resistance in microorganisms.

5- Study the synergistic and/or antagonistic effects of both nanoparticles and antibiotics mixed together in vivo and in vit.

Reference

1- Pendyala, Chaitanya, et al. "Contemporary apprise on LASERS and its applications in dentistry." International Journal of Oral Health and Medical Research 4 (2017): 47-51.

2- Riveiro, Antonio, et al. "Laser surface texturing of polymers for biomedical applications." Frontiers in physics 6 (2018): 16.

3-Guisbiers, Grégory, et al. "Nanomaterial properties: size and shape dependencies." Journal of Nanomaterials 2012 (2012).

4- Dhanalakshmi, M., et al. "Silver nanoparticles and its antibacterial activity." Int J Pharm Biol Arch 4 (2013): 819-826.

5- Anzaldo Montoya, et al. "Technical standards in nanotechnology as an instrument of subordinated governance: Mexico case study." Journal of responsible innovation 3.2 (2016): 135-153.

6- Mangematin, Vincent, et al. "The future of nanotechnologies." Technovation 32.3-4 (2012): 157-160.

7- Gao, Weiwei, et al. "Nanomaterials arising amid antibiotic resistance." Nature Reviews Microbiology 19.1 (2021): 5-6.

8- Du, Hongli, et al. "Rare-earths doped-nanoparticles prepared by pulsed laser ablation in liquids." Ceramics International 46.16 (2020): 26299-26308.

9- Carrouel, Florence, et al. "Nanoparticles as anti-microbial, anti-inflammatory, and remineralizing agents in oral care cosmetics: a review of the current situation." Nanomaterials 10.1 (2020): 140.

10- Dong, Xiao-Yun, et al. "Nanosilver as a new generation of silver catalysts in organic transformations for efficient synthesis of fine chemicals." Catalysis Science & Technology 5.5 (2015): 2554-2574.

11- Motelica, Ludmila, et al. "Innovative antimicrobial chitosan/ZnO/Ag NPs/citronella essential oil nanocomposite—Potential coating for grapes." Foods 9.12 (2020): 1801.

12- Zimmerli, W. "Clinical presentation and treatment of orthopaedic implant-associated infection." Journal of internal medicine 276.2 (2014): 111-119.

13- Pendyala, Chaitanya, et al. "Contemporary apprise on LASERS and its applications in dentistry." International Journal of Oral Health and Medical Research 4 (2017): 47-51.

14- Behera, Ajit, et al. "Nanomaterials: Fundamental Principle and Applications." Nanotechnology and Nanomaterial Applications in Food, Health, and Biomedical Sciences. Apple Academic Press, 2019. 163-194.

15- Shirvan, Anahita Rouhani, et al. "Recent advances in application of chitosan and its derivatives in functional finishing of textiles." The impact and prospects of green chemistry for textile technology (2019): 107-133.

16-Aizat, Muhd Arif, et al. "Chitosan nanocomposite application in wastewater treatments." Nanotechnology in Water and Wastewater Treatment. Elsevier, 2019. 243-265.

17-Kumar, Majeti NV Ravi. "A review of chitin and chitosan applications." Reactive and functional polymers 46.1 (2000): 1-27.

18-Zhao, Li-Ming, et al. "Preparation and application of chitosan nanoparticles and nanofibers." Brazilian Journal of Chemical Engineering 28 (2011): 353-362.

19- Li, Q., et al. "Applications and properties of chitosan." Applications of chitin and chitosan. CRC Press, 2020. 3-29.

20-Zhao, Dongying, et al. "Biomedical applications of chitosan and its derivative nanoparticles." Polymers 10.4 (2018): 462 .

21-Morin-Crini, Nadia, et al. "Applications of chitosan in food, pharmaceuticals, medicine, cosmetics, agriculture, textiles, pulp and paper, biotechnology, and environmental chemistry." Environmental Chemistry Letters 17.4 (2019): 1667-1692.

22- Reshad, Riyan Al Islam, et al. "Chitosan and its broad applications: A brief review." Available at SSRN 3842055 (2021).

23-Zu, Sheng-Zhen, et al. "Aqueous dispersion of graphene sheets stabilized by pluronic copolymers: formation of supramolecular hydrogel." The Journal of Physical Chemistry C 113.31 (2009): 13651-13657.

24- Huang, Zhenzhen, et al. "Toxicity mechanisms and synergies of silver nanoparticles in 2, 4-dichlorophenol degradation by Phanerochaete chrysosporium." Journal of hazardous materials 321 (2017): 37-46.

25- Guo, Zhi, et al. "Determination of inequable fate and toxicity of Ag nanoparticles in a Phanerochaete chrysosporium biofilm system through different sulfide sources." Environmental Science: Nano 3.5 (2016): 1027-1035.

26-Mohamed Abd El-Galil, Mona, et al. "IMPACT OF CRUDE ALOE VERA GEL ON SILVER NANOPARTICLE-INDUCED LUNG CYTOTOXICITY IN ADULT MALE ALBINO RATS: FUNCTIONAL, HISTOLOGICAL AND IMMUNOHISTOCHEMICAL STUDY." Al-Azhar Medical Journal 51.1 (2022): 563-604.

27-Huang, Tao, et al. "Synthesis and characterization of tunable rainbow colored colloidal silver nanoparticles using single-nanoparticle plasmonic microscopy and spectroscopy." Journal of materials chemistry 20.44 (2010): 9867-9876.

28-Baig, Nadeem, et al. "Nanomaterials: A review of synthesis methods, properties, recent progress, and challenges." Materials Advances 2.6 (2021): 1821-1871 .

29- Calderón-Jiménez, Bryan, et al. "Silver nanoparticles: Technological advances, societal impacts, and metrological challenges." Frontiers in chemistry 5 (2017): 6.

30- Sabir, Sidra, et al. "Zinc oxide nanoparticles for revolutionizing agriculture: synthesis and applications." The Scientific World Journal 2014 (2014).

31- Kadhim, Hiba Basim Abbas, et al. "Ablation of ZnO in liquid by Nanosecond Laser." Journal of Physics: Conference Series. Vol. 1032. No. 1. IOP Publishing, 2018.

32-Siddiqi, Khwaja Salahuddin, et al. "Properties of zinc oxide nanoparticles and their activity against microbes." Nanoscale research letters 13.1 (2018): 1-13.

33-Jiang, Jinhuan, et al."The advancing of zinc oxide nanoparticles for biomedical applications." Bioinorganic chemistry and applications 2018 (2018).

34-Buşilă, Mariana, et al. "Synthesis and characterization of antimicrobial textile finishing based on Ag: ZnO nanoparticles/chitosan biocomposites." Rsc Advances 5.28 (2015): 21562-21571.

35-Li, Li-Hua, et al. "Preparation, characterization and antimicrobial activities of chitosan/Ag/ZnO blend films." Chemical Engineering Journal 160.1 (2010): 378-382 .

36-Duan, Huiyu, et al. "Recent progress and challenges in plasmonic nanomaterials." Nanotechnology Reviews 11.1 (2022): 846-873.

37- Hammond, Oliver S., et al. "Ionic liquids and deep eutectics as a transformative platform for the synthesis of nanomaterials." Chemical Communications 58.24 (2022): 3865-3892.

38-Yin, Yadong, et al. "Formation of hollow nanocrystals through the nanoscale Kirkendall effect." Science 304.5671 (2004): 711-714.

39-Kong, Xiang Yang, et al. "Single-crystal nanorings formed by epitaxial self-coiling of polar nanobelts." Science 303.5662 (2004): 1348-1351 .

40- Pfleger, Jiri, et al. "Preparation of Ag nanoparticles by two-wavelength laser ablation and fragmentation." Advanced Organic and Inorganic Optical Materials. Vol. 5122. SPIE, 2003.

41-Shaw, S. J., et al. "A study of the interaction of a laser-generated cavity with a nearby solid boundary." Journal of Physics D: Applied Physics 32.14 (1999): 1612 .

42-Amendola, Vincenzo, et al. "What controls the composition and the structure of nanomaterials generated by laser ablation in liquid solution?." Physical Chemistry Chemical Physics 15.9 (2013): 3027-3046 .

43-Sakka, Tetsuo, et al. "Laser ablation at solid–liquid interfaces: An approach from optical emission spectra." The Journal of Chemical Physics 112.19 (2000): 8645-8653 .

44-Brause, R., et al. "Characterization of laser-ablated and chemically reduced silver colloids in aqueous solution by UV/VIS spectroscopy and STM/SEM microscopy." Applied Physics B 75.6 (2002): 711-716 .

45-Henglein, Arnim. "Physicochemical properties of small metal particles in solution:" microelectrode" reactions, chemisorption, composite metal particles, and the atom-to-metal transition." The Journal of Physical Chemistry 97.21 (1993): 5457-5471.

46-Kawabata, Arisato, et al. "Electronic properties of fine metallic particles. II. Plasma resonance absorption." Journal of the physical society of Japan 21.9 (1966): 1765-1772.

47- Geusic, J. , et al"Laser oscillations in Nd-doped yttrium aluminum, yttrium gallium and gadolinium garnets." Applied Physics Letters 4.10 (1964): 182-184.

48- Milonni, P. W., et al " Laser Physics", John Wiley and Sons, 2010.

49-Aguilera-Correa, John Jairo, et al. "Effect of Gold Nanostars Plus Amikacin against Carbapenem-Resistant Klebsiella pneumoniae Biofilms." Biology 11.2 (2022): 162 .

50-Pareek, Vikram, et al. "Silver nanoparticles induce a triclosan-like antibacterial action mechanism in multi-drug resistant Klebsiella pneumoniae." Frontiers in microbiology 12 (2021): 183 .

51-Hamza, Ammar M., et al. "Enhancement the Efficiency of ZnOnanofiber mats antibacterial Using Novel PVA/Ag nanoparticles." Energy Procedia 119 (2017): 615-621 .

52-Maruthupandy, Muthuchamy, et al. "Highly efficient antibacterial activity of graphene/chitosan/magnetite nanocomposites against ESBL-producing Pseudomonas aeruginosa and Klebsiella pneumoniae." Colloids and Surfaces B: Biointerfaces 202 (2021): 111690 .

53- Zamiri, Reza, et al. "Laser based fabrication of chitosan mediated silver nanoparticles." Applied Physics A 105.1 (2011): 255-259

54-Li, Bei, et al. "Molecular pathogenesis of Klebsiella pneumoniae." Future microbiology 9.9 (2014): 1071-1081.

55-Zhu, Jie, et al. "Virulence factors in hypervirulent Klebsiella pneumoniae." Frontiers in Microbiology 12 (2021): 642484.

56-Lawlor, Matthew S., et al. "Yersiniabactin is a virulence factor for Klebsiella pneumoniae during pulmonary infection." Infection and immunity 75.3 (2007): 1463-1472.

57-Zhang, Xi-Feng, et al. "Silver nanoparticles: synthesis, characterization, properties, applications, and therapeutic approaches." International journal of molecular sciences 17.9 (2016): 1534.

58-Amin, Rehab M., et al. "Rapid and sensitive microplate assay for screening the effect of silver and gold nanoparticles on bacteria." Nanomedicine 4.6 (2009): 637-643.

59-Asamoah, R. B., et al. "A comparative study of antibacterial activity of CuO/Ag and ZnO/Ag nanocomposites." Advances in Materials Science and Engineering 2020 (2020).

60-Zhang, Tianlu, et al. "Cytotoxic potential of silver nanoparticles." Yonsei medical journal 55.2 (2014): 283-291.

61-Zhao, Yuyun, and Xingyu Jiang. "Multiple strategies to activate gold nanoparticles as antibiotics." Nanoscale 5.18 (2013): 8340-8350 .

62-Huang, Zhenzhen, et al. "Toxicity mechanisms and synergies of silver nanoparticles in 2, 4-dichlorophenol degradation by Phanerochaete chrysosporium." Journal of hazardous materials 321 (2017): 37-46.

63-Singh, Priyanka, et al. "Silver nanoparticles produced from Cedecea sp. exhibit antibiofilm activity and remarkable stability." Scientific Reports 11.1 (2021): 1-13 .

64-Yilmaz Atay, Hüsnügül. "Antibacterial activity of chitosan-based systems." Functional chitosan. Springer, Singapore, 2019. 457-489 .

65-Al-Nemrawi, Nusaiba K., et al. "Formulation and characterization of tobramycin-chitosan nanoparticles coated with zinc oxide nanoparticles." Saudi Pharmaceutical Journal 30.4 (2022): 454-461.

66-Sirelkhatim, Amna, et al. "Review on zinc oxide nanoparticles: antibacterial activity and toxicity mechanism." Nano-micro letters 7.3 (2015): 219-242 .

67-Chen, Yu-Hung, and Chen-Sheng Yeh. "Laser ablation method: use of surfactants to form the dispersed Ag nanoparticles." Colloids and Surfaces A: Physicochemical and Engineering Aspects 197.1-3 (2002): 133-139.

68-Zamiri, Reza, et al. "Laser based fabrication of chitosan mediated silver nanoparticles." Applied Physics A 105.1 (2011): 255-259

69-Tajdidzadeh, M., et al. "Synthesis of silver nanoparticles dispersed in various aqueous media using laser ablation." The Scientific World Journal 2014 (2014).

70-Zhao, Yan, et al. "Synthesis and properties of Ag/ZnO core/shell nanostructures prepared by excimer laser ablation in liquid." APL Materials 3.8 (2015): 086103.

71-Bui, Vu Khac Hoang, et al. "Chitosan combined with ZnO, TiO2 and Ag nanoparticles for antimicrobial wound healing applications: a mini review of the research trends." Polymers 9.1 (2017): 21.

72-Kumar, S. Raj, and P. Gopinath. "In situ synthesis of chitosan coated silver-zinc oxide nanocomposites and its enhanced antibacterial properties." Journal of Nanoscience and Nanotechnology 17.12 (2017): 8797-8805.

73-Jemal, Kero, et al. "Synthesis, characterization, and evaluation of the antibacterial activity of Allophylus serratus leaf and leaf derived callus extracts mediated silver nanoparticles." Journal of Nanomaterials 2017 (2017).

74-Kalaivani, R., et al. "Synthesis of chitosan mediated silver nanoparticles (Ag NPs) for potential antimicrobial applications." Frontiers in Laboratory Medicine 2.1 (2018): 30-35.

75-Tajdidzadeh, Mojgan, et al. "Improving stability of zinc nanoparticles in chitosan solution with a nanosecond pulsed laser." Laser Physics Letters 16.5 (2019): 055603.

76-Gavrilenko, Ekaterina A., et al. "Comparative study of physicochemical and antibacterial properties of ZnO nanoparticles prepared by laser ablation of Zn target in water and air." Materials 12.1 (2019): 186.

77- Al-Abboodi, Sabah M. Thahab, et al. "Preparation and Characterization of Chitosan/ZnO/Ag Nanocomposites as Antibacterial Hydrogel for Wound Dressing." IOP Conference Series: Materials Science and Engineering. Vol. 978. No. 1. IOP Publishing, 2020.

78-Motelica, Ludmila, et al. "Innovative antimicrobial chitosan/ZnO/Ag NPs/Citronella essential oil nanocomposite—Potential coating for grapes." Foods 9.12 (2020): 1801.

79-Menazea, A. A., et al. "Antibacterial activity of TiO2 doped ZnO composite synthesized via laser ablation route for antimicrobial application." Journal of Materials Research and Technology 9.4 (2020): 9434-9441.

80-Asamoah, R. B., et al. "A comparative study of antibacterial activity of CuO/Ag and ZnO/Ag nanocomposites." Advances in Materials Science and Engineering 2020 (2020).

81-Ke, Cai-Ling, et al. "Antimicrobial actions and applications of chitosan." Polymers 13.6 (2021): 904.

82-Awed, Nasser S., et al. "Green synthesis of different ratios from bimetallic gold: Silver nanoparticles core@ shell via laser ablation scattered in Chitosan-PVA matrix and its electrical conductivity behavior." Composites Communications 24 (2021): 100678.

83- Avicenna, Syifa, et al. "Synthesis of colloidal silver nanoparticles in various liquid media using pulse laser ablation method and its antibacterial properties." Indonesian Journal of Chemistry 21.3 (2021): 761-768.

84-Elsayed, Khaled A., et al. "Fabrication of ZnO-Ag bimetallic nanoparticles by laser ablation for anticancer activity." Alexandria Engineering Journal 61.2 (2022): 1449-1457.

85-Abdelmigid, Hala M., et al. "Green Synthesis of Zinc Oxide Nanoparticles Using Pomegranate Fruit Peel and Solid Coffee Grounds vs. Chemical Method of Synthesis, with Their Biocompatibility and Antibacterial Properties Investigation." Molecules 27.4 (2022): 1236 .

86-Aadim Ph D, Kadhim A., and Awatif Sabir Jasim Ph D. "Silver nanoparticles synthesized by Nd: YAG laser ablation technique: characterization and antibacterial activity." Karbala International Journal of Modern Science 8.1 (2022): 71-82 .

87- Scherrer, Paul. "Bestimmung der inneren Struktur und der Größe von Kolloidteilchen mittels Röntgenstrahlen." Kolloidchemie Ein Lehrbuch. Springer, Berlin, Heidelberg, 1912. 387-409.

88- Rudolph, Peter, ed. Handbook of crystal growth: Bulk crystal growth. Elsevier, 2014.

89-Ingham, B., and M. F. Toney. "X-ray diffraction for characterizing metallic films." Metallic Films for Electronic, Optical and Magnetic Applications. Woodhead Publishing, 2014. 3-38 .

90- Alyamani, A. M. O. L., and O. M. Lemine. "FE-SEM characterization of some nanomaterial." Scanning electron microscopy. IntechOpen, 2012.

91-Saal, Hilkka, Michael Binnewies, et al. "Unusual Optical Properties of Mn-doped ZnO: The Search for a New Red Pigment—A Combined Experimental and Theoretical Study." Chemistry–A European Journal 15, no. 26 (2009): 6408-6414.

92- Ibraheim, Adil M., and Maki A. Sameer. "Effect of The Cu Doping on The Structural and Optical Properties of AlSb Thin Films Deposited by Thermal Evaporation Method." Journal of Physics: Conference Series. Vol. 1879. No. 3. IOP Publishing, 2021.

93- Mustafa, F. A., "The Structural and Optical Characteristics of Polyvinylpyrrolidone Doped with Nano Crystal NaF Films." Academic Research International, Vol. 4, No. 3, pp. 125, 2013.

94-Ambily, S., and C. S. Menon. "Electrical conductivity studies and optical absorption studies in copper phthalocyanine thin films." Solid state communications 94, no.6 (1995): 485-487.

95-Abbasipour, Mina, et al. "Coated cotton gauze with Ag/ZnO/chitosan nanocomposite as a modern wound dressing." Journal of Engineered Fibers and Fabrics 9.1 (2014): 155892501400900114.

96- Stenzel, Olaf. The physics of thin film optical spectra. Berlin/Heidelberg, Germany: Springer, 2015.

97- Klingshirn, Claus F. Semiconductor optics. Springer Science & Business Media, 2012.

98-Kasap, Safa O. Principles of electronic materials and devices. Vol. 2. New York: McGraw-Hill, 2006.

99-Garl, z., "Operating Intruduction Abbe-Refroctrometer", west Germany oberkochn, pp. 3-25, 1985.

100-Mustafa, F. A., "The Structural and Optical Characteristics of Polyvinylpyrrolidone Doped with Nano Crystal NaF Films." Academic Research International, Vol. 4, No. 3, pp. 125, 2013.

101-Sparavigna, Amelia Carolina. "Light-emitting diodes in the solid-state lighting systems." arXiv preprint arXiv:1411.6620 (2014).

102- Lev, Anastasia I., et al. "Comparative analysis of Klebsiella pneumoniae strains isolated in 2012–2016 that differ by antibiotic resistance genes and virulence genes profiles." Pathogens and global health 112.3 (2018): 142-151.

103-Dunckley, Travis, and R. Parker. "RNA turnover." Brenner's Encyclopedia of Genetics: Second Edition. Elsevier Inc., 2013. 295-297 .

104-Derakhshan, Safoura, et al. "Association between presence of virulence genes and antibiotic resistance in clinical Klebsiella pneumoniae isolates." Laboratory medicine 47.4 (2016): 306-311.

105-Marques, Cátia, et al. "Klebsiella pneumoniae causing urinary tract infections in companion animals and humans: population structure, antimicrobial resistance and virulence genes." Journal of Antimicrobial Chemotherapy 74.3 (2019): 594-602.

106-Aljanaby, Ahmed Abduljabbar Jaloob, and Alaa Hassan Abdulhusain Alhasani. "Virulence factors and antibiotic susceptibility patterns of multidrug resistance Klebsiella pneumoniae isolated from different clinical infections." African Journal of Microbiology Research 10.22 (2016): 829-843. **107**-Remya, P. A., M. Shanthi, and Uma Sekar. "Characterisation of virulence genes associated with pathogenicity in Klebsiella pneumoniae." Indian journal of medical microbiology 37.2 (2019): 210-218.

108-Luo, Y., et al. "Molecular epidemiology and virulence factors of pyogenic liver abscess causing Klebsiella pneumoniae in China." Clinical Microbiology and Infection 20.11 (2014): O818-O824.

109-Aljanaby, Ahmed Abduljabbar Jaloob, and Alaa Hassan Abdulhusain Alhasani. "Virulence factors and antibiotic susceptibility patterns of multidrug resistance Klebsiella pneumoniae isolated from different clinical infections." African Journal of Microbiology Research 10.22 (2016): 829-843.

110-Nwanya, A. C., et al. "Structural and optical properties of chemical bath deposited silver oxide thin films: Role of deposition time." Advances in Materials Science and Engineering 2013 (2013).

111-Aziz, A., et al. "STRUCTURAL, MORPHOLOGICAL AND OPTICAL INVESTIGATIONS OF SILVER NANOPARTICLES SYNTHESIZED BY SOL-GEL AUTO-COMBUSTION METHOD." Digest Journal of Nanomaterials & Biostructures (DJNB) 13.3 (2018).

112-Islam, S. M. Z., et al. "Energy band gap of Zinc (Hydr) oxide using absorption, fluorescence and photoconductivity." Frontiers in Optics. Optical Society of America, 2012.

113-Nazrin, S. N., et al. "Comparison study of optical properties on erbium-doped and silver-doped zinc tellurite glass system for non-linear application." Journal of Materials Science: Materials in Electronics 30.7 (2019): 6378-6389.

114-Akmaz, Solmaz, et al. "The effect of Ag content of the chitosan-silver nanoparticle composite material on the structure and antibacterial activity." Advances in Materials Science and Engineering 2013 (2013).

115-AbdElhady, M. M. "Preparation and characterization of chitosan/zinc oxide nanoparticles for imparting antimicrobial and UV protection to cotton fabric." International journal of carbohydrate chemistry 2012 (2012).

116-Dolatabadi, Aghigh, et al. "Ecofriendly biomolecule-capped Bifidobacterium bifidum-manufactured silver nanoparticles and efflux pump genes expression alteration in Klebsiella pneumoniae." Microbial Drug Resistance 27.2 (2021): 247-257.

117-Siddiqi, Khwaja Salahuddin, and Azamal Husen. "Properties of zinc oxide nanoparticles and their activity against microbes." Nanoscale research letters 13.1 (2018): 1-13.

118- Prasad, Durga, et al. "A study on the antibacterial activity of ZnO nanoparticles prepared by combustion method against E. coli." International Journal of Engineering Research and Applications 4.6 (2014): 84-89.

119- Kirchner, Christian, et al. "Cytotoxicity of colloidal CdSe and CdSe/ZnS nanoparticles." Nano letters 5.2 (2005): 331-338.

120- Milliron, Delia J., et al. "Colloidal nanocrystal heterostructures with linear and branched topology." Nature 430.6996 (2004): 190-195.

121- Clement, Julia L., and Penelope S. Jarrett. "Antibacterial silver." Metal-based drugs 1.5-6 (1994): 467-482.

122- Zhang, Huanjun, and Guohua Chen. "Potent antibacterial activities of Ag/TiO2 nanocomposite powders synthesized by a one-pot sol− gel method." Environmental science & technology 43.8 (2009): 2905-2910.

123- Dixit, H., et al. "Electronic structure and band gap of zinc spinel oxides beyond LDA: ZnAl2O4, ZnGa2O4 and ZnIn2O4." New Journal of Physics 13.6 (2011): 063002.

124-Bechiri, A., F. Benmakhlouf, and N. Bouarissa. "Calculation of electronic and optical properties of Zn-based II–VI semiconductors." Physics Procedia 2.3 (2009): 803-812.

125-Huang, Xiaofei, et al. "A novel silver-loaded chitosan composite sponge with sustained silver release as a long-lasting antimicrobial dressing." RSC advances 7.55 (2017): 34655-34663.

126-Wrońska, Natalia, et al. "Antimicrobial effect of chitosan films on food spoilage bacteria." International journal of molecular sciences 22.11 (2021): 5839.

127- Wali, Hawra, et al ."Study and characterization of the antibacterial activity of chemically synthesized CdS and Au/CdS nanocomposites and their effect on the molecular level of Gram-negative bacteria" To obtain a master's degree in life sciences, microbiology (2017).

FIGURE LIST

الخلاصة

توليف المواد الفيزيائية والبيولوجية وعلم النانو كلها مواضيع ذات أهمية في التطبيقات الطبية والصناعية وغيرها. يؤدي دمج الجسيمات النانوية باستخدام تقنية الاستئصال بالليزر النبضي بالسوائل (PLAL) إلى إنتاج مركبات نانوية عالية الجودة تساهم في إنتاج المواد المضادة للبكتيريا ، بما في ذلك الالتهاب الرئوي *Klebsiella*.

بعد وضع العينات النانوية على شرائح زجاجية وإخضاعها لسلسلة من الاختبارات ، أعطت المركبات (Cs- Zno) / (Cs-Ag) / (Cs-Ag-Zno) النتائج التالية: فحص الخواص البصرية للأشعة فوق البنفسجية- أظهر vis وجود قمتين ، أحدهما مرتبط بـ Ag NPs ويقع عند ٤٠٠ نانومتر والآخر بأكسيد الزنك ويقع عند ٢٤٤ نانومتر. يكون معامل الامتصاص للمركب النانوي عند قيمته القصوى في النطاق ٢٠٠-٥٥٠ نانومتر وأن فجوة النطاق المباشر للفضة هي (٢.٨) فولت ، وفجوة الطاقة المباشرة للزنك هي (٤.٧) فولت وفجوة الطاقة المباشرة لـ Cs، Ag و Zn عند (٢.٧) eV بينما (٢.٥) eV هي فجوة الطاقة غير المباشرة للفضة وفجوة الطاقة غير المباشرة لمركب (Cs-Ag-ZnO) هي ٢.٦ eV و ٤.٢ eV لـ Zno.

كانت هناك أيضًا ثلاث قمم لكل مركب في نتائج FTIR لمسح المركبات النانوية ولاحظنا رابطة O-H \ NH2. وكذلك روابط C = O و N-H: OH.

كشف البحث عن الخصائص الهيكلية للمركب النانوي (Cs-Ag-Zno) عن وجود مستويات بلورية ووجود قمم مقابلة لمحلول الشيتوزان عند (٢٤.٦١١٨ درجة) ، بالإضافة إلى وجود قمم مماثلة من الفضة والزنك. الجسيمات النانوية. تم الحصول على الجسيمات النانوية عند (٣٠.٣٧٢٩ و ٤٥.٩٩٠٢ درجة) مع معاملات ميلر (١٠٠ ، ٢٠٠) ، والجسيمات النانوية كانت FCC لجسيمات الفضة النانوية وسداسية لأكسيد الزنك.

كشف اختبار TEM أن الجسيمات النانوية الكروية لها حجم نانوي يبلغ ١٨.١٩٦ نانومتر. وفقًا لنتائج FE-SEM ، تم اكتشاف أن جزيئات الفضة النانوية وجسيمات الزنك النانوية مرتبطة بإحكام بالبوليمر (Cs) وظهرت كعصيات من المركب الثلاثي بينما ظهرت على شكل قطع هلام الزنك والشيتوزان أثناء إضافة جزيئات الفضة النانوية لمحلول البوليمر قاموا بتشكيل أشكال مخروطية متحدة المركز.

عندما تعرضت بكتيريا *Klebsiella pneumonia* التي يمكن أن تسبب أمراضًا متنوعة إلى المركبات النانوية المتولدة ، أظهرت النتائج أن نسبة التثبيط أو القتل تراوحت بين (٢٢-٣٥) ملم.

تزداد النسبة المئوية للبكتيريا المقتولة مع زيادة تركيز المركبات النانوية. أظهرت النتائج أن تراكيز الحمض النووي البكتيري تراوحت بين ٠.٠٣ و ٠.٢٩١ ، وأعلى تركيز كان عند مركب (Cs-Zno).

أخيرًا ، تمت دراسة خمسة أنواع من جينات الالتهاب الرئوي*Klebsiella (1 Fimh ،. Ycfm entB، Kfu، rpmA)* واتضح أنها تأثرت بالمركبات النانوية بطرق مختلفة) ، ولكن في التخفيف الثاني ، كان تأثير المركب النانوي (Cs- Ag -Zno) واضحًا ، لأنه لوحظ أن جميع

الجينات المدروسة قد تأثرت بهذا المركب النانوي عند مقارنتها بالعينة. غير معالج بالمواد النانوية.

جمهورية العراق

وزارة التعليم العالي والبحث العلمي

كلية العلوم للبنات

جامعة بابل

قسم فيزياء الليزر

توليف ودراسة تأثير المركب النانوي (شيتوزان-اوكسيد الزنك-الفضة) بطريقة الليزر النبضي على الامراض وعوامل الضراوة لكلبسيلا الرئوية

أطروحة

مقدمة الى مجلس كلية العلوم للبنات / جامعة بابل ضمن متطلبات الحصول على درجة الماجستير في فيزياء الليزر

رسالة

انوار عبد الرزاق عباس الجشعمي

بكلوريوس (٢٠١٢)

بأشراف

أ.م .د .امير خضير النافعي

أ. د .علي حسين المرزوكي

1444 2022